Charles University

Faculty of Science

Department of Physical and Macromolecular Chemistry

MSc. Beata Anna Zasońska

Preparation and characterization of superparamagnetic inorganic/polymer particles for biomedical application

Doctoral Thesis

Supervisor: Ing. Daniel Horák, CSc.

Institute of Macromolecular Chemistry AS CR, v.v.i.

Prague, 2016

Univerzita Karlova

Přírodovědecká fakulta

Katedra fyzikální a makromolekulární chemie

Mgr. Beata Anna Zasońska

Příprava a vlastnosti superparamagnetických anorganicko/polymerních částic pro biolékařské aplikace

Doktorská dizertační práce

Školitel: Ing. Daniel Horák, CSc.

Ústav makromolekulární chemie AV ČR, v.v.i.

Praha, 2016

I declare that I have written this thesis independently under the supervision of Ing. Daniel Horák, CSc. I did not submit this work, or a part of it, to obtain another university degree. To the best of my knowledge, I have cited all the sources I have used.

Prague, 22.11.2016 Beata Anna Zasońska

Acknowledgments

I would like to thank to my supervisor, Ing. Daniel Horák, CSc., for leading, support, and help with this doctoral thesis. I wish to express many thanks to my colleagues, coworkers, and coauthors for many fruitful discussions and assistance. I am also grateful to the Charles University for opportunity of the doctoral studies and to the Institute of Macromolecular Chemistry, where I did the experimental work. Additionally, I would like to thank to my family for its support.

TABLE OF CONTENTS

ABSTRACT

Superparamagnetic γ-Fe_2O_3 nanoparticles were synthesized by coprecipitation of ferric and ferrous salts with a base. Resulting nanoparticles were coated with shells, such as poly(*N,N*-dimethylacrylamide) (PDMAAm), neat and functionalized silica (SiO_2 and SiO_2-NH_2), and polyaniline (PANI). PDMAAm shell was introduced by modification of iron oxide nanoparticle surface with an initiator and *N,N*-dimethylacrylamide was polymerized producing γ-Fe_2O_3&PDMAAm core-shell particles. In case of SiO_2-NH_2 shell, tetramethyl orthosilicate was used to yield γ-Fe_2O_3&SiO_2 nanoparticles, which were subsequently modified by (3-aminopropyl)triethoxysilane to prepare γ-Fe_2O_3&SiO_2-NH_2 particles. Oxidation of aniline hydrochloride with ammonium persulfate in an aqueous solution of poly(*N*-vinylpyrrolidone) in the presence of iron oxides produced γ-Fe_2O_3&PANI nanoparticles. Finally, the last type of the particles was based on thionin-modified poly(carboxymethyl methacrylate) (PCMMA&Th).

The particles were characterized by techniques, such as scanning and transmission electron microscopy (SEM and TEM) and dynamic light scattering (DLS) to determine the particle morphology and hydrodynamic diameter. The presence of the functional groups, chemical composition, and the iron content were investigated by Fourier-transform infrared (FTIR) spectroscopy, elemental analysis (AAS), atomic absorption, energy dispersive X-ray (EDAX), and X-ray photoelectron spectroscopy (XPS). Vibrating sample magnetometry (VSM) determined the magnetic properties of the iron oxide particles.

Last, but not least, γ-Fe_2O_3&PDMAAm, γ-Fe_2O_3&SiO_2, and γ-Fe_2O_3&SiO_2-NH_2 particles were applied in biological experiments, namely they were incubated with murine macrophages of J774.2 line and engulfment of the particles by the cells was quantified. Cytotoxicity of γ-Fe_2O_3&PANI particles was evaluated on human neuroblastoma cells, while cytotoxicity and immune response of porous silica-coated magnetic nanoparticles was determined on proliferating human peripheral blood cells. The particles were localized within the cytoplasm of treated cells and proved to be non-toxic even at high doses and after long incubation periods. The particles might be suitable in cell applications as the cells labeled with the developed nanoparticles can be non-invasively monitored by magnetic resonance imaging (MRI); optionally they can be easily magnetically separated and redispersed in water solutions on removing of the external magnetic field. Especially, γ-Fe_2O_3&PDMAAm nanoparticles seem to be promising for diagnosis of phagocytic activity, as well as delivery of various biomolecules, such as specific proteins. Finally, PCMMA&Th particles represent a highly sensitive and universal tool for labeling of antibodies in enzyme-based sandwich-type immunosensors.

Keywords: polymer; nanoparticles; superparamegnetism; iron oxide; cell.

ABSTRAKT

Superparamagnetické γ-Fe_2O_3 nanočástice byly syntetizovány srážením železitých a železnatých solí alkalickými činidly. Výsledné nanočástice byly povlečeny slupkami, jako je poly(*N,N*-dimethylakrylamid) (PDMAAm), výchozí i funkcionalizovaná silika (SiO_2 a SiO_2-NH_2) a polyanilin (PANI). PDMAAm slupka byla zavedena modifikací povrchu nanočástic oxidů železa iniciátorem a *N,N*-dimethylakrylamid byl polymerizován za vzniku γ-Fe_2O_3&PDMAAm částic. V případě SiO_2-NH_2 slupky byl použit tetramethyl-orthosilikát a vznikly γ-Fe_2O_3&SiO_2 nanočástice, které byly následně modifikovány (3-aminopropyl)triethoxysilanem (γ-Fe_2O_3&SiO_2-NH_2 částice). Oxidací anilin hydrochloridu persulfátem amonným ve vodném roztoku poly(*N*-vinylpyrolidonu) v přítomnosti oxidů železa vznikly γ-Fe_2O_3&PANI nanočástice. Poslední typ částic byl pak na bázi thioninem modifikovaného poly(karboxymethyl-methakrylátu) (PCMMA&Th).

Částice byly charakterizovány technikami, jako je rastrovací a transmisní elektronová mikroskopie (SEM a TEM) a dynamický rozptyl světla (DLS), které stanovily morfologii a hydrodynamický průměr částic. Přítomnost funkčních skupin, chemické složení a obsah železa byly prokázány infračervenou spektroskopií s Fourierovou transformací (FTIR), dále atomovou absorpční spektroskopií (AAS), prvkovou a mikroprvkovou analýzou (EDAX) a rentgenovou fotoelektronovou spektroskopií (XPS). Vibrační magnetometrií (VSM) se stanovily magnetické vlastnosti částic oxidů železa.

V neposlední řadě byly γ-Fe_2O_3&PDMAAm, γ-Fe_2O_3&SiO_2 a γ-Fe_2O_3&SiO_2-NH_2 částice použity v biologických experimentech, kde byly inkubovány se savčími makrofágy linie J774.2 a bylo kvantifikováno pohlcování částic buňkami. Cytotoxicita γ-Fe_2O_3&PANI částic byla vyhodnocena na lidských neuroblastomech; cytotoxicita a imunitní reakce magnetických nanočástic povlečených porézní silikou byly stanoveny na proliferujících lidských periferních krevních buňkách. Částice byly lokalizovány v buněčné cytoplazmě a bylo prokázáno, že jsou netoxické i za vysokých koncentrací a po dlouhé inkubační době. Částice mohou být vhodné pro buněčné aplikace; buňky označené nanočásticemi mohou být neinvazivně monitorovány magnetickým rezonančním zobrazením (MRI); mohou být rovněž snadno magneticky odděleny a poté opět redispergovány ve vodných roztocích, je-li vnější magnetické pole odstraněno. Zejména γ-Fe_2O_3&PDMAAm nanočástice jsou slibné pro diagnostiku fagocytární aktivity a rovněž pro dávkování různých biomolekul, např. proteinů. PCMMA&Th částice pak představují vysoce citlivý a univerzální prostředek pro značení protilátek v ELISA imunosenzorech.

Klíčová slova: polymer; nanočástice; superparamagnetický; oxid železa; buňka.

ABBREVIATIONS

AAS	atomic absorption spectroscopy
ABHA	2,2'-azobis(*N*-hydroxy-2-methylpropanimidamide) dihydrochloride
AMPA	2,2'-azobis(2-methylpropanimidamide) dihydrochloride
APTES	(3-aminopropyl)triethoxysilane
B_d	flux density
CCHPA	4-cyano-4-{[1-cyano-3-(*N*-hydroxycarbamoyl)-1-methylpropyl]azo}pentanoic acid
CTAB	cetyltrimethylammonium bromide
D_h	hydrodynamic diameter
DLS	dynamic light scattering
DMAAm	*N*,*N*-dimethylacrylamide
D_n	number-average particle diameter
D_w	weight-average particle diameter
EDAX	energy dispersive X-ray spectroscopy
EDC	*N*-(3-dimethylaminopropyl)-*N*'-ethylcarbodiimide
ELISA	enzyme-linked immunosorbent assay
FTIR	Fourier-transform infrared spectroscopy
GMA	glycidyl methacrylate
GM-CSF	granulocyte macrophage colony stimulating factor
H	magnetic field
HRP	horseradish peroxidase
M	magnetization
M_n	number-average molecular weight
M_s	saturation magnetization
M_w	weight-average molecular weight
MRI	magnetic resonance imaging
NHS	*N*-hydroxysulfosuccinimide
PANI	polyaniline
PCMMA	poly(carboxymethyl methacrylate)
PCMMA&Th	thionin-modified poly(carboxymethyl methacrylate)
PDI	polydispersity index (according to TEM)
PDMAAm	poly(*N*,*N*-dimethylacrylamide)

PGMA	poly(glycidyl methacrylate)
PHA	phytohemagglutinin
PI	polydispersity (according to DLS)
PVP	poly(*N*-vinylpyrrolidone)
S_{BET}	specific surface area
SEM	scanning electron microscopy
TEM	transmission electron microscopy
TEOS	tetraethyl orthosilicate
Th	thionine
TMOS	tetramethyl orthosilicate
UV-vis	ultraviolet-visible spectroscopy
VSM	vibrating sample magnetometry
XPS	X-ray photoelectron spectroscopy
σ	conductivity
μ	magnetic permeability
μ_0	magnetic permeability constant
χ	magnetic susceptibility

LIST OF PUBLICATIONS AND CONTRIBUTIONS AT CONFERENCES

1. Zasońska B.A., Boiko N., Horák D., Klyuchivska O., Macková H., Beneš M., Babič M., Trchová M., Hromádková J., Stoika R., The use of hydrophilic poly(*N,N*-dimethylacrylamide) grafted from magnetic γ-Fe_2O_3 nanoparticles to promote engulfment by mammalian cells, *J. Biomed. Nanotechnol.* 9, 479-491, **2013** (IF = 5.338).

2. Zasońska B.A., Boiko N., Klyuchivska O., Trchová M., Petrovský E., Stoika R., Horák D., Silica-coated γ-Fe_2O_3 nanoparticles: Preparation and engulfment by mammalian macrophages, *J. Nanopharm. Drug Delivery* 1, 182-192, **2013**.

3. Zasońska B.A., Líšková A., Kuricová M., Tulinská J., Pop-Georgievski O., Ilavská S., Horváthová M., Jahnová E., Horák D., Functionalized porous silica&maghemite core-shell nanoparticles for applications in medicine: Design, synthesis and immunotoxicity, *Croat. Med. J.* 57, 165-179, **2016** (IF = 1.483).

4. Zasońska B.A., Bober P., Jošt P., Boštík P., Horák D., Magnetoconductive maghemite core/polyaniline shell nanoparticles: Physico-chemical and biological assessment, *Colloids Surf. B* 141, 382-389, **2016** (IF = 3.9).

5. Zasońska B.A., Čadková M., Kovářová L., Bílková Z., Korecká L., Horák D., Thionin-modified poly(glycidyl methacrylate) nanospheres as label of antibodies for biosensing applications, *ACS Appl. Mater. Interfaces* 7, 24926-24931, **2015** (IF = 7.145).

Monograph

Zasońska B.A., Patsula V., Stoika R., Horák D., Surface-modified magnetic nanoparticles for cell labeling, in: The Chemistry and Physics of Engineering Materials, Vol. 1: Modern Analytical Methodologies, Berlin A.A., Joswik R., Vatin N.I., eds., Apple Academic Press, Oakville 2015, Canada, pp. 145-164. ISBN 9781771880794.

Other author's publications

1. Podhorodecki A., Noculak A., Banski M., Sojka B., Zelazo A., Misiewicz J., Cichos J., Karbowiak M., Zasońska B.A., Horak D., Sikora B., Elbaum D., Dumych T., Bilyy R., Szewczyk M., Lanthanides fluorides doped nanocrystals for biomedical applications, *ECS Trans.* 61, 115-125, **2014**.

2. Huk A., Izak-Nau E., El Yamani N., Uggerud H., Vadset M., Zasońska B.A, Duschl A., Dušinska M., Impact of nanosilver on various DNA lesions and HPRT gene mutations - effects of charge and surface coating, *Part. Fibre Toxicol.* 12, 25, **2015** (IF = 8.6).

3. Bober P., Zasońska B.A., Humpolíček P., Kuceková Z., Vargae M., Horák D., Babayan V., Kazantseva N., Prokeš J., Stejskal J., Polyaniline-maghemite based dispersion: Electrical, magnetic properties and their cytotoxicity, *Synth. Met.* 214, 23-29, **2016** (IF = 2.299).

Contributions on conferences (selected)

Oral presentation

Zasońska B., Boiko N., Horák D., Stoika R., PDMAAm-coated γ-Fe_2O_3 nanoparticles for cell labeling, Bridges in Life Sciences Annual Conference, Biopolymers & Cells, Budapest, Hungary 2012, Abstract Book, p. 79.

Poster presentations

1. Zasońska B.A., Boiko N., Horák D., Stoika R., Poly(*N,N*-dimethylacrylamide) shell/γ-Fe_2O_3 core nanoparticles for labeling of mammalian cells, Polymers in Medicine, Prague, Czech Republic 2012, Abstract Book, p. 113.

2. Zasońska B.A., Horák D., Superparamagnetic iron oxide nanoparticles coated with organic and inorganic polymer shell for imaging and tracking of macrophages, International Polymer Colloid Group Research Conference, Shanghai, People's Republic of China 2013.

3. Zasońska B.A., Horák D., Boiko N., Stoika R., Silica-coated superparamagnetic nano- and microparticles for cell labeling, Bridges in Life Sciences Annual Conference, Prague, Czech Republic 2013, Abstract Book, p. 93.

4. Zasońska B.A., Horák D., Boiko N., Stoika R., Silica/iron oxide nano- and microparticles for cell labeling, Career in Polymers V., Prague, Czech Republic 2013, Abstract Book, P 4.

5. Zasońska B.A., Líšková A., Tulinská J., Kuricová M., Bartušová M., Horák D., Functionalized core-shell porous silica/maghemite nanoparticles: Design, synthesis and immunotoxicity, Bridges in Life Sciences Annual Scientific Conference, Split, Croatia 2014, Abstract Book, p. 69.

6. Zasońska B.A., Tulinská J., Horák D., Líšková A., Kuricová M., Bartušová M., Immunotoxicity of functionalized core-shell maghemite/porous silica nanoparticles, Frontiers of Polymer Colloids: From Synthesis to Macro-Scale and Nano-Scale Applications, 78th Prague Meeting on Macromolecules, Prague, Czech Republic 2014, Abstract Book, p. 151.

7. Zasońska B.A., Bober P., Jošt P., Boštík P., Horák D., Cytotoxicity of maghemite core/polyaniline shell nanoparticles, Bridges in Life Sciences Annual Scientific Conference, Wroclaw, Poland 2015, Abstract Book, p. 61.

8. Zasońska B.A., Bober P., Jošt P., Boštík P., Horák D., Cytotoxicity of maghemite/ polyaniline nanoparticles using human neuroblastoma cells, Functional Polymers at Bio-Material Interfaces, 79th Prague Meeting on Macromolecules, Prague, Czech Republic 2015, Abstract Book, p. 66.

Author's contribution in publications 1-5: 50-60%

Co-authors (selected)

Daniel Horák - supervisor.
Milan J. Beneš - consultations (publications No. 1, 2 and 3).
Patrycja Bober - help with polyaniline coating, UV-vis spectroscopy (publication No. 4).
Jiřina Hromádková - TEM, SEM micrographs and EDAX analysis.
Eduard Petrovský - magnetic measurements (publications No. 2 and 4).
Hana Macková - help with synthesis of initiator, molecular mass measurement (publication No. 1).
Ognen Pop-Georgievski - XPS measurement (publication No. 3).
Miroslava Trchová - help with FTIR spectroscopy (publications No. 1 and 2).

1. LITERATURE OVERVIEW

Nanotechnology is one of the most rapidly developing scientific branches[1]. It allows fabrication of innovative, nanostructured materials, featured with unique properties and multiple application possibilities. By the definition, at least one dimension of nanomaterials is in nanoscale size (typically ≤ 100 nm)[2]. Compared to the single-component structures, core-shell particles are composed of two or more materials; the latter type has a wider range of useful applications, especially in biological and medical field, such as drug delivery systems, magnetic resonance imaging (MRI)[3], specific targeting, and biosensors[4,5].

Recently, a plethora of publications about design of the nanoparticles and their toxicity are appearing each year[6,7]. Nevertheless, the current knowledge is still incomplete. One of the reasons is that a material of the same composition can exhibit various properties due to differences in synthesis, purification, modification, storage, etc. It is therefore essential to completely characterize properties of the particles, their stability, and toxicity not only in *in vitro* studies, but also *in vivo* on different mammalian cells.

1.1. Magnetic nanoparticles

Magnetic nanoparticles are mostly based on iron oxides, which play a prominent role in life, since iron is indispensable component of organisms and is non-toxic at moderate concentration[8]. Surface-modified iron oxide nanoparticles have been thus found very attractive for cell separations[9] and labeling[10], cancer therapy[11], drug delivery[12], hyperthermia[13], and as contrast agents for magnetic resonance imaging (MRI)[14].

Nanoparticle magnetism

Magnetic properties of materials are the result of action of magnetic field on magnetic moments of electrons and atoms[15]. Magnetic field is characterized by magnetic induction, or the magnetic flux density (B_d), intensity of the external magnetic field (H), and magnetization of the substance (M)[16]. The relation between these parameters is given by the following equations:

$$B_d = \mu_0 \cdot (M + H) \quad (1)$$

$$B_d = \mu \cdot H \quad (2)$$

Here, μ_0 represents universal magnetic permeability constant and μ is permeability of the material. The magnetic induction is generated by the field alone and $\mu_0 M$ is the additional magnetic induction contributed by the material. The magnetic susceptibility χ is defined as the ratio of magnetization M to magnetic field H[17]:

$$\chi = \frac{M}{H} \tag{3}$$

From these equations, the correlation between permeability and susceptibility of given material can be easily found[18]:

$$\mu = \mu_0 \cdot (1 + \chi) \tag{4}$$

The susceptibility plays a major role in characterization of magnetic properties of a material. The magnitude of the susceptibility, as well as its temperature and field dependencies, provide information on magnetic behavior of different types of magnetic materials, which can be classified into three main groups: diamagnetic, paramagnetic, and ferromagnetic[15-17]. Furthermore, three types of materials with ferromagnetic behavior are recognized: ferromagnets, ferrimagnets and antiferromagnets.

Diamagnetism is determined by the distortion of electron orbits due to external magnetic field and is present in all materials. This response is negative, small and temperature-independent. Paramagnetism is present in materials with atoms containing unpaired electrons resulting thus in non-zero atomic magnetic moment. Exchange interaction between neighboring atoms is absent or weak ($\chi = 10^{-6}$-10^{-1} m^3/kg) compared to the thermal energy. In the ferromagnets (strong exchange interactions between atoms), the magnetization is the result of the parallel alignment of all the atomic magnetic moments in the same direction. Ferrimagnets, such as γ-Fe_2O_3 and Fe_3O_4, however, are composed of two magnetic sub-lattices of unequal magnetic moment, which are aligned anti-parallel to each other. This unbalance in the sub-lattice magnetization leads to a net magnetization in the solid. In the bulk, materials with a net magnetization minimize their free magnetic energy by splitting their magnetic structure into domains. Orientation of each magnetization within domains varies, which results in zero total magnetization at a zero magnetic field. If the magnetic material has a size of a single domain and is small enough (< 20 nm), energy of thermal vibrations of such particles prevents alignment of their magnetic moments and the behavior resembles that of a paramagnet in a large temperature region; such a material is called superparamagnetic[16].

With applied external magnetic field H, the material acquires induced magnetization M, which increases with increasing H until maximum value (saturation magnetization, M_s) is

reached; the same is happening in the opposite direction. In case of paramagnets, this behavior is linear and reversible until saturation at high fields (typically > 7 T). In ferrimagnets, this behavior is non-linear, irreversible, and saturation is reached at much smaller fields (in magnetite at 300 mT). Such behavior is called a hysteresis loop (Figure 1)[17]. Superparamagnetic substances show behavior similar to that of paramagnets, but they reach saturation at fields as ferrimagnet of the same composition, or lower[16]. Temperature acts against magnetic alignment. Once increasing temperature reaches value at which magnetic alignment vanishes (Curie point), the material starts to behave paramagnetically. Curie point is characteristic for different materials with aligned magnetic moments and is called Curie temperature (ferro/ferrimagnetic material) or the Néel temperature (antiferromagnetic material)[15,16].

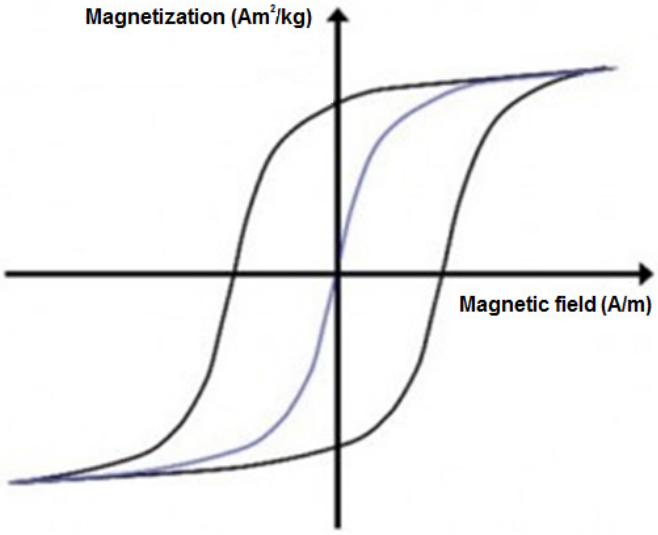

Figure 1. Hysteresis loops of ferromagnetic (black) and superparamagnetic materials (violet).

Synthesis of magnetic nanoparticles

There are many methods to obtain various types of iron oxide nanoparticles differing in shape, size, and availability of the reactive groups on the surface[19]. The oldest preparation involves the size reduction[20], i.e., grinding of bulk magnetite in the presence of large amounts of a surfactant in a ball mill for 500-1,000 h. Other synthetic approaches include coprecipitation[21,22], thermal decomposition[23], spray pyrolysis[24], microemulsion[25], hydrothermal[26], sol-gel[27], bacterial[28], and other methods[29]. However, the most common technique for preparation of such particles is coprecipitation of Fe(III) and Fe(II) salts in the presence of an aqueous base (e.g., NH_4OH or NaOH). The latter method was used for

synthesis of the particles in this work, where ferric and ferrous chlorides were mixed with ammonia[30]. Using appropriate reactant ratios, it was possible to obtain quite uniform spherical-like particles.

Maghemite

Since this work deals mostly with maghemite nanoparticles, let us to mention some of their properties. γ-Fe_2O_3 is a brownish mineral, second most common polymorph of iron oxide with saturation magnetization of *ca*. 80 $A \cdot m^2/kg$ (bulk material)[18,21,31]. Its crystal structure is similar to that of magnetite, but with vacancies in octahedral sites due to oxidation of divalent iron ions; maghemite is ferrimagnetic. Small γ-Fe_2O_3 particles (< 20 nm) have large specific surface area, high magnetic susceptibility, and exhibit superparamagnetism at ambient temperatures. High surface to volume ratio makes the particles thermodynamically metastable[15,18]. To compensate the excess of surface energy, they tend to form bigger structures (aggregates) in water[32]. In the next chapter, some approaches how to prevent the particle aggregation are discussed.

1.2. Core-shell nanoparticles

Iron oxide nanoparticles have plenty of distinctive advantages, but on the other hand, neat (uncoated) particles exhibit high nonspecific adsorption of biomolecules, undesirable *in vitro* and *in vivo* interactions, as well as tendency to aggregation. This can be avoided by the surface modification with a biocompatible shell[33]. Typical polymer shells are made from organic (poly(ethylene glycol)[34], poly(vinyl alcohol)[35], poly(*N,N*-dimethylacrylamide)[36]) or inorganic materials (silica[37]). This additional layer renders the particles with colloidal stability, avoids interactions with the surrounding environment, and introduces specific functional groups on the surface to allow attachment of a cargo (protein or drug), and to boost cellular uptake. There are four main types of nanoparticle morphologies: single core, multicore, strawberry, and hairy (Figure 2).

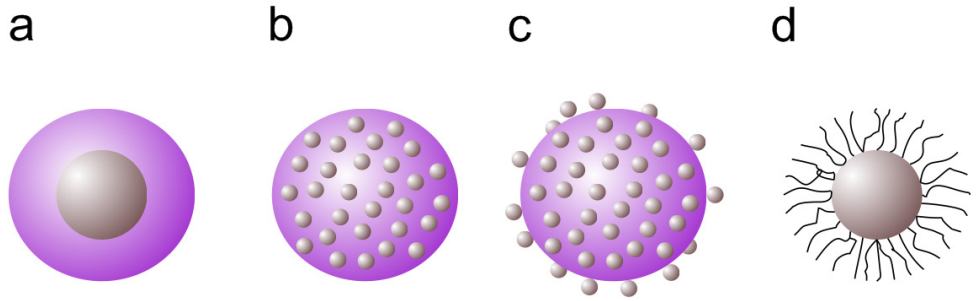

Figure 2. Scheme of four main core-shell particle morphologies: (a) single core, (b) multicore, (c) strawberry, and (d) hairy[38].

In this thesis, the following macromolecular modification agents were chosen: poly(*N,N*-dimethylacrylamide), porous and non-porous silica including its amino derivative, and polyaniline. Below, basic information about these coatings is shown.

Poly(*N,N*-dimethylacrylamide)

Highly hydrophilic poly(*N,N*-dimethylacrylamide) (PDMAAm) is well-known not only for its excellent solubility both in water and various organic solvents, but also for very good biocompatibility[39,40]. PDMAAm rapidly polymerizes under azo- and/or peroxy-initiation by free-radical mechanisms (Figure 3).

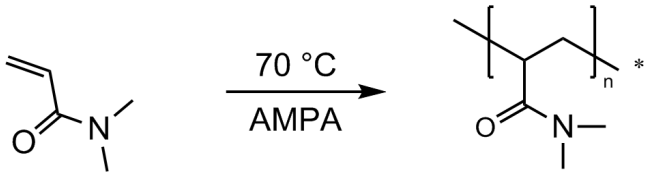

Figure 3. Polymerization of *N,N*-dimethylacrylamide; AMPA - 2,2'-azobis(2-methyl-propanimidamide) dihydrochloride.

DMAAm can be also copolymerized with other monomers[41,42], such as methyl methacrylate[43], acrylic acid[44], styrene, and butadiene[45]; polysiloxane and cellulose can be grafted on the main PDMAAm chain. PDMAAm has been used as a support improving dying, hygroscopic, and antistatic properties of synthetic fibers and gels[46], adhesiveness of polyamide resins, and for manufacture of contact lenses[47]. Cosmetic industry uses PDMAAm as a skin protecting agent from UV irradiation. Recently, PDMAAm has attracted increasing interest in drug delivery systems and medicinal diagnostics[48-50].

Silica

Silica includes several types of silicon dioxides, which can be soluble, amorphous or crystalline; silicon atom is surrounded by four or six oxygen atoms. Silica is generally thermally stable, optically transparent, biocompatible, and relatively environmentally friendly inert material, with minimum non-specific protein adsorptions[51]; silica is thus not the subject of microbial attacks. There are many methods of synthesis of the silica nanoparticles involving reverse microemulsion, aerosol pyrolysis, sol-gel technique[52], etc. The synthesis and reproducibility of the sol-gel method including particle nucleation and growth have been intensively investigated[51-53].

In this thesis, Stöber sol-gel approach was chosen for the SiO_2 synthesis, because it is efficient, fast, low-cost, and surfactant-free method for preparing monodisperse spherical particles with diameters between 20 and 2000 nm[52]. The process involves hydrolysis (Eq. 5) and condensation (Eq. 6 and 7) of a silica precursor, typically TEOS or TMOS, at room temperature in an ethanolic medium in the presence of acid or base (catalysts)[54]. Under acidic conditions, hydrolysis is slow and silica preferably forms linear chains, which later undergo branching and gelation. At higher pH (basic conditions), hydrolysis is fast and highly branched spherical particles are formed (Figure 4). Condensation occurs between two silanols or silanol and ethoxy groups resulting in siloxane (Eq. 6 and 7),

$$\equiv Si-OR + H_2O \rightleftharpoons \equiv Si-OH + ROH \quad (6)$$

$$\equiv Si-OR + HO-Si\equiv \rightleftharpoons \equiv Si-O-Si\equiv + ROH \quad (7)$$

$$\equiv Si-OH + HO-Si\equiv \rightleftharpoons \equiv Si-O-Si\equiv + H_2O \quad (8),$$

where OR is alkoxide.

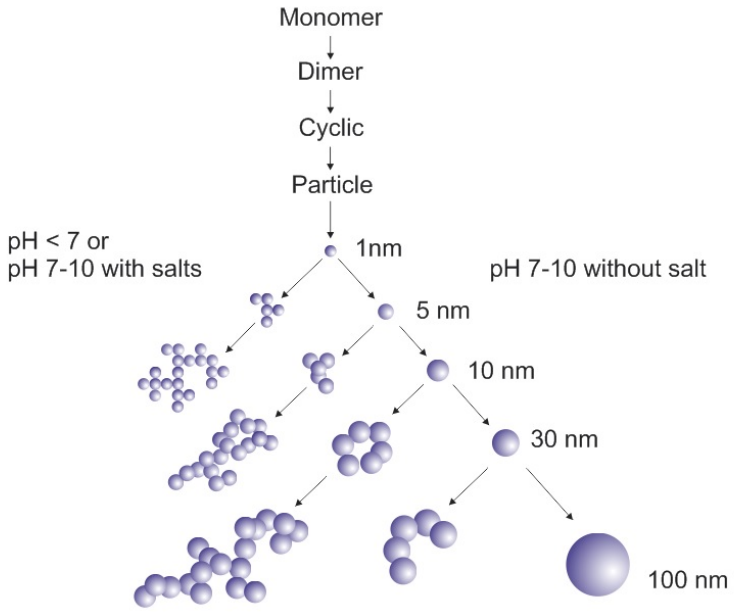

Figure 4. Formation of silica nanoparticles by hydrolysis and condensation of alkoxy orthosilicates. Acid-catalyzed reaction leads to a three-dimensional gel and base-catalyzed reaction results in individual spherical particles[55].

Recently, mesoporous silica nanoparticles (pores 2-50 nm) are receiving growing attention not only as packings in chromatography, but also as multifunctional platforms for nanomedicine, especially, in drug delivery systems[56]. Synthesis of ordered mesoporous SiO_2 takes advantage of templates, typically amphiphilic surfactants[57,58].

Polyaniline

Polyaniline (PANI) is one of the most intensively studied polymers due to its mixed ionic and electronic conductivity, excellent electronic and optical properties, good redox and ion-exchange activity, environmental stability, ease of preparation from common chemicals, and relatively low cost[59,60]. PANI exists in various forms that differ in the degree of oxidation or extent of protonation (Figure 5)[60].

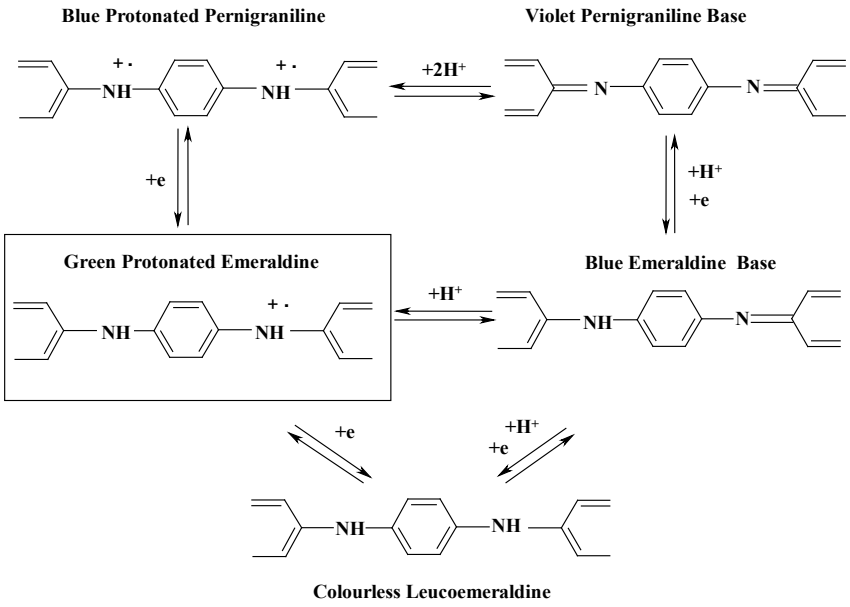

Figure 5. Oxidation and protonation of aniline[60].

PANI is usually obtained by oxidative polymerization of aniline or its salts (aniline hydrochloride or sulfate) with an oxidant in water or acidic solutions, respectively[61]. The most important PANI form is emeraldine salt obtained by aniline polymerization (Figure 5). The product is green, stable, and highly conducting ($\sigma \sim 4$ S/cm)[62]. Emeraldine salt can be converted to its base, a blue non-conducting PANI form, by the deprotonation with hydroxides. Depending on the polymerization conditions (pH, temperature), PANI can be prepared in various morphologies; globules and nanotubes are the most common[60].

Many useful properties of conducting polymers are exploited in numerous technological and biomedical applications, such as electromagnetic shielding for computers and other electronic devices[63], sensors[64], anti-corrosion coatings[65], and photothermal therapy[66].

Biological and biomedical applications

Nanotechnology, nanomedicine, and nanotoxicology are three interconnected and closely dependent fields. As any new nanomaterial can have an impact on the biological environment with consequences on the living organism, a series of toxicology studies has to be carried out before any medical application. The toxicological studies should include *in vitro* characterization of the nanomaterial behavior in cells, uptake by the cells, effects on living tissues, and evaluation of therapeutic or diagnostic efficiency[67]. It is worth of mentioning that biological fate of the nanoparticles strictly depends on their composition and physico-

chemical properties, such as size, surface, charge, morphology, stability, and coating[68]. If intravenously injected in an animal, majority of the iron oxide nanoparticles is distributed in liver (80 %), but also in spleen (< 8 %), kidneys, and lungs[69]. It is a big advantage, that magnetite and maghemite have been already approved for clinical use by US Food and Drug Administration[70].

2. PARTICLE CHARACTERIZATION

There is no universal method to determine size, structure, and composition of the particles. Each of the characterization method has its own limitations and always more techniques are required to determine properties of the particles.

Transmission electron microscopy (TEM) provides information about morphology, size and distribution of the nanoparticles. The number-average diameter (D_n), as well as the weight-average diameter (D_w), and uniformity (polydispersity index PDI = D_w/D_n) were calculated from at least 400 individual nanoparticles on the micrographs using Atlas software (Tescan Digital Microscopy Imaging; Brno, Czech Republic) according to Eq. 8 and 9:

$$D_n = \frac{\sum n_i \cdot D_i}{\sum n_i} \tag{8}$$

$$D_w = \frac{\sum n_i \cdot D_i^4}{\sum n_i \cdot D_i^3} \tag{9},$$

where n_i and D_i are the number and diameter of the i^{th} particle, respectively. In this work, a Tecnai Spirit G2 transmission electron microscope and a Quanta 200 FEG scanning electron microscope (both from FEI; Brno, Czech Republic) were used.

Energy dispersive X-ray spectroscopy (EDAX) determines elemental composition of the particle surface. This analysis was performed using a Quanta 200 FEG SEM microscope equipped with an energy dispersive X-ray spectrometer (Mahwah, NJ, USA).

Iron content was analyzed by atomic absorption spectroscopy (AAS PerkinElmer 3110, Wellesley, MA, USA) of an extract from a sample obtained with dilute HCl (1:1) at 80 °C for 1 h.

Nitrogen content was determined on a PerkinElmer 2400 CHN elemental analyzer (Waltham, MA, USA).

X-ray photoelectron spectroscopy (XPS) provides information about elemental composition and electronic state of the particles. XPS spectra were recorded with a K-Alpha+ spectrometer (ThermoFisher Scientific; East Grinstead, UK).

Dynamic light scattering (DLS) is one of the most important characterization techniques for measurement of particles dispersed in a liquid. It gives information about the hydrodynamic particle size and its distribution[71]. Translational diffusion coefficient depends not only on the size of the particle core, but also on surface modification, as well as on concentration and type of ions present in the medium and pH. ζ-potential (electrokinetic potential) is a measure of the effective charge on the nanoparticle surface. ζ-potential also provides information about the particle colloidal stability; higher ζ-potential increases electrostatic repulsion and colloidal stability. Particles with ζ-potential < -30 mV and > +30 mV are generally considered as stable. Hydrodynamic diameter, ζ-potential, and conductivity were determined using a Zetasizer Nano-ZS Model ZEN3600 (Malvern Instruments; Malvern, UK) equipped with a HeNe laser operating at 632.8 nm and a scattering detector at 173°.

Fourier transform infrared spectroscopy (FTIR) reveals presence of functional groups on the nanoparticle surface and efficiency of the chemical modification. FTIR was measured in an attenuated total reflection (ATR) mode using a Thermo Nicolet NEXUS 870 FTIR spectrometer (Madison, WI, USA).

Ultraviolet–visible spectroscopy (UV-vis) was recorded in two buffer solutions (pH 3 and 7) with a PerkinElmer Lambda 950 spectrometer (Waltham, MA, USA).

Vibrating sample magnetometry allows determination of the magnetic properties of a material as a function of magnetic field, temperature, and time. In this work, all measurements were done on an EV9 vibrating-sample magnetometer (DSM Magnetics; ADE Corporation; Lowell, MA, USA) with the maximum magnetic field of 2 T. The temperature dependence of magnetic susceptibility was measured using a KLY-4S/CS-3 kappabridge (AGICO; Brno, Czech Republic) from 77 K (liquid nitrogen) to *ca*. 1000 K.

Size-exclusion chromatography (SEC) separates molecules according to their molecular weight. In the thesis, M_w and M_n were determined by a Shimadzu SIL-HT Chromatograph (Tokyo, Japan) with acetate buffer eluent at pH 4.5 and flow rate 0.5 ml/min using a TSK GEL G6000PW column (7.5 mm ID, 300 mm length; Tosoh Biosciences; Stuttgart, Germany), RI and multiangle light scattering DAWN 8 detection (Wyatt Technology; Santa Barbara, CA, USA).

Specific surface area (S_{BET}) of the nanoparticles was determined by dynamic desorption of nitrogen using a Gemini VII 2390 Analyzer (Micromeritics; Norcross, GA, USA).

3. AIMS

- Synthesis of superparamagnetic γ-Fe_2O_3 nanoparticles by coprecipitation method.
- Coating of magnetic nanoparticles with biocompatible shells based on
    - poly(*N,N*-dimethylacrylamide),
    - non-porous and porous silica, optionally functionalized with amino groups,
    - polyaniline.
- Synthesis of thionin-modified poly(carboxymethyl methacrylate) particles.
- Control of particle size and thickness of the shell.
- Characterization of the particles.
- Application of the particles in biological and biomedical experiments.

4. RESULTS AND DISCUSSIONS

4.1. Magnetic nanoparticles

In this work, magnetic iron oxide particles were selected, as they are well tolerated by a living organism, in contrast to, e.g., ferrites containing toxic Ni, Co, Mn, and other ions. Among the iron oxides, maghemite (γ-Fe_2O_3) was preferred for biological experiments since it is chemically more stable in air and water than magnetite (Fe_3O_4). In the synthesis of the nanoparticles, Fe_3O_4 nanoparticles were first obtained by conventional coprecipitation of Fe(II) and Fe(III) salts with ammonia[40]. It was followed by controlled oxidation of Fe_3O_4 with NaOCl to obtain γ-Fe_2O_3 nanoparticles (Figure 6; Eq. 10 and 11).

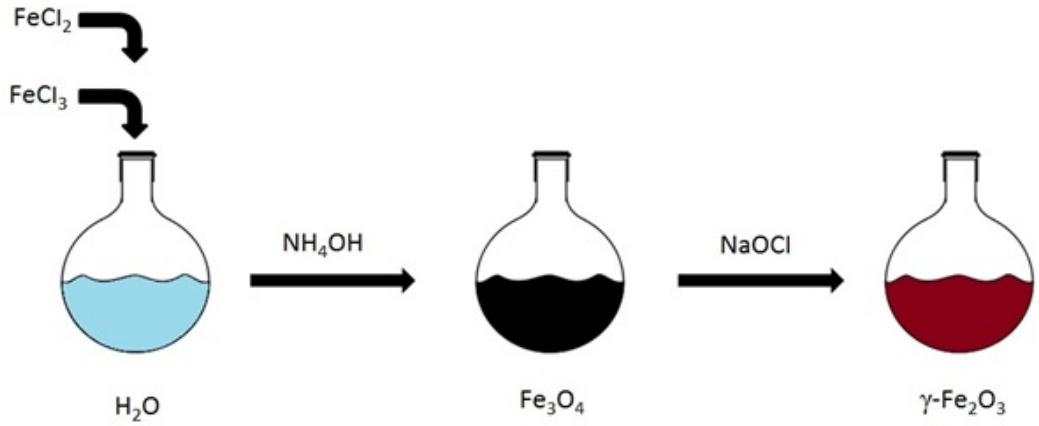

Figure 6. Scheme of γ-Fe_2O_3 synthesis.

$$FeCl_2 + 2\,FeCl_3 + 8\,NH_4OH \longrightarrow Fe_3O_4 + 8\,NH_4Cl + 4\,H_2O \quad (10)$$

$$2\,Fe_3O_4 + NaOCl \longrightarrow 3\,\gamma\text{–}Fe_2O_3 + NaCl \quad (11)$$

According to TEM micrographs, γ-Fe_2O_3 particles were almost spherical and their D_n ranged 9-11 nm (Figure 7); width of the particle size distribution was moderate (PDI ~ 1.2).

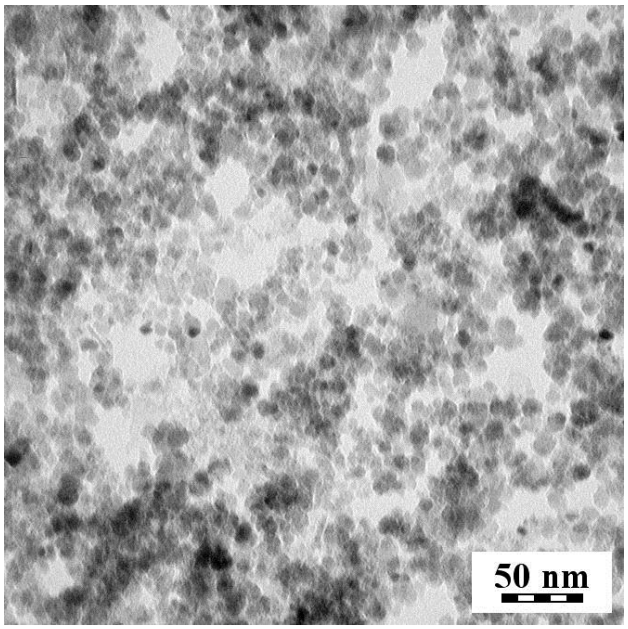

Figure 7. TEM micrograph of maghemite nanoparticles.

Hydrodynamic particle size (D_h) in water according to DLS ranged 108-192 nm depending on pH and ionic strength. D_h was always larger than D_n, which can be ascribed to the fact that while TEM determines number-average diameter of dry particles, DLS measures them in water, where solvent hydration layer contributes to the increased size. Moreover, DLS is an intensity-based measurement (proportional to sixth power of the size), which is sensitive to large particles. Another important point, which should be considered, is that the particles can interact in water. Many studies suggest that D_h is one of the most important parameter for understanding the nanoparticle performance in biological assays.

Structure of the particles was verified using FTIR, XPS, and EDAX spectroscopy, elemental analysis, and magnetic measurements. Amount of Fe in the uncoated maghemite particles, ~ 66 and ~ 61 wt.%, was determined according to AAS and VSM, respectively, was in agreement with literature[23]. After applying the external magnetic field, the particles were attracted to a magnet facilitating thus their purification in water. VSM measurements proved that the particles were superparamagnetic.

Details about synthesis and characterization of the γ-Fe_2O_3 nanoparticles are described in the attached publications No. 1-4. In the following sections, core-shell nanoparticles containing two or more separate phases with different chemical composition and structure are described; core is magnetic and shell is a polymer. The coating has to be biocompatible to avoid unwanted biological responses and nonspecific protein adsorption.

4.2. Poly(*N*,*N*-dimethylacrylamide)-coated γ-Fe_2O_3

γ-Fe_2O_3&PDMAAm core-shell nanoparticles were obtained in a two-steps reaction. In the first step, initiator was attached to the iron oxide surface. Three various initiators, such as 2,2'-azobis(2-methylpropanimidamide) dihydrochloride (AMPA), 2,2'-azobis(*N*-hydroxy-2-methylpropanimidamide) dihydrochloride (ABHA), and 4-cyano-4-{[1-cyano-3-(*N*-hydroxycarbamoyl)-1-methylpropyl]azo}pentanoic acid (CCHPA), were selected and effect of the initiator/γ-Fe_2O_3 ratio on the particle size and polydispersity of the γ-Fe_2O_3 nanoparticles was determined. With the increasing initiator/γ-Fe_2O_3 ratio, the particles were larger; D_h > 1 μm then indicated aggregation of the particles at the AMPA and CCHPA initiator/γ-Fe_2O_3 ratio = 0.12 and 0.32 w/w, respectively. If ABHA/γ-Fe_2O_3 ratio was < 0.64 w/w, the subsequent polymerization of DMAAm produced colloidally stable γ-Fe_2O_3&PDMAAm nanoparticles (Figure 8 a). In the dependence of ζ-potential of initiator-modified γ-Fe_2O_3 nanoparticles on the initiator/γ-Fe_2O_3 ratio, the ζ-potential of AMPA- and CCHPA-γ-Fe_2O_3 increased from -45 to -13 mV with the ratio increasing up to 0.3 w/w, approaching then a plateau (Figure 8 b). In contrast, ζ-potential of ABHA-γ-Fe_2O_3 was positive amounting to 40 mV irrespectively of the ABHA/γ-Fe_2O_3 ratio.

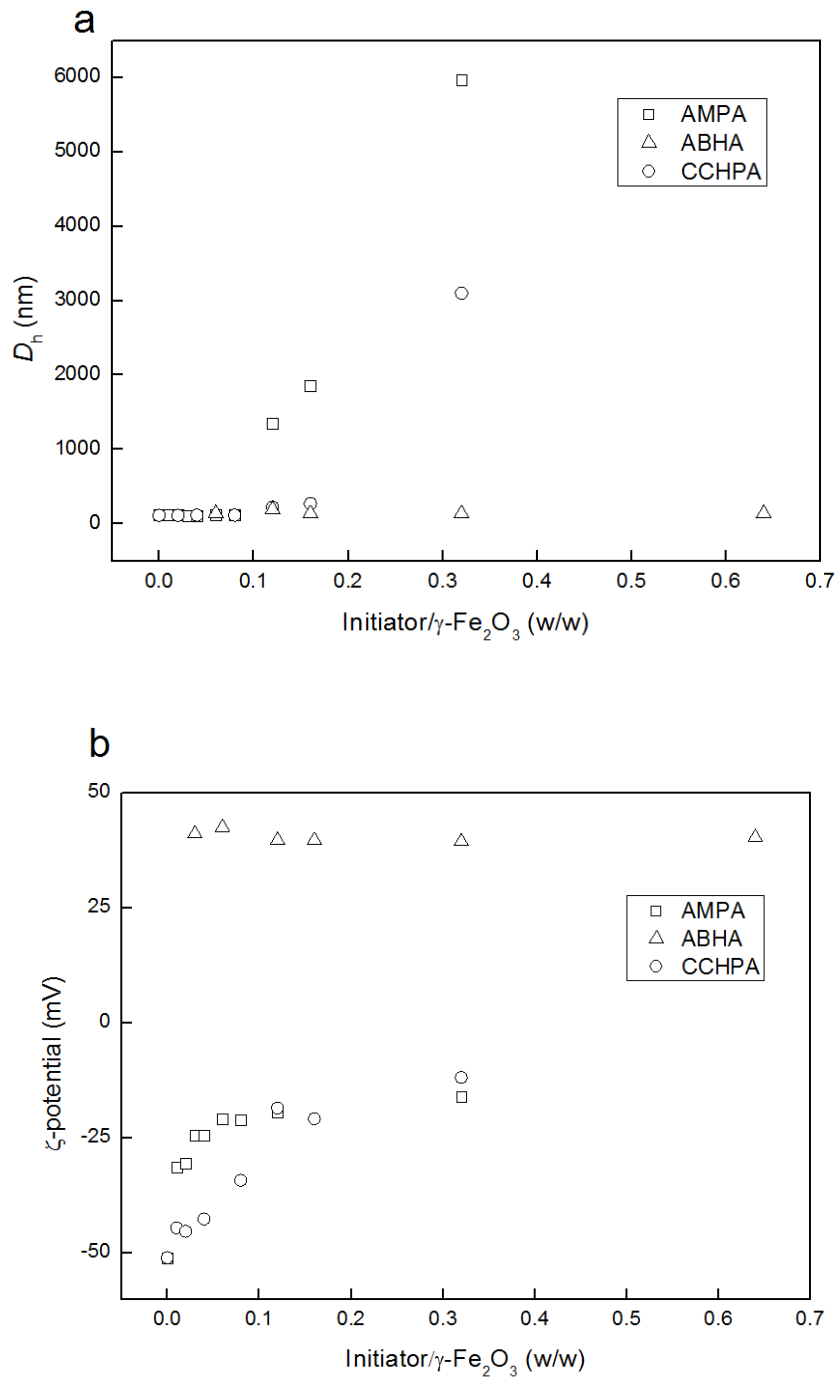

Figure 8. Dependence of (a) hydrodynamic diameter D_h and (b) ζ-potential of initiator-modified γ-Fe_2O_3 nanoparticles on the initiator/γ-Fe_2O_3 ratio.

In the second step, initiator-modified γ-Fe_2O_3 nanoparticles were "grafted from" by free-radical polymerization of DMAAm, as exemplified on Figure 9 a for ABHA-γ-Fe_2O_3. TEM micrograph is on Figure 9 b.

a

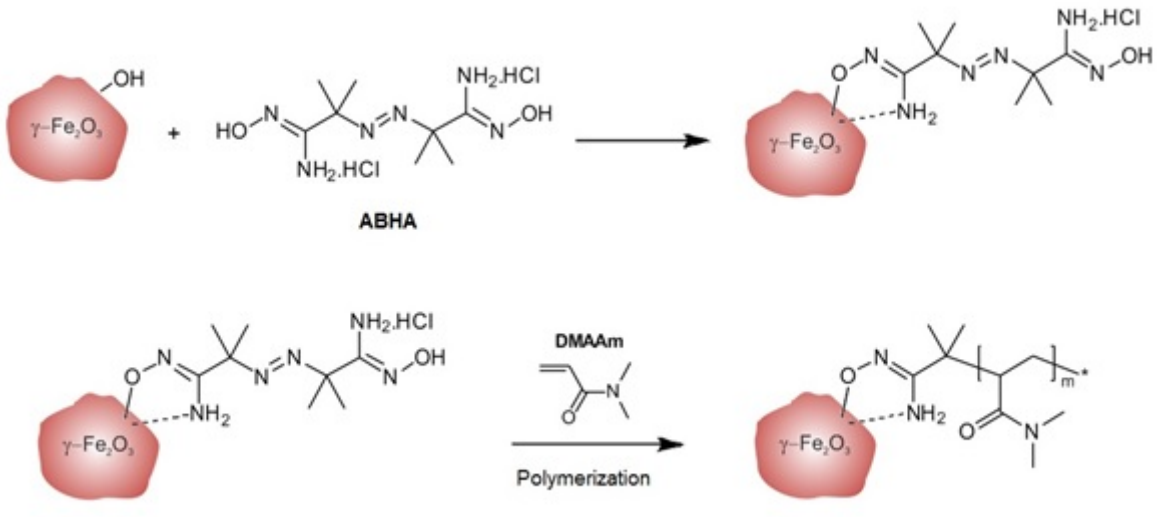

b

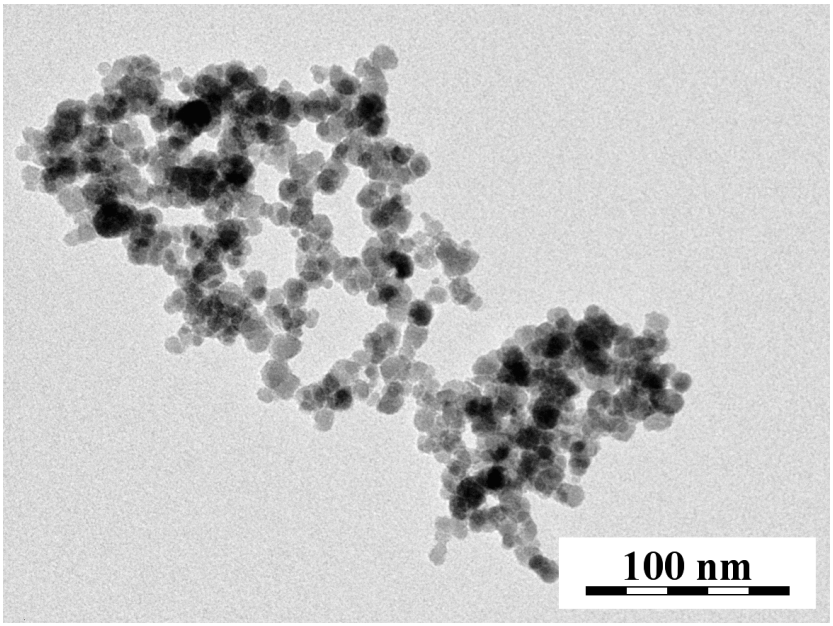

Figure 9. Scheme of (a) preparation and (b) TEM micrograph of γ-Fe_2O_3&PDMAAm nanoparticles obtained by "grafting-from" method. ABHA - 2,2'-azobis(*N*-hydroxy-2-methylpropanimidamide) dihydrochloride. DMAAm - *N,N*-dimethylacrylamide.

Using different initiators, γ-Fe_2O_3&PDMAAm particle size (D_n) could be controlled from 9 to 16 nm. Typically, D_n of PDMAAm-coated AMPA-γ-Fe_2O_3, ABHA-γ-Fe_2O_3, and CCHPA-γ-Fe_2O_3 nanoparticles was 12, 16, and 13 nm, respectively, with PDI = 1.18, 1.24, and 1.46, respectively. This means that polydispersities of PDMAAm-coated ABHA- and

AMPA-γ-Fe_2O_3 were narrower than that of CCHPA-γ-Fe_2O_3 nanoparticles. Hydrodynamic size of all γ-Fe_2O_3&PDMAAm particle clusters D_h was large, ~ 206 nm, compared to that obtained from TEM micrographs. The PI values approached 0.2 reflecting polydisperse nature of the product. γ-Fe_2O_3&PDMAAm particles were colloidally stable for several months.

Also second type of grafting, "grafting to" method, was investigated, but the interaction between PDMAAm and metal oxide particles was too weak to make the particles applicable in the next experiments.

Grafting of PDMAAm shell on the particles was thoroughly described in publication No. 1.

4.3. Silica-coated γ-Fe_2O_3

Silica used as an inorganic inert coating of the γ-Fe_2O_3 nanoparticles proved to be also a suitable modification agent preventing aggregation of the particles and enhancing their chemical stability. Silica is also easily susceptible to additional chemical modifications, which makes synthesis of the particles for combined diagnosis and therapy possible. Silica shell on the γ-Fe_2O_3 particles was obtained according to Stöber method using hydrolysis and condensation of TMOS under base catalysis[55]. Amino-functionalized particles were then prepared by modification of γ-Fe_2O_3&SiO_2 nanoparticles with APTES (Figure 10).

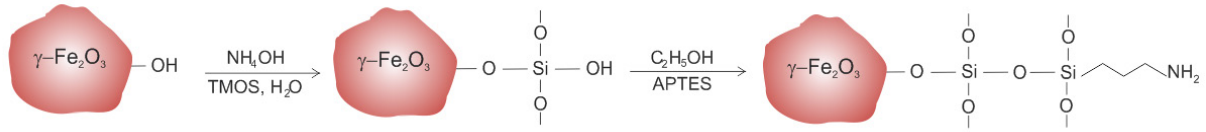

Figure 10. Silanization of γ-Fe_2O_3 nanoparticles with tetramethyl orthosilicate (TMOS) and subsequent modification with (3-aminopropyl)triethoxysilane (APTES).

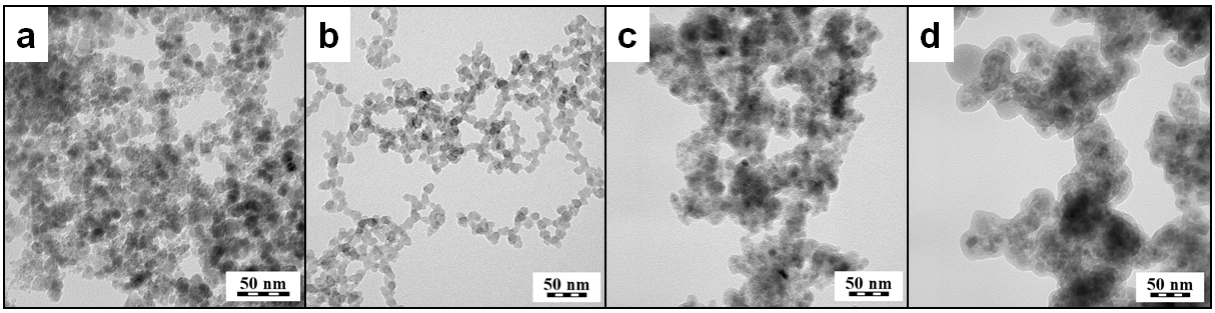

Figure 11. TEM micrographs of γ-Fe_2O_3&SiO_2 particles obtained at γ-Fe_2O_3/TMOS = (a) 0.8, (b) 0.4, (c) 0.2, and (d) 0.1 w/w.

During the synthesis, γ-Fe_2O_3/TMOS ratio was changed in the range 0.1-0.8 w/w to control morphology and size of the γ-Fe_2O_3&SiO_2 nanoparticles (Figure 11). As expected, a "hallo" was observed on TEM micrograph at a high γ-Fe_2O_3/TMOS ratio (0.8 w/w) suggesting the presence of a silica shell. At γ-Fe_2O_3/TMOS = 0.4 w/w, the particles were 12 nm in size with 2.2 nm thick shell and a quite narrow size distribution (PDI = 1.07). With increasing amounts of TMOS relative to iron oxide (γ-Fe_2O_3/TMOS = 0.2 w/w) number-average diameter again increased (D_n = 19 nm). Hydrodynamic diameter D_h was again much larger than D_n, increasing from ~ 100 nm for neat γ-Fe_2O_3 nanoparticles to ~ 300 nm for γ-Fe_2O_3&SiO_2 particles. Polydispersity PI of the nanoparticles prepared at low γ-Fe_2O_3/TMOS ratios indicated their broad particle size distribution. After the last modification with APTES, amino groups were introduced on the particles, which can be employed for prospective attachment of a target biomolecule. Synthesis, magnetic properties, and characterization of the γ-Fe_2O_3&SiO_2 and γ-Fe_2O_3&SiO_2-NH_2 particles was fully described in publication No. 2.

To obtain porous silica shell, cationic surfactant, cetyltrimethylammonium bromide (CTAB), was added in the second reaction step during the modification with APTES. Also in this synthesis, several reaction parameters were changed to prepare a thick shell around the nanoparticles. S_{BET} increased from ~ 66 (neat γ-Fe_2O_3) to 206 m^2/g for γ-Fe_2O_3&SiO_2-NH_2 particles documenting thus porous character of the silica shell. Complete preparation and characterization of the porous γ-Fe_2O_3&SiO_2-NH_2 particles was presented in publication No. 3.

4.4. Polyaniline-coated magnetic nanoparticles

Another class of multifunctional materials consisting of a superparamagnetic core and a conductive shell is exemplified by γ-Fe_2O_3&PANI particles. Combination of these unique material properties can make the particle susceptible to both magnetic imaging and targeting, e.g., to tumor tissues, and at the same time it enables stimulation of cell growth and/or differentiation. Presence of PANI shell on the γ-Fe_2O_3 nanoparticles also increases absorption of NIR light boosting thus possible hyperthermic effect, if the particles are applied in cancer treatment.

Conductive PANI shell was introduced on the γ-Fe_2O_3 surface by oxidation of aniline hydrochloride with ammonium persulfate at 0 and 25 °C in the presence of PVP stabilizer

(Figure 12). PANI shell, thickness of which was regulated by the reaction temperature, was physically adsorbed on the iron oxide surface[72].

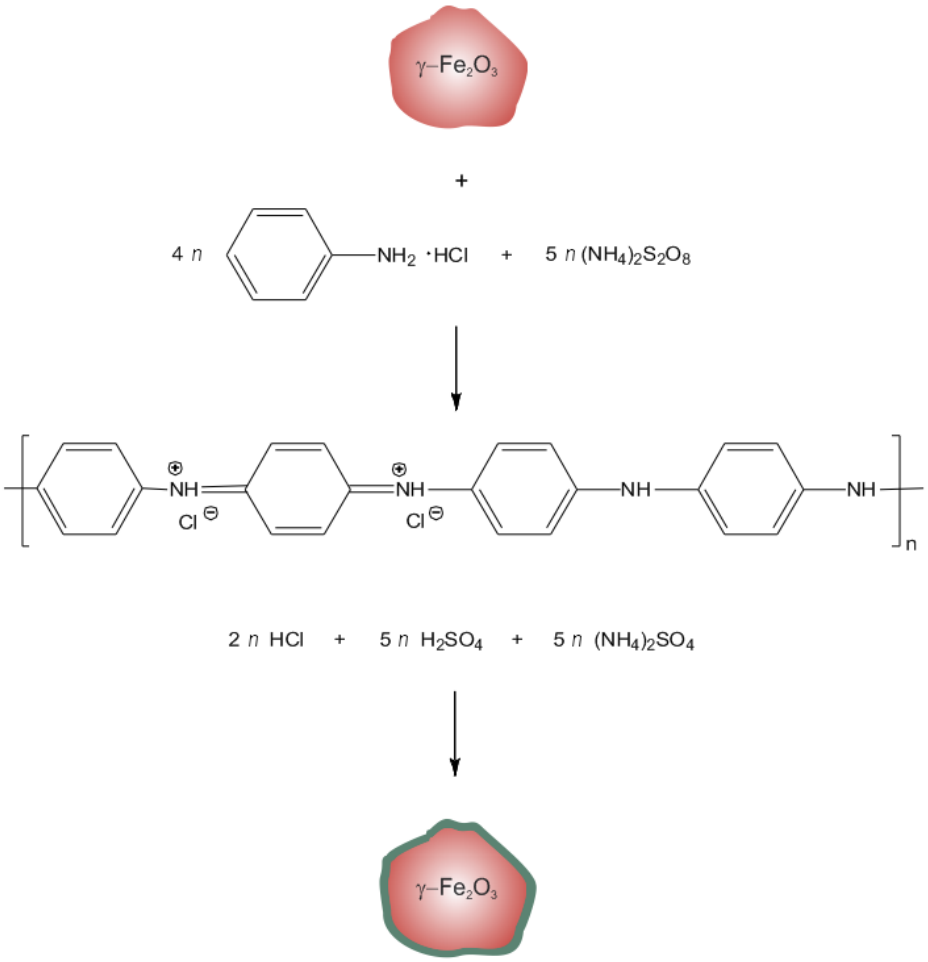

Figure 12. Oxidation of aniline hydrochloride by ammonium persulfate in the presence of poly(*N*-vinylpyrrolidone)-stabilized γ-Fe_2O_3 dispersion.

Changes in the γ-Fe_2O_3&PANI particle synthesis caused differences in the particles properties, such as morphology, size, size distribution, etc. For example, D_n of γ-Fe_2O_3&PANI core-shell particles prepared at 0 °C was by 9 nm larger than that of the particles synthesized at 25 °C (Figure 13) due to an increase of molecular weight of PANI with decreasing temperature[73]. D_n, as well as D_h, increased after PANI modification from 11 to 25 nm and from 192 to 257 nm, respectively.

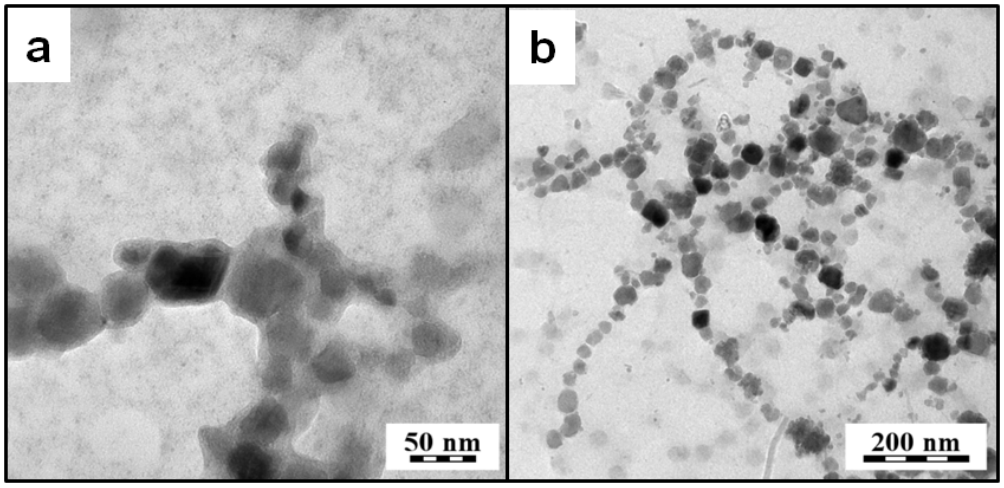

Figure 13. TEM micrographs and of γ-Fe_2O_3&PANI particles prepared at (a) 0 and (b) 25 °C.

Saturation magnetization of uncoated γ-Fe_2O_3 particles was ~ 50 A·m^2/kg suggesting that the concentration of maghemite was 61 wt.% (assuming M_s of bulk maghemite was ~ 80 A·m^2/kg)[23]. After coating, saturation magnetization of the γ-Fe_2O_3&PANI nanoparticles decreased to ~ 14 A·m^2/kg suggesting presence of 28 wt.% γ-Fe_2O_3 in the composite nanoparticles. Full characterization of the particles was described in publication No. 4.

4.5. Thionin-modified poly(carboxymethyl methacrylate) nanospheres

Recently, biosensors represent one of the most important analytical devices. Their development is greatly influenced by the design of new nanomaterials to improve the performance.

Purpose of this research was to synthesize particles, namely, monodisperse poly(glycidyl methacrylate) nanospheres (PGMA; Figure 14),

a

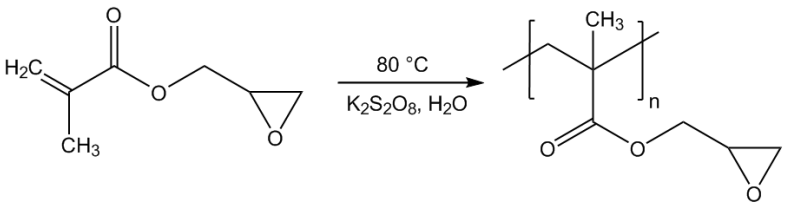

b

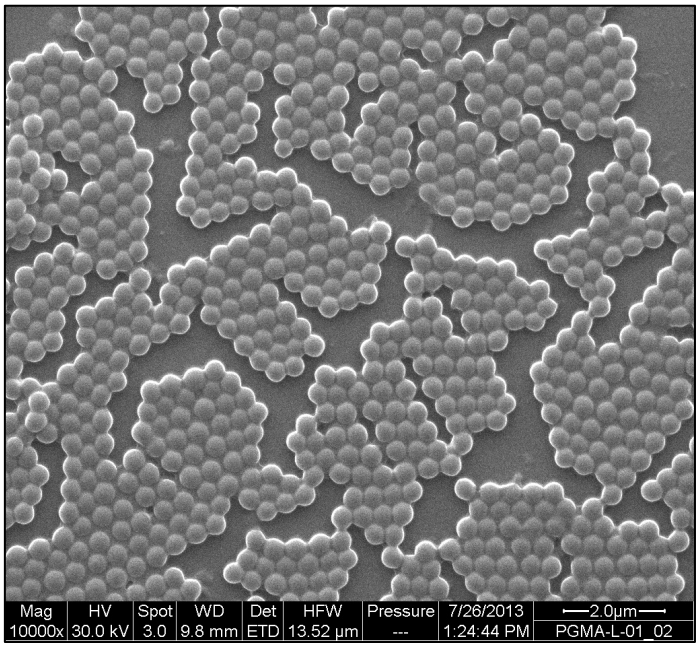

Figure 14. (a) Polymerization of glycidyl methacrylate and (b) SEM micrograph of PGMA nanospheres.

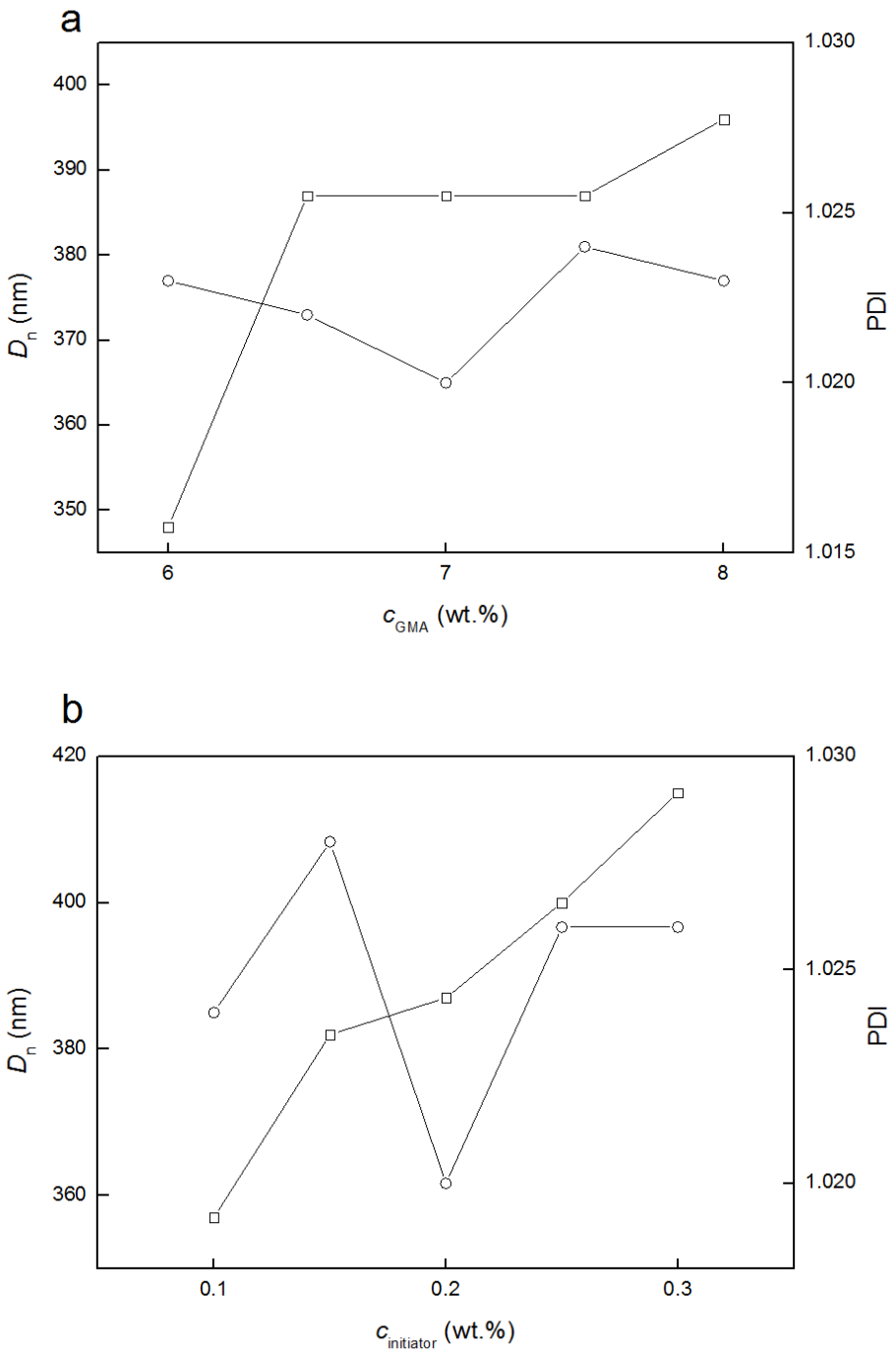

Figure 15. Dependence of (□) number-average diameter D_n and (○) polydispersity index PDI of PGMA nanospheres on concentration of (a) GMA (0.2 wt.% $K_2S_2O_8$); and (b) $K_2S_2O_8$ in water (7 wt.% GMA).

The particles were spherical with D_n ranging 350-400 nm depending on the GMA concentration in water (Figure 15 a). The PGMA nanosphere diameter was slightly larger with increasing monomer concentration, which can be ascribed to the fact that the monomer is

a good solvent for the polymer increasing thus the oligomer critical chain length before the precipitation. The dependence of the PGMA nanosphere diameter on the concentration of the initiator in water showed that the particle size increased from 360 to 420 nm with increasing initiator concentration due to higher radical-to-monomer molar ratio (Figure 15 b). Typically, the particles had a very narrow size distribution.

To introduce carboxyl groups, the PGMA nanospheres were hydrolyzed with H_2SO_4 and oxidized with $KMnO_4$ yielding poly(carboxymethyl methacrylate) (PCMMA). Finally, thionin (Th) as an electron mediator was covalently attached to the particles using carbodiimide chemistry (Figure 16). Complete results pertaining PCMMA&Th nanospheres were described in publication No. 5.

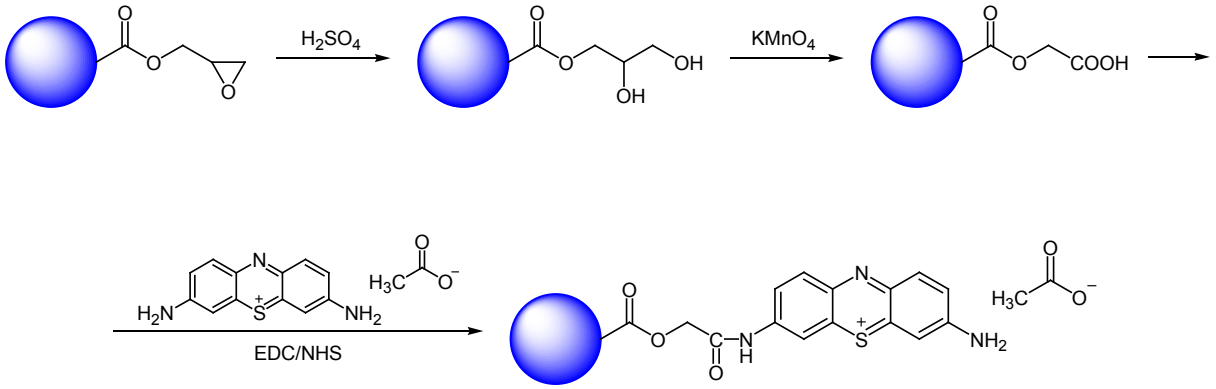

Figure 16. Preparation of PCMMA&Th nanospheres by hydrolysis of PGMA, oxidation with H_2SO_4, and reaction with thionin acetate. EDC - *N*-(3-dimethylaminopropyl)-*N*'-ethylcarbodi-imide, NHS - *N*-hydroxysulfosuccinimide.

4.6. Biological experiments

There is urgent need of reliable toxicity test systems capable of identifying the potential risks of the nanoparticles prior to their application in biomedicine. Superparamagnetic inorganic/polymer particles developed during this thesis were investigated in terms of their toxicity. The uptake of the surface-coated iron oxide nanoparticles by phagocytic monocytes and macrophages provided a valuable *in vivo* tool, by which magnetic resonance imaging can monitor cell introduction and movement, and short- and long-term fate of the cells in the organism. Biological experiments demonstrated that γ-Fe_2O_3&PDMAAm, γ-Fe_2O_3&SiO_2, and γ-Fe_2O_3&SiO_2-NH_2 core-shell nanoparticles were recognized and

engulfed by the macrophages (Figure 17; publications No. 1 and 2). γ-Fe_2O_3&PDMAAm and γ-Fe_2O_3&SiO_2 nanoparticles, in contrast to neat γ-Fe_2O_3, were proved to be non-cytotoxic.

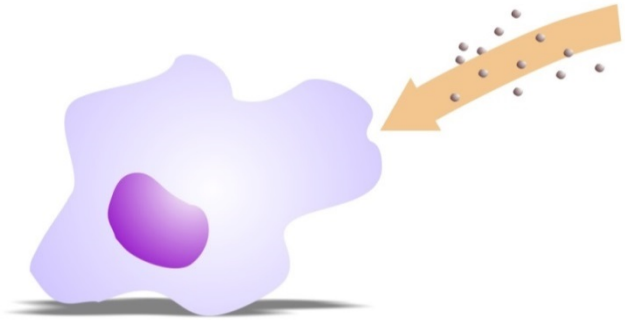

Figure 17. Schematic illustration of γ-Fe_2O_3&PDMAAm and γ-Fe_2O_3&SiO_2 nanoparticle uptake by a macrophage.

No cell irritation was observed during the phagocytosis of the γ-Fe_2O_3&PDMAAm nanoparticles. In contrast, time-dependent vacuolization in cytoplasm of macrophages treated with neat γ-Fe_2O_3 nanoparticles suggested their cytotoxicity. Details pertaining internalization of the particles by macrophages can be found in publication No. 1.

Because more biological assessments are needed before possible use of the surface-modified superparamagnetic γ-Fe_2O_3 nanoparticles in human medicine, cytotoxicity and effect of porous γ-Fe_2O_3&SiO_2-NH_2 nanoparticles was determined also on immune response. Lymphocyte proliferative and phagocytic activity, leukocyte respiratory burst, and *in vitro* production of cytokine granulocyte macrophage colony stimulating factor (GM-CSF) were examined in the presence of the particles. The nanoparticles proved to be non-toxic even at a high doses (75 μg/cm^2) and after a long-time incubation (72 h). Significantly increased production of GM-CSF cytokine by human blood cells treated with this high dose of the particles was observed in cell cultures stimulated with PHA mitogen. However, no significant differences in proliferative response of T-lymphocytes, as well as T-dependent B-cells, treated with γ-Fe_2O_3&SiO_2-NH_2 particles in all concentrations and time exposures were found compared to the control untreated cells. The particles did not interfere with the phagocytic activity of monocytes and granulocytes and did not affect respiratory burst of phagocytes. Our findings thus demonstrated that an interaction between human immune cells and high doses of nanoparticles needs to be taken into account when considering their use in human medicine. Detailed description of biological results of γ-Fe_2O_3&SiO_2-NH_2 particles was given in publication No. 3.

Cell viability of γ-Fe_2O_3&PANI nanoparticles was investigated on SH-SY5Y cell line using a novel real-time cytotoxicity test - xCELLigence system (Figure 18). The system combines real-time impedance-based monitoring of cell behavior with visual inspection (dynamic monitoring) enabling observation of cellular changes, e.g., morphology and proliferative state. Inhibition of the cell growth increased at high γ-Fe_2O_3&PANI particle concentrations, but morphology of the cells exposed to both uncoated γ-Fe_2O_3 and γ-Fe_2O_3&PANI nanoparticles at a concentration 100 µg/ml did not change and no cell damage was observed in comparison with the control cells.

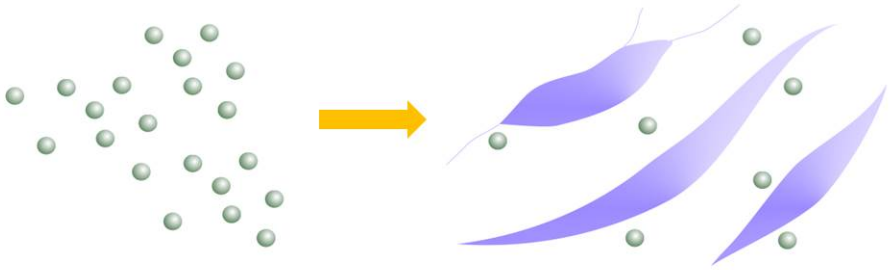

Figure 18. Schematic illustration of γ-Fe_2O_3&PANI nanoparticle interaction with SH-SY5Y neuroblastoma cells.

This indicated that also the γ-Fe_2O_3&PANI particles can be considered as safe for biomedical applications. Details were included in publication No. 4.

Final biological experiment involved application of PCMMA&Th nanospheres in an immunosensor, where horseradish peroxidase (HRP) was used as an enzyme to generate electrochemical signal (Figure 19). Bioconjugation of HRP on both PCMMA and PCMMA&Th nanoparticles was achieved via EDC/sulfo-NHS chemistry.

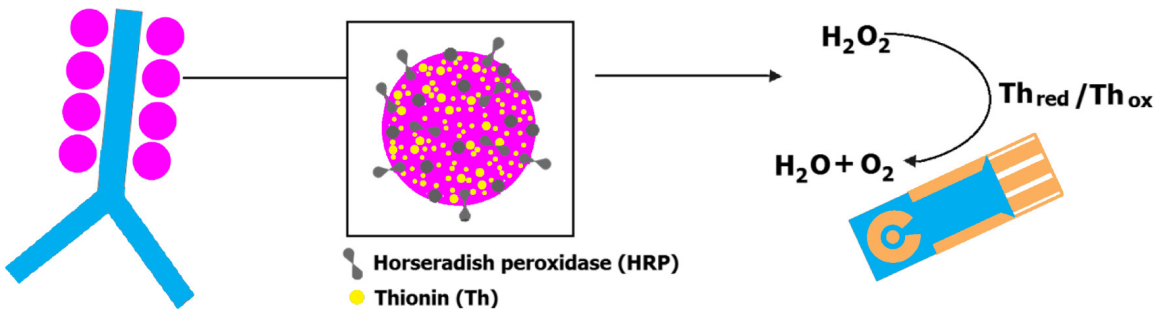

Figure 19. Schematic illustration of application of PCMMA&Th-HRP nanospheres for electrochemical detection.

The PCMMA&Th-HRP nanospheres improved the electrochemical signal and the sensitivity of the biosensor. The nanospheres thus represent a highly sensitive and universal tool for labeling of antibodies in enzyme-based sandwich-type immunosensors, which are promising for immunochemical analyses not only in biology, but also in personalized medical care devices.

High potential of all types of developed nanoparticles (γ-Fe_2O_3&PDMAAm, porous and non-porous γ-Fe_2O_3&SiO_2 and γ-Fe_2O_3&SiO_2-NH_2, γ-Fe_2O_3&PANI, and PCMMA&Th-HRP) can be envisioned in many biological applications. The superparamagnetic particles can be easily magnetically separated and redispersed in water solutions upon removing of the external magnetic field. Magnetically labeled cells can be steered and concentrated inside the body by a magnet. The iron oxide particles, modified with organic, as well as inorganic polymer coatings, seem to be very promising not only for cell imaging and tracking, but also for drug and gene delivery systems, and capture of various cells and biomolecules required for diagnostics of cancer, infectious diseases, and neurodegenerative disorders.

5. CONCLUSIONS

In this work, γ-Fe_2O_3 particles were successfully prepared and their surface was modified with (i) PDMAAm by the radical polymerization using "grafting from" method, (ii) silica obtained by hydrolysis and condensation of Si precursors, and (iii) polyaniline prepared by oxidation of aniline HCl with ammonium persulfate.

Last but not least, thionin-modified monodisperse poly(glycidyl methacrylate) particles, ~ 390 nm in diameter, were developed by emulsifier-free emulsion polymerization.

All surface modifications of the particles were confirmed by a range of physico-chemical methods. The particles proved to be chemically and colloidally stable even after several months of storage.

In biological experiments, all synthesized magnetic particles were incubated with both animal and human cells including macrophages, peripheral blood and neuroblastoma cells, and particle (immuno)toxicity and engulfment were evaluated.

As the developed surface-modified γ-Fe_2O_3 particles proved to be non-toxic and readily internalized in the living cells, they are promising tool for diagnostics, as well as for delivery of various biomolecules, such as specific proteins.

Finally, monodisperse PCMMA&Th-HRP nanospheres were found to amplify the electrochemical signal in the biosensor improving thus its sensitivity.

6. REFERENCES

1. Nouailhat A., An Introduction to Nanoscience and Nanotechnology, ISTE, London 2008, UK.

2. Whitesides G.M., The 'right' size in nanobiotechnology, *Nat. Biotechnol*. 21, 1161-1165, (2003).

3. Strijkers G.J., van Tilborg G.A., Geelen T., Reutelingsperger C.P., Nicolay K., Current applications of nanotechnology for magnetic resonance imaging of apoptosis, *Methods Mol. Biol.* 624, 325-342 (2010).

4. Jianronga C., Yuqing M., Nongyue H., Xiaohua W., Sijiao L., Nanotechnology and biosensors, *Biotechnol. Adv*. 22, 505-518 (2004).

5. Vashist S.K., Venkatesh A.G., Mitsakakis K., Nanotechnology-based biosensors and diagnostics: Technology push versus industrial/healthcare requirements, *BioNanoSci*. 2, 115-126 (2012).

6. Jarockyte G., Daugelaite E., Stasys M., Statkute U., Poderys V., Tseng T.C., Hsu S.H., Karabanovas V., Rotomskis R., Accumulation and toxicity of superparamagnetic iron oxide nanoparticles in cells and experimental animals, *Int. J. Mol. Sci.* 17, 1193 (2016).

7. Bagheri S., Julkapli N.M., Modified iron oxide nanomaterials: Functionalization and application, *J.Magn. Magn. Mater.* 416,117-133 (2016).

8. Jeng H.A., Swanson J., Toxicity of metal oxide nanoparticles in mammalian cells, *J. Environ. Sci. Health, Part A: Toxic Hazard Subst. Environ. Eng.* 4, 12699-12711 (2006).

9. Gupta A.K., Gupta M., Synthesis and surface engineering of iron oxide nanoparticles for biomedical applications, *Biomaterials* 26, 3995-4021 (2005).

10. Arbab A.S., Bashaw L.A., Miller B.R., Jordan E.K., Lewis B.K., Kalish H., Frank J.A., Characterization of biophysical and metabolic properties of cells labeled with superparamagnetic iron oxide nanoparticles and transfection agent for cellular MR imaging, *Radiology* 229, 838-846 (2003).

11. Schleich N., Sibret P., Danhier P., Ucakar B., Laurent S., Muller R.N., Jérôme C., Gallez B., Préat V., Danhier F., Dual anticancer drug/superparamagnetic iron oxide-loaded PLGA-based nanoparticles for cancer therapy and magnetic resonance imaging, *Int. J. Pharm*. 15, 94-101 (2013).

12. Alexiou C., Schmid R.J., Jurgons R., Kremer M., Wanner G., Bergemann C., Huenges E., Nawroth T., Arnold W., Parak F.G., Targeting cancer cells: Magnetic nanoparticles as drug carriers, *Eur. Biophys. J*. 35, 446-450 (2006).

13. Bauer L.M., Situ S.F., Griswold M.A., Samia A.C.S., High-performance iron oxide nanoparticles for magnetic particle imaging - guided hyperthermia (hMPI), *Nanoscale* 8, 12162-12169 (2016).

14. Li L., Jiang W., Luo K., Song H., Lan F., Wu Y., Gu Z., Superparamagnetic iron oxide nanoparticles as MRI contrast agents for non-invasive stem cell labeling and tracking, *Theranostics* 3, 595-615 (2013).

15. Stacey F.D., Banerjee S.K., The Physical Principles of Rock Magnetism. Developments in Solid Earth Geophysics. Elsevier, New York 1974, USA.

16. Coey J.M.D., Magnetism and Magnetic Materials, Cambridge University Press, Cambridge 2010, UK.

17. Evans M.E., Heller F., Environmental Magnetism: Principles and Applications of Enviromagnetics, Academic Press, San Diego 2003, USA.

18. Rawlings R.D., Materials Science and Engineering II, EOLSS Publishers, Oxford 2009, UK.

19. Ling D., Hyeon T., Chemical design of biocompatible iron oxide nanoparticles for medical applications, *Small* 9, 1450-1466 (2013).

20. Papell S.S., Low viscosity magnetic fluid obtained by the colloidal suspension of magnetic particles, US Pat. 3,215,572 (1965).

21. Cornell R.M., Schwertmann U., The Iron Oxides: Structure, Properties, Reactions, Occurrences and Uses, 2nd Ed., Wiley, Darmstadt 2000, Germany.

22. Laurent S., Forge D., Port M., Roch A., Robic C., van der Elst L., Muller R.N., Magnetic iron oxide nanoparticles: Synthesis, stabilization, vectorization, physicochemical characterizations, and biological applications, *Chem. Rev.*108, 2064-2110 (2008).

23. Patsula V., Kosinová L., Lovrić M., Ferhatovic-Hamzić L., Rabyk M., Konefal R., Paruzel A., Šlouf M., Herynek V., Gajović S., Horák D., Superparamagnetic Fe_3O_4 nanoparticles: Synthesis by thermal decomposition of iron(III) glucuronate and application in magnetic resonance imaging, *ACS Appl. Mater. Interfaces* 23, 7238-7247 (2016).

24. Strobel R., Pratsinis S., Direct synthesis of maghemite, magnetite and wustite nano-particles by flame spray pyrolysis, *Adv. Powder Technol*. 20, 190-194 (2009).

25. Okoli C., Boutonnet M., Mariey L., Jaras S., Rajarao G, Application of magnetic iron oxide nanoparticles prepared from microemulsions for protein purification, *J. Chem. Technol. Biotechnol.* 86, 1386-1393 (2011).

26. Viswanathiah M., Tareen K., Krishnamurthy V., Low temperature hydrothermal synthesis of magnetite, *J. Cryst. Growth* 49, 189-192 (1980).

27. Sugimoto T., Sakata K., Preparation of monodisperse pseudocubic α-Fe_2O_3 particles from condensed ferric hydroxide gel, *J. Colloid Interface Sci.* 152, 587-590 (1992).
28. Arakaki A., Nakazawa H., Nemoto M., Mori T., Matsunaga T., Formation of magnetite by bacteria and its application, *J. R. Soc. Interface* 6, 977-999 (2008).
29. Majidi S., Sehrig F.Z., Farkhani S.M., Goloujeh M.S., Akbarzadeh A., Current methods for synthesis of magnetic nanoparticles, *Artif. Cells Nanomed. Biotechnol*. 44, 722-734 (2016).
30. Horák D., Babic M., Macková H., Benes M.J., Preparation and properties of magnetic nano- and microsized particles for biological and environmental separations, *J. Sep. Sci.* 30, 1751-1772 (2007).
31. Serna C.J., Morales M.P., Maghemite (γ-Fe_2O_3): A versatile magnetic colloidal material, in Surface and Colloid Science Vol. 17, Matijevic E., Borkovec M., eds., Springer Science & Business Media, New York 2011, USA, pp. 27-81.
32. Baalousha M., Manciulea A., Cumberland S., Kendall K., Lead J.R., Aggregation and surface properties of iron oxide nanoparticles: Influence of pH and natural organic matter, *Environ. Toxicol. Chem*. 27, 1875-1882 (2008).
33. Ghosh Chaudhuri R., Paria S., Core/shell nanoparticles: Classes, properties, synthesis mechanisms, characterization, and applications, *Chem. Rev*. 11, 2373-2433 (2012).
34. Barrera C., Herrera A.P., Rinaldi C., Colloidal dispersions of monodisperse magnetite nanoparticles modified with poly(ethylene glycol), *J. Colloid Interface Sci*. 329, 107-113 (2009).
35. Chastellain M., Petri A., Hofmann H., Particle size investigations of a multistep synthesis of PVA coated superparamagnetic nanoparticles, *J. Colloid Interface Sci*. 278, 353-260 (2004).
36. Babič M., Horák D., Jendelová P., Glogarová K., Herynek V., Trchová M., Likavčanová K., Hájek M., Syková E., Poly(*N,N*-dimethylacrylamide)-coated maghemite nanoparticles for stem cell labeling, *Bioconjugate Chem*. 20, 283-294 (2009).
37. Lu Y., Yin Y., Mayers B.T., Xia Y., Modifying the surface properties of super-paramagnetic iron oxide nanoparticles through a sol-gel approach, *Nano Lett*. 2, 183-186 (2002).
38. Horák D., Babič M., Macková H., Beneš M.J., Preparation and properties of magnetic nano- and microsized particles for biological and environmental separations, *J. Sep. Sci.* 30, 1751-1772 (2007).

39. Yang J., Kopeček J., Macromolecular therapeutics**,** *J. Controlled Release* 28, 288-303 (2014).

40. Babič M., Horák D., Poly(*N,N*-dimethylacrylamide)-based microspheres prepared by heterogeneous polymerizations, *Macromol. React. Eng.* 1, 86-94 (2007).

41. Shibanuma T., Aoki T., Sanui K., Ogata N., Kikuchi A., Sakurai Y., Okano T. Thermo-sensitive phase-separation behavior of poly(acrylic acid)-*graft*-poly(*N,N*-dimethylacrylamide) aqueous solution, *Macromolecules* 33, 444-450 (1999).

42. Liu S.Q., Tong Y.W., Yang Y.Y., Thermally sensitive micelles self-assembled from poly(*N*-isopropylacrylamide-*co*-*N,N*-dimethylacrylamide)-*b*-poly(D,L-lactide-*co*-glycolide) for controlled delivery of paclitaxel, *Mol. BioSyst.* 43, 4771-4781 (2005).

43. Yan L., Wei T.J., Graft copolymerization of *N,N*-dimethylacrylamide to cellulose in homogeneous media using atom transfer radical polymerization for hemocompatibility, *Biomed. Sci. Eng*. 10, 37-43 (2008).

44. Macková H., Horák D., Donchenko G.V., Andriyaka V.I. Palyvoda O.M.; Chernishov V.I., Chekhun V.F., Todor I.N., Kuzmenko O.I., Colloidally stable surface-modified iron oxide nanoparticles: Preparation, characterization and anti-tumor activity, *J. Magn. Magn. Mater.* 380, 125-131 (2015).

45. Nakhmanovich B.I., Prudskova T.N., Arest-Yakubovich A.A., Müller A.H.E., Copolymerization of *N,N*-dimethylacrylamide with styrene and butadiene: The first example of polar growing chain end/nonpolar monomer cross-initiation, *Macromol. Rapid Commun*. 22, 1243-1248 (2001).

46. He X., Oishi Y., Takahara A., Kajiyama T., Higher order structure and thermo-responsive properties of polymeric gel with crystalline side chains, *Polym. J.* 28**,** 452-457 (1996).

47. Kopeček J., Hydrogels from soft contact lenses and implants to self-assembled nanomaterials, *J. Polym. Sci., Part A: Polym. Chem.* 47, 5929-5946 (2009).

48. Kopeček J., Polymer-drug conjugates: Origins, progress to date and future directions, *Adv. Drug Delivery Rev.* 65, 49-59 (2013).

49. Yang J., Kopeček J., Macromolecular therapeutics, *J. Controlled Release* 28, 288-303 (2014).

50. Ishihara T., Maeda T., Sakamoto H., Takasaki N., Shigyo M., Ishida T., Kiwada H., Mizushima Y., Mizushima T., Evasion of the accelerated blood clearance phenomenon by coating of nanoparticles with various hydrophilic polymers, *Biomacromolecules* 11, 2700-2706 (2010).

51. Bergna H.E., Roberts W.O., Colloidal Silica: Fundamentals and Applications, CRC Press, Santa Barbara 2005, USA.

52. Brinker C.J., Scherer G.W., Sol-Gel Science, Academic Press, New York 1990, USA.

53. Stöber W., Fink A., Controlled growth of monodisperse silica spheres in the micron size range, *J. Colloid Interface Sci*. 26, 62-69 (1968).

54. Otterstedt J.-E., Brandreth D.A., Small Particles Technology, Springer Science & Business Media, New York 1998, USA.

55. Iler R.K., The Chemistry of Silica, Wiley, New York 1979, USA.

56. Mamaeva V, Sahlgren C., Lindén M., Mesoporous silica nanoparticles in medicine-recent advances, *Adv. Drug Deliv. Rev*. 65, 689-702 (2013).

57. Inagaki S., Guan S., Ohsuna T., Terasaki O., An ordered mesoporous organosilica hybrid material with a crystal-like wall structure, *Nature* 416, 304-307 (2002).

58. Nooney R.I., Thirunavukkarasu D., Chen Y., Josephs R., Ostafin A.E, Synthesis of nanoscale mesoporous silica spheres with controlled particle size, *Chem. Mater.* 14, 4721-4728 (2002).

59. Stejskal J., Kratochvíl P., Jenkins A.D., Polyaniline: Forms and formation, *Collect. Czechoslovak Chem. Commun.* 60, 1747-1755 (1995).

60. Stejskal J., Sapurina I., Trchová M., Polyaniline nanostructures and the role of aniline oligomers in their formation, *Prog. Polym. Sci.* 35 1420-1481 (2010).

61. Tzou K., Gregory R.V., Kinetic study of the chemical polymerization of aniline in aqueous solutions, *Synth. Met.* 47, 267-277 (1992).

62. Stejskal J., Gilbert R.G., Polyaniline. Preparation of a conducting polymer, *Pure Appl. Chem.* 74, 857-867 (2002).

63. Babayan V., Kazantseva N.E., Sapurina I., Moucka R., Stejskal J., Saha P., Increasing the high-frequency magnetic permeability of MnZn ferrite in polyaniline composites by incorporating silver, *J. Magn. Magn. Mater.* 333, 30-38 (2013).

64. Virji S., Kaner R. B., Weiller B. H., Hydrogen sensors based on conductivity changes in polyaniline nanofibers, *J. Phys. Chem. B* 110, 22266-22270 (2006).

65. Kalendová A., Veselý D., Sapurina I., Stejskal J., Anticorrosion efficiency of organic coatings depending on the pigment volume concentration of polyaniline phosphate, *Prog. Org. Coat*. 63, 228-237 (2008).

66. Jiang B.-P., Zhang L., Zhu Y., Shen X.-C., Ji S.-C, X.-Y. Tan, L. Cheng, H. Liang, Water-soluble hyaluronic acid–hybridized polyaniline nanoparticles for effectively targeted photothermal therapy, *J. Mater. Chem. B* 3, 3767-3776 (2015).

67. Mahmoudi M., Hofmann H., Rothen-Rutishauser B., Petri-Fink A., Assessing the *in vitro* and *in vivo* toxicity of superparamagnetic iron oxide nanoparticles, *Chem. Rev.* 112, 2323-2338 (2012).

68. Duguet E., Vasseur S., Mornet S., Devoisselle J.M., Magnetic nanoparticles and their applications in medicine, *Nanomedicine (London U.K.)* 1, 157-168 (2006).

69. Cedervall T., Lynch I., Lindman S., Berggard T., Thulin E., Nilsson H., Dawson K. A., Linse S., Understanding the nanoparticles-protein corona using methods to quantify exchange rates and affinities of proteins for nanoparticles, *Proc. Natl. Acad. Sci.* USA. 104, 2050-2055 (2007).

70. Lei L., Ling-Ling J., Yun Z., Gang L., Toxicity of superparamagnetic iron oxide nanoparticles: Research strategies and implications for nanomedicine, *Chin. Phys. B* 22, 127503 (2013).

71. Schmitz K.S., An Introduction to Dynamic Light Scattering by Molecules, Academic Press, Oxford 1990, UK.

72. Stejskal J., Sapurina I., Polyaniline: Thin films and colloidal dispersions (IUPAC technical report), *Pure Appl. Chem.* 77, 815-826 (2005).

73. Stejskal J., Riede A., Hlavatá D., Prokeš J., Helmstedt M., Holler P., The effect of polymerization temperature on molecular weight, crystallinity, and electrical conductivity of polyaniline, *Synth. Met.* 96, 55-61 (1998).

7. ATTACHED PUBLICATIONS

Publication No. 1

Article

Journal of Biomedical Nanotechnology
Vol. 9, 1–13, 2012
www.aspbs.com/jbn

The Use of Hydrophilic Poly(*N*,*N*-dimethylacrylamide) for Promoting Engulfment of Magnetic γ-Fe_2O_3 Nanoparticles by Mammalian Cells

Beata Anna Zasońska[1], Nataliya Boiko[2], Daniel Horák[1,*], Olga Klyuchivska[2], Hana Macková[1], Milan J. Beneš[1], Michal Babič[1], Miroslava Trchová[1], Jiřina Hromádková[1], and Rostyslav Stoika[2]

[1] *Institute of Macromolecular Chemistry, Academy of Sciences of the Czech Republic, Heyrovského Sq. 2, 162 06 Prague 6, Czech Republic*
[2] *Institute of Cell Biology, National Academy of Sciences of Ukraine, Drahomanov Street, 14/16, 79005, Lviv, Ukraine*

γ-Fe_2O_3 nanoparticles obtained by coprecipitation of Fe(II) and Fe(III) chlorides with a base and subsequent oxidation were coated with a shell of hydrophilic biocompatible poly(*N*,*N*-dimethylacrylamide) (PDMAAm). Various initiators were attached to the iron oxide surface to enable the use of the "grafting-from" approach for immobilization of PDMAAm. They included 2,2′-azobis(2-methylpropanimidamide) dihydrochloride (AMPA), 2,2′-azobis(*N*-hydroxy-2-methylpropanimidamide) dihydrochloride (ABHA) and 4-cyano-4-{[1-cyano-3-(*N*-hydroxycarbamoyl)-1-methylpropyl]azo}pentanoic acid (CCHPA). Engulfment of PDMAAm-coated γ-Fe_2O_3 nanoparticles by murine J774.2 macrophages was investigated. Only some nanoparticles were engulfed by the macrophages. PDMAAm-AMPA-γ-Fe_2O_3 and PDMAAm-ABHA-γ-Fe_2O_3 nanoparticles were rapidly engulfed by the cells. In contrast, neat γ-Fe_2O_3 and PDMAAm-CCHPA-γ-Fe_2O_3 particles induced formation of transparent vacuoles indicating toxicity of the particles. Thus, PDMAAm-coated AMPA- and ABHA-γ-Fe_2O_3 nanoparticles can be recommended as non-toxic labels for mammalian cells.

KEYWORDS: *Nanoparticles, Superparamagnetic, Poly(N,N-dimethylacrylamide), Maghemite, Engulfment, Mammalian Cells.*

INTRODUCTION

Superparamagnetic iron oxide nanoparticles provide a promising platform for a variety of biomedical applications both in diagnostics[1,2] and therapeutics such as in magnetic resonance imaging,[3–5] drug delivery[6,7] and hyperthermia.[8,9] The nanoparticles are very useful also in other areas, e.g., in catalysis,[10] separations of cells,[11] proteins, nucleic acids and genes.[12] Typical superparamagnetic nanoparticles are based on mixed Fe(II) and Fe(III) oxides, i.e., magnetite (Fe_3O_4) and maghemite (γ-Fe_2O_3) that in solutions do not have typical reducing or oxidizing properties of Fe(II) or Fe(III), respectively. This is due to their insolubility in water and heterogeneous character of the reactions. Magnetite can be thus transformed to maghemite only by strongly oxidizing agents, such as H_2O_2, Fe(III) ions and NaClO. Under physiological conditions, both magnetite and maghemite are sufficiently stable. Commercially available iron oxide nanoparticles, e.g., Ferridex®, Endorem® and Resovist® are approved as contrast agents. An important condition for biological and medicinal applications of iron oxide nanoparticles is the coating of their surface with a suitable shell preventing interactions with microenvironment.[13] A disadvantage of uncoated nanoparticles consists in high nonspecific adsorption of many biopolymers including proteins and nucleic acids. Moreover, appropriate surface coating provides colloid stability of the nanoparticles under physiological conditions and makes it possible to immobilize useful ligands like drugs, fluorescent labels and transfection agents.

There is a considerable number of approaches that provide coating of magnetic iron oxide nanoparticles

*Author to whom correspondence should be addressed.
Email:
Received: 6 June 2012
Revised/Accepted: 28 August 2012

with low- or high-molecular-weight substances.[14–17] All these methods are based on strong binding interactions between the selected functionalities, such as chelating groups (including COOH[18] and OH groups, phosphates or phosphonates[19] and unsaturated sites on the iron oxide surface. If a polymer should be used as a coating, it has to contain a strongly interacting group o several moderately binding groups. Polymers containing one telechelic or semitelechelic group strongly interacting with the iron oxide surface can be prepared separately in solution and subsequently used for modification of the iron oxide surface by the "grafting-to" approach. The method allows grafting of polymers with well-defined chain length. However, the "grafting-to" method suffers from several drawbacks. For example, it is difficult to obtain high grafting density; moreover, the neighbouring polymer chains are often sterically hindered. Hence, the thickness of the shell layer is usually limited (below 100 nm).[20]

In the "grafting-from" method, polymerization starts from the initiator bound to magnetic iron oxide; as a result, polymer brushes are formed. The "grafting-from" method, also called "surface-initiated polymerization" provides good control of functionality, grafting density, and the thickness of polymer brushes.[21] The shell thickness and brush density can be easily controlled by varying the concentrations of the hydrophilic monomer and initiator. A typical example of preparation of the "grafting-from" magnetic iron oxide nanoparticles is living atom transfer radical polymerization (ATRP) where the initiator (typically a bromoisobutyrate) is bound to iron oxide.[22–28] Since the attachment of the initiator to solid support requires two reaction steps including the introduction of amino groups to the particle surface and reaction with 2-bromoisobutyryl bromide, our aim was to simplify the process using azoinitiators containing hydroxamic or amidoxime groups. Such initiators are known as complexing (chelating) agents for ferric ions[29–36] or, e.g., amidoxime-containing sorbents selectively bind cations such as UO_2^{2+}, Cu^{2+} and Fe^{3+}.

Macrophages participate in many pathological processes including heart disorders, Alzheimer disease, diabetes, infectious diseases, and obesity. Estimation of their phagocytary activity by monitoring the efficiency of engulfment of various artificial objects is therefore very important. Various labels are used for that purpose including superparamagnetic nanoparticles[37–41] that can additionally be applied to targeting macrophages loaded with biological "waste" (microorganisms, damaged and old cells and bio-molecules, fat particles, etc.). Magnetically labeled macrophages are useful also for magnetic resonance imaging (MRI) detection of macrophages in mixed cell population, and/or for their attraction to pathological loci, e.g., to the inflammation site or atherosclerotic plaques. Chemical nature of the particle shell strongly affects their biocompatibility and cytotoxicity.[42] MRI noninvasively monitored microvascular lesions in transgenic mouse in Alzheimer disease models. The strength and number of foci of signal attenuation detected in cortical and thalamic brain regions of aged APP23 mice, was considerably enhanced by intravenous administration of iron oxide nanoparticles that were taken up by macrophages through an absorptive endocytosis.[43]

In this report, highly hydrophilic poly(*N*,*N*-dimethylacrylamide) (PDMAAm) was grafted from the functionalized surfaces of iron oxide nanoparticles. PDMAAm is well known not only for its remarkable solubility both in water and in various organic solvents, but also for its excellent biocompatibility.[44, 45] Recently, it has attracted increasing interest in drug delivery and medicinal diagnostics.[46–50] An additional aim of this report was to investigate the engulfment of PDMAAm-coated iron oxide nanoparticles by macrophages since the biocompatible particles are required for adequate evaluation of the phagocytary activity of these immunocompetent cells. The size of the particles should be uniform. They should be coated with a suitable polymer to achieve an efficient engulfment by macrophages. The prospects of biomedicinal applications of the nanoparticles are considered.

EXPERIMENTAL DETAILS

Materials

Aqueous ammonia was from Lach-Ner (Neratovice, Czech Republic), $FeCl_2 \cdot 4H_2O$, $FeCl_3 \cdot 6H_2O$, 2,2′-azobisisobutyronitrile (AIBN), hydroxylamine (50% water solution), 4,4′-azobis-(4-cyanopentanoic acid) and 4-(dimethylamino)pyridine (DMAP) were purchased from Fluka (Buchs, Switzerland), 2,2′-azobis(2-methylpropanimidamide) dihydrochloride (AMPA; Scheme 1(a)) and dicyclohexylcarbodiimide (DCCI) were from Aldrich (St. Louis, MO, USA). Sodium hypochlorite (NaOCl) solution (5 wt%) was from Bochemie (Bohumín, Czech Republic); *N*,*N*-dimethylacrylamide (DMAAm; Aldrich) was distilled (boiling point 56 °C/266 Pa). Ultrapure *Q*-water ultrafiltered in a Milli-*Q* Gradient A10 system (Millipore, Molsheim, France) was used for the preparation of solutions. All other solvents and chemicals were from Lachner (Neratovice, Czech Republic) or Aldrich.

2,2′-Azobis(*N*′-hydroxy-2-methylpropanimidamide) Dihydrochloride (ABHA)

The initiator was prepared by a modified procedure[51, 52] (Scheme 1(b)). AIBN (1 g; 6.09 mmol) was dissolved in ethanol (40 ml) and 50% aqueous solution of hydroxylamine (1 g; 15.1 mmol) was added at room temperature under stirring for 4 h. Ethanol was partly (10%) evaporated on a rotary evaporator to initiate crystallization. The product was left to stand for 2 h at −18 °C, collected by

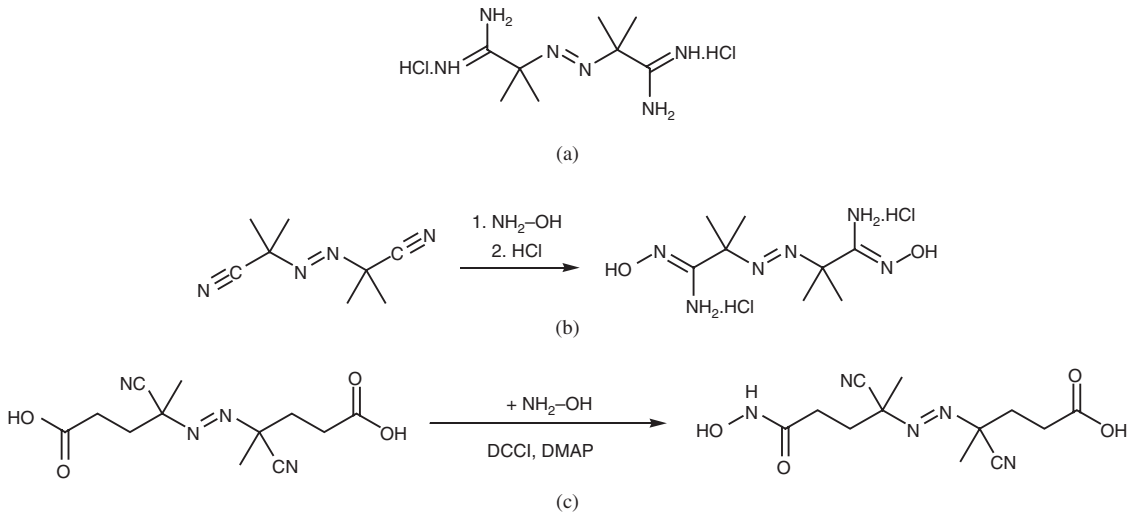

Scheme 1. Azoinitiators with anchoring groups. (a) 2,2′-Azobis(2-methylpropanimidamide) dihydrochloride (AMPA), (b) 2,2′-azobis(*N*-hydroxy-2-methylpropanimidamide) dihydrochloride (ABHA) and (c) 4-cyano-4-{[1-cyano-3-(*N*-hydroxycarbamoyl)-1-methylpropyl]azo}pentanoic acid (CCHPA).

filtration and washed with ethanol. Yield: 1.25 g (89%); m.p. 154 °C (literature[51] 153 °C). Finally, the product (1.25 g; 3.71 mmol) was mixed with ethanol (18 ml) and 35% hydrochloric acid (0.93 ml; 10.9 mmol) was dropwise added under stirring at 23 °C for 4 h. ABHA was collected by filtration. Found, %: C 31.91; H 6.46; N 27.46. Calculated, %: C 31.69; H 6.65; N 27.72. M.p. 163–165 °C (decomposition). Additional crystalline product was obtained by evaporation of the filtrate.

4-Cyano-4-{[1-cyano-3-(*N*-hydroxycarbamoyl)-1-methylpropyl]azo} Pentanoic Acid (CCHPA)

CCHPA was obtained by modification of a literature procedure.[53,54] 4,4′-Azobis-(4-cyanopentanoic acid) (2.8 g; 10 mmol) and dicyclohexylcarbodiimide (4.13 g; 20 mmol) were dissolved in tetrahydrofuran (THF; 100 ml), cooled to −10 °C and 4-(dimethylamino)pyridine (10 mg; 0.082 mmol) and aqueous hydroxylamine (2 g; 30 mmol) were added. The mixture was kept at 4 °C for 12 h and the precipitate was collected by filtration. THF was evaporated on a vacuum evaporator and CCHPA (Scheme 1(c)) was recrystallized from methanol. Yield: 2 g (70%). Found, %: C 50.17; H 6.9; N 21.8. Calculated, %: C 48.81; H 5.80; N 23.72.^{1}H NMR ($CDCl_3$), δ, ppm: 1.70 (*s*, 3H), 1.70 (*s*, 3H), 2.48 (*m*, 2H), 2.44 (*m*, 2H), 2.11 (*m*, 2H), 2.08 (*m*, 2H).

Colloidal γ-Fe_2O_3

The colloid was prepared according to literature.[51] 0.2 M aqueous iron(III) chloride (100 ml) and 0.2 M iron(II) chloride solutions (50 ml) were mixed with 0.5 M aqueous NH_3 (100 ml) under 5 min sonication. The solution was added to 0.5 M aqueous NH_3 solution (400 ml) and the mixture stirred for 1 h (200 rpm). The resulting precipitate was magnetically separated, washed with *Q*-water until peptization and sonicated with 5 wt% sodium hypochlorite solution (16 ml) for 5 min. The precipitate was again magnetically separated and washed with *Q*-water until peptization that was accompanied by the formation of colloidal γ-Fe_2O_3. Its concentration was 47 mg of γ-Fe_2O_3 per ml.

Complexation of Initiators on γ-Fe_2O_3 Surface and Polymerization of DMAAm

For DLS measurements, aqueous initiator solutions (0.02–0.16 mg AMPA/ml; 0.02–0.64 mg ABHA/ml and 0.02–0.32 mg CCHPA/ml) were mixed with colloidal γ-Fe_2O_3 (1 mg γ-Fe_2O_3/ml) under shaking; the resulting nanoparticles are denoted as AMPA-, ABHA- and CCHPA-γ-Fe_2O_3.

Polymerizations were run in a 30-ml glass reactor equipped with an anchor-type stirrer. First, the initiator (4.8 mg) was added to the colloid (10 ml; 47 mg γ-Fe_2O_3/ml) during 5 min, then DMAAm (0.3 g) was dissolved in the colloid and the mixture was purged with nitrogen for 10 min. The polymerization was started by heating at 70 °C for 16 h under stirring (400 rpm). After completion of the polymerization, PDMAAm-coated γ-Fe_2O_3 particles (PDMAAm-AMPA-γ-Fe_2O_3, PDMAAm-ABHA-γ-Fe_2O_3 or PDMAAm-CCHPA-γ-Fe_2O_3) were magnetically separated and washed ten times with Q-water until all reaction byproducts were removed.

Characterization of the Nanoparticles

The particle size in the dry state and particle size distribution were obtained from TEM micrographs (JEM

20CX, Jeol; Tokyo, Japan) and Quanta FEG 200F SEM (FEI; Brno, Czech Republic). The number-average diameter (D_n), weight-average diameter (D_w), and polydispersity index (PDI = D_w/D_n) were calculated with Atlas software (Tescan Digital Microscopy Imaging; Brno, Czech Republic) by counting at least 400 individual particles in the micrographs. The hydrodynamic diameter (D_h) and zeta-potential of particles in water (1 mg/ml; pH ~ 6) were measured using a Zetasizer Nano-ZS Model ZEN3600 instrument (Malvern Instruments; Malvern, UK).

Infrared spectra were measured using a Thermo Nicolet NEXUS 870 Fourier Transform Infrared (FTIR) spectrometer (Madison, WI, USA). Spectra of the powdered samples were measured with Golden Gate™ Heated Diamond Attenuated Total Reflection (ATR) Top-Plate (MKII single reflection ATR system; Specac; Orpington, UK). The Fe content was analyzed with a Perkin-Elmer 3110 (Norwalk, CT, USA) AAS spectrometer using a solution obtained by mineralization of a sample with dilute HCl (1:1) at 80 °C for 1 h. The M_w and M_n were determined by size-exclusion chromatography (SEC; Shimadzu SIL-HT, Tokyo, Japan) with acetate buffer eluent, pH 4.5, flow rate 0.5 ml/min, using a TSK GEL G6000PW column 7.5 mm ID × 300 mm length (Tosoh Biosciences; Stuttgart, Germany), RI and multiangle light scattering DAWN 8 detection (Wyatt Technology, Santa Barbara, CA, USA).

Cell Experiments

Cell culture. Murine macrophages of J774.2 line and murine transformed fibroblasts of L929 line were obtained from the William Harvey Institute (London, UK) and Ludwig Institute for Cancer Research (Uppsala, Sweden), respectively. Cells were cultured in Dulbecco's modified Eagle's medium (DMEM; Sigma, St. Louis, USA) supplemented with 10% fetal bovine serum (FBS; Sigma). Cells were kept in incubator in 5% CO_2 atmosphere at 37 °C and 100% humidity.

Opsonization of PDMAAm-coated γ-Fe_2O_3 nanoparticles and their phagocytosis by macrophages. The PDMAAm-AMPA-γ-Fe_2O_3, PDMAAm-ABHA-γ-Fe_2O_3, PDMAAm-CCHPA-γ-Fe_2O_3 and neat γ-Fe_2O_3 nanoparticles (4.4 mg/ml) were opsonized with proteins of fetal bovine serum (FBS) at 37 °C for 24 h. The opsonized particles (concentration 0.025 wt%; the stock solution diluted 200 times) were added to cultured macrophages J774.2 or fibroblasts L929, and the cultures were kept at 37 °C in incubator under CO_2 atmosphere for 30 min, 1 h, 2 h, 3 h, or 24 h for engulfment of the particles. The engulfment of neat γ-Fe_2O_3 nanoparticles and the culture medium without particles were used as controls.

Light and fluorescence microscopy. Cells were stained with Acridine Orange and Hoechst 33342 and observed under a Carl Zeiss AxioImager A1 light and fluorescence microscope (Carl Zeiss, Germany). Final concentration of both fluorescent dyes equaled 0.3 μg/ml and the staining time was 15 min. For Hoechst 33342, the excitation and emission wavelengths were 365–395 nm and 445–450 nm, respectively, while for Acridine Orange the excitation and emission wavelengths were 470–495 nm and 525–550 nm, respectively, with green filter and 546–560 nm and 575–640 nm, respectively, with red filter. Cells were photographed with a microscope digital camera (Carl Zeiss, Germany).

Cytotoxicity of the PDMAAm-AMPA-γ-Fe_2O_3, PDMAAm-ABHA-γ-Fe_2O_3, PDMAAm-CCHPA-γ-Fe_2O_3 and neat γ-Fe_2O_3 nanoparticles was estimated using a hemocytometric chamber for counting the number of cells treated in the presence of nanoparticles (0.025, 0.5 and 1 wt%; the stock solution diluted 200, 100 and 50 times) in culture medium after 24 h treatment.

RESULTS AND DISCUSSION

γ-Fe_2O_3 Nanoparticles

Iron oxide nanoparticles were synthesized by coprecipitation of aqueous $FeCl_3$ and $FeCl_2$ solutions with aqueous ammonia. Since the resulting magnetite (Fe_3O_4) is not chemically stable in air or water, its controlled oxidation with sodium hypochlorite to maghemite (γ-Fe_2O_3) was preferred. The γ-Fe_2O_3 particles in the dry state were observed under TEM microscope. The γ-Fe_2O_3 particles were of spherical shape, their number-average diameter was 9 nm and PDI 1.24 suggesting that the particles were polydisperse (Fig. 1(a)).

Complexation of Initiators on γ-Fe_2O_3 Surface

To initiate polymerization of DMAAm, three water-soluble initiators were selected to modify γ-Fe_2O_3 surface: 2,2′-azobis(2-methylpropanimidamide) dihydrochloride (AMPA), 2,2′-azobis(*N*′-hydroxy-2-methylpropanimidamide) dihydrochloride (ABHA) and 4-cyano-4-{[1-cyano-3-(*N*-hydroxycarbamoyl)-1-methylpropyl]azo}pentanoic acid (CCHPA). All the initiators possess a functional group capable of interacting with the iron oxide. Protonated amidine groups of AMPA are assumed to interact electrostatically with the negatively charged iron oxide surface analogously to other cationic molecules.[55] Complexation of amidoxime and hydroxamate anchoring groups of ABHA and CCHPA, respectively, with the iron oxide surface was then confirmed by experiments described below.

Partial aggregation of the initiator-modified γ-Fe_2O_3 particles was observed after drying as documented by TEM micrographs (Figs. 1(b)–(d)). The morphology, size (~ 10 nm) and polydispersity (PDI ~ 1.2) of the initiator-modified γ-Fe_2O_3 nanoparticles (Figs. 1(b)–(d); Table I) did not substantially differ from those of the neat γ-Fe_2O_3 colloid (Fig. 1(a)).

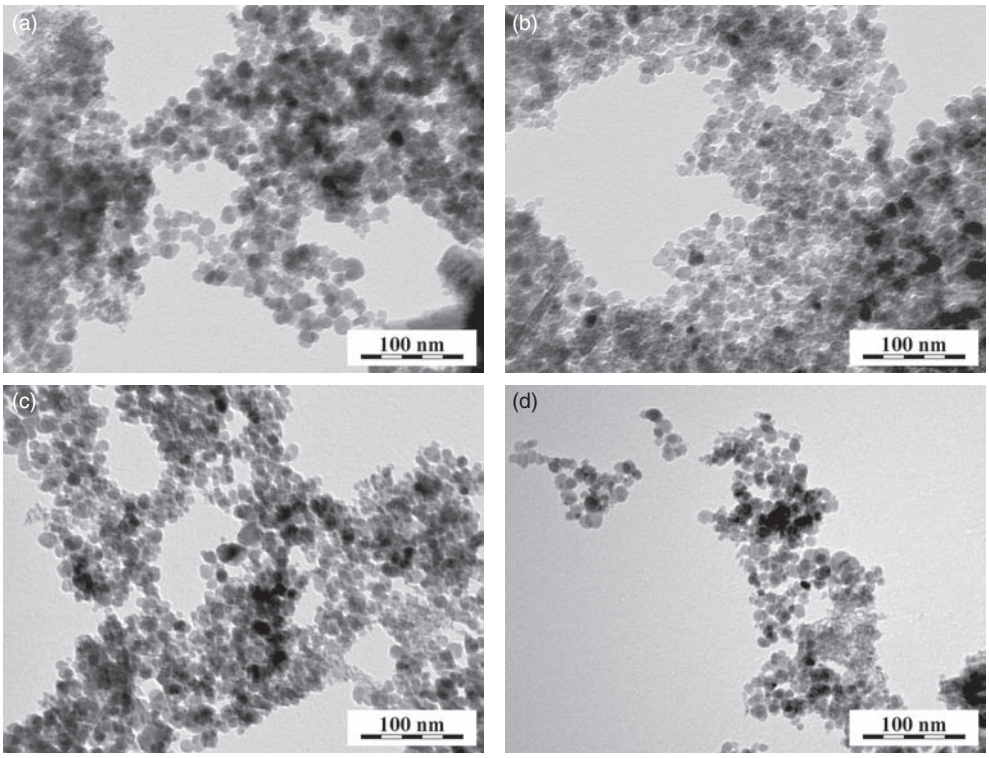

Figure 1. **TEM micrographs of nanoparticles (a) neat γ-Fe_2O_3, (b) AMPA-γ-Fe_2O_3, (c) ABHA-γ-Fe_2O_3 and (d) CCHPA-γ-Fe_2O_3.**

In addition to TEM analysis of the particles in the dry state, the aqueous initiator-modified γ-Fe_2O_3 colloids were investigated by DLS. Here, the concentrations of γ-Fe_2O_3 in water had to be low (1 mg/ml) to prevent particle aggregation; the concentration was then used in all experiments within this report. As TEM observes the number-average diameters of individual dry particles while DLS measures hydrodynamic size (z-diameter; sensitive to large sizes) of the particles, their dimers and aggregates swollen in water, it is not surprising that much larger sizes were obtained by DLS ($\sim$ 115–120 nm) than by TEM (Table I). DLS provides also polydispersity (PI) derived from cumulative analysis.[56] Generally, PI varies in the range 0–1, where 0 is for monodisperse particles while 1 for very broad particle size distributions. Since PI of both neat and initiator-modified γ-Fe_2O_3 equaled to 0.13–0.19, we concluded that polydispersity PI was within the standard range. Moreover, it is apparent that polydispersities determined by both the independent methods (TEM and DLS) correlate quite well.

In another series of experiments, the effect of the initiator/γ-Fe_2O_3 ratio on morphology, particle size and polydispersity of AMPA-, ABHA- and CCHPA-γ-Fe_2O_3 nanoparticles was investigated (Fig. 2). The particles showed a very similar hydrodynamic size ($D_h \sim 120$ nm). With the increasing initiator/γ-Fe_2O_3 ratio the particles were larger; $D_h > 1$ μm then indicated sedimentation of the particles due to aggregation occurring at the initiator/γ-Fe_2O_3 ratio = 0.12 and 0.32 w/w for AMPA and CCHPA, respectively. PDMAAm particles obtained from ABHA-γ-Fe_2O_3 nanoparticles were stable within the investigated range ABHA/γ-Fe_2O_3 ratios (up to

Table I. **Some characteristics of initiator-modified γ-Fe_2O_3 and PDMAAm-coated initiator-modified γ-Fe_2O_3 particles according to TEM, DLS and AAS.**

	D_n^a (nm) (TEM)	PDI[b] (TEM)	D_h^c (nm) (DLS)	PI[d] (DLS)	Fe (wt%) (AAS)	Coating (wt%)
$\gamma-Fe_2O_3$	9	1.24	113	0.15	66.14	–
AMPA-γ-Fe_2O_3	10	1.23	120	0.19	–	–
ABHA-γ-Fe_2O_3	10	1.23	123	0.18	–	–
CCHPA-γ-Fe_2O_3	11	1.19	114	0.13	–	–
PDMAAm-AMPA-γ-Fe_2O_3	12	1.18	209	0.20	64.47	2.5
PDMAAm-ABHA-γ-Fe_2O_3	16	1.24	206	0.16	64.54	2.4
PDMAAm-CCHPA-γ-Fe_2O_3	13	1.46	206	0.18	63.92	3.3

Notes: [a]Number average particle diameter (TEM); [b]polydispersity index (TEM); [c]hydrodynamic diameter (DLS); [d]polydispersity (DLS).

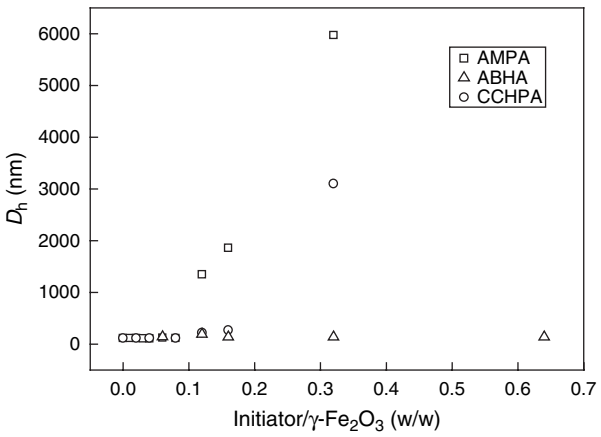

Figure 2. Dependence of the diameter of initiator-modified γ-Fe_2O_3 nanoparticles on the initiator/γ-Fe_2O_3 ratio. Initiators: (□) AMPA, (Δ) ABHA and (○) CCHPA.

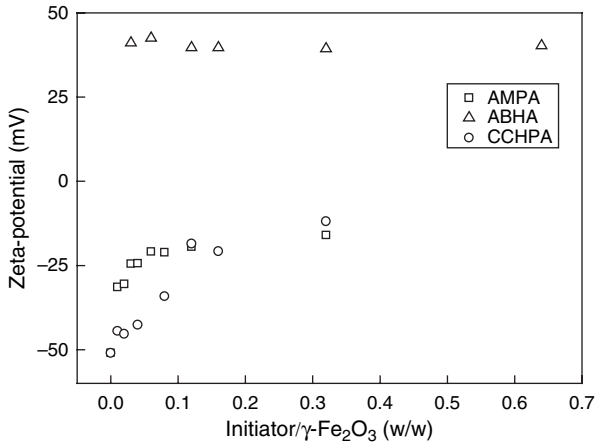

Figure 3. Dependence of zeta-potential of initiator-modified γ-Fe_2O_3 nanoparticles on the initiator/γ-Fe_2O_3 ratio. Initiators: (□) AMPA, (Δ) ABHA and (○) CCHPA.

0.64 w/w). This could be due to diminishing the effective thickness of a stabilizing electric double layer.[57] Thus, ABHA-modified nanoparticles exhibited the highest stability.

Zeta-potential of neat (uncoated) γ-Fe_2O_3 was equal to −51 mV (pH 5.5), which means that the solution was very stable. In the dependence of zeta-potential of initiator-modified γ-Fe_2O_3 nanoparticles on the initiator/γ-Fe_2O_3 ratio, the potential of AMPA- and CCHPA-γ-Fe_2O_3 increased from −45 to −13 mV with the ratio increasing up to 0.3 w/w, approaching then a plateau (Fig. 3). In contrast, zeta-potential of ABHA-γ-Fe_2O_3 was positive amounting to 40 mV irrespectively of the ABHA/γ-Fe_2O_3 ratio. It is known that the zeta-potential of stable colloidal particles should be lower than −30 mV or higher than 30 mV.[58] Similar behavior was observed also with other types of initiators.[59, 60]

Polymerization of DMAAm from the Initiator-Modified-γ-Fe_2O_3 Nanoparticles

Generally, surface-initiated polymerizations involving ATRP, RAFT, cationic, anionic or radical polymerization are considered as a convenient methods for controlled introduction of functional groups to the surface of nanoparticles.[61, 62] In particular, controlling brush density can be achieved by living polymerization. The method enables modification of surface properties of a wide range of materials.

However, in the present report, radical polymerization was used to graft PDMAAm from γ-Fe_2O_3 surface (Scheme 2). Polymerizations were run for 16 h when the conversions approached 100% as shown in the previous paper.[55] SEM micrographs of PDMAAm-coated-AMPA-γ-Fe_2O_3 nanoparticles documented that the tiny particles aggregated in the course of deposition on

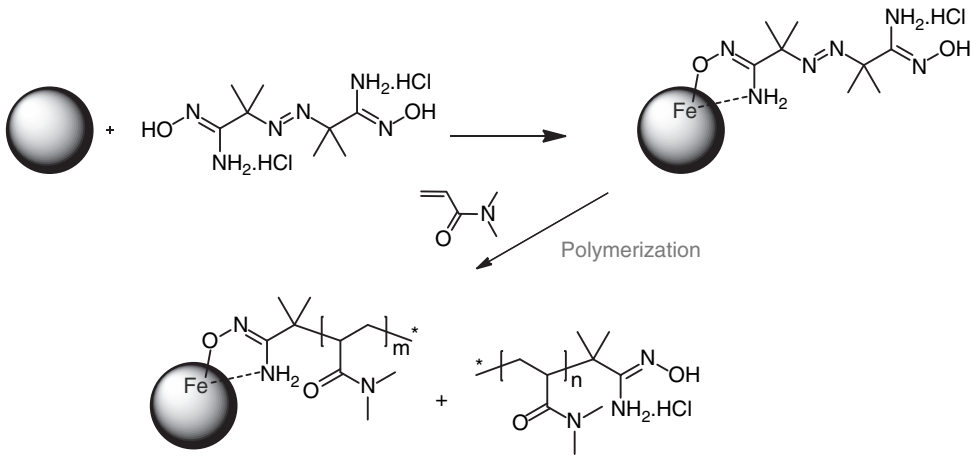

Scheme 2. Preparation of PDMAAm-γ-Fe_2O_3 particles by "grafting-from" ABHA-γ-Fe_2O_3.

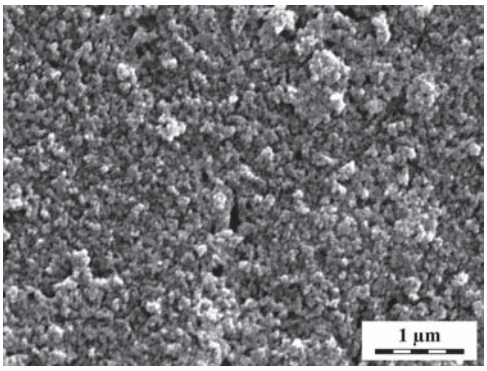

Figure 4. SEM micrograph of PDMAAm-AMPA-γ-Fe_2O_3 nanoparticles.

support microscopic slide and subsequent drying (Fig. 4). The aggregates, however, were rather regular with $D_n \sim$ 45 nm and PDI 1.09 indicating a narrow size distribution. As SEM did not provide high resolution because of a very small particle size, TEM was used to view PDMAAm-coated γ-Fe_2O_3 particles. As in the TEM analysis a dilute suspension of the nanoparticles was dropped on the microscopic copper grid covered with electron-transparent carbon film, the observed particles were rather individual. According to TEM, D_n of PDMAAm-coated AMPA-γ-Fe_2O_3 nanoparticles was 12 nm and PDI was 1.18 (Fig. 5(a); Table I). The PDMAAm-coated ABHA-γ-Fe_2O_3 nanoparticles varied in size from 8 to 32 nm, with $D_n = 16$ nm and PDI = 1.24 (Fig. 5(b); Table I). The PDMAAm-coated CCHPA-γ-Fe_2O_3 nanoparticles varied in size from 6 to 39 nm, their D_n was 13 nm and PDI 1.46 (Fig. 5(c); Table I), i.e., the polydispersities of PDMAAm-coated ABHA- and AMPA-γ-Fe_2O_3 were narrower than that of CCHPA-γ-Fe_2O_3 nanoparticles.

DLS provided information on the hydrodynamic size of particle clusters. As a consequence, the D_h size was larger, 206 nm, for both PDMAAm-coated AMPA-, ABHA- and CCHPA-γ-Fe_2O_3, compared with that obtained from TEM micrographs (Table I). The PI value approaching 0.2 reflects polydisperse nature of the product.

The amount of PDMAAm coating and the content of maghemite in the particles were calculated from Fe content (by AAS). Since PDMAAm does not contain Fe, the Fe content may be used for calculating the percentage of γ-Fe_2O_3 in PDMAAm-coated γ-Fe_2O_3 nanoparticles using the following equation: $\%Fe_2O_3 = (\%Fe \times 100)/66.14$, where %Fe was obtained from AAS of the investigated microspheres, 66.14 was the percentage of Fe in neat γ-Fe_2O_3. For example, AAS showed the Fe percentage 64.47, hence the calculated percentage of γ-Fe_2O_3 in PDMAAm-coated γ-Fe_2O_3 nanoparticles was 97.5 wt%, i.e., the percentage of coating was 2.5 wt% (by AAS) (Table I). The AAS results suggest that the PDMAAm amount bound to the γ-Fe_2O_3 nanoparticle surface was rather low, ranging from 2.4 to 3.3 wt%.

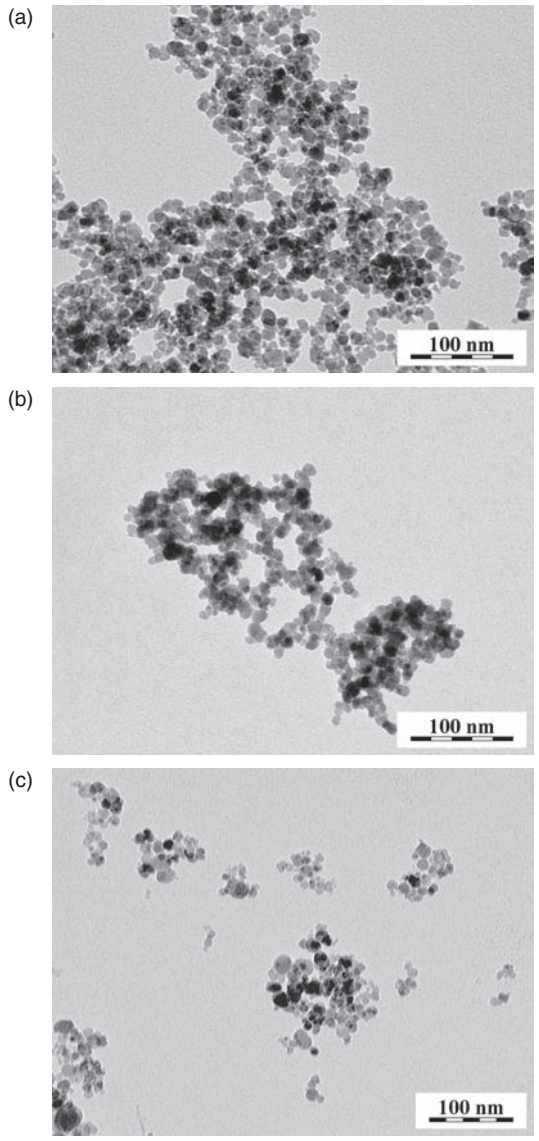

Figure 5. TEM micrographs of (a) PDMAAm-AMPA-γ-Fe_2O_3, (b) PDMAAm-ABHA-γ-Fe_2O_3 and (c) PDMAAm-CCHPA-γ-Fe_2O_3 nanoparticles.

The surface of γ-Fe_2O_3 nanoparticles coated with PDMAAm by the "grafted-from" method was also analyzed by surface-sensitive ATR FTIR spectroscopy (Fig. 6). In IR spectra of γ-Fe_2O_3 nanoparticles, absorption bands at 3400, 1558 and 856 cm^{-1} corresponding to various O–H vibration modes of water adsorbed on the surface were observed. First, the IR spectra of γ-Fe_2O_3 particles after surface modification with AMPA, ABHA and CCHPA initiators were compared with the spectrum of neat magnetic particles (Figs. 6(a)–(c)). In all the three cases, the spectra were different after modification indicating that the initiators have been attached to the γ-Fe_2O_3 surface. When the initiator-modified surfaces were coated with PDMAAm by the "grafting-from" method, small peaks corresponding to PDMAAm were observed in the spectra of PDMAAm-AMPA-γ-Fe_2O_3

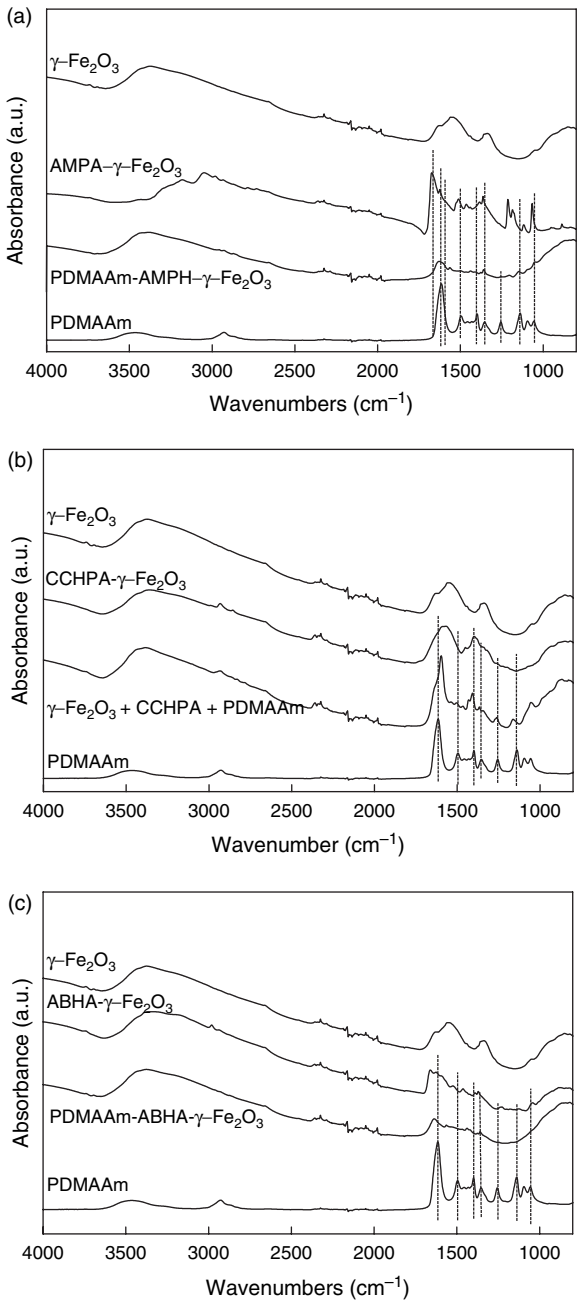

Figure 6. ATR FTIR spectra of magnetic γ-Fe_2O_3 nanoparticles before and after surface modification with (a) AMPA, (b) ABHA and (c) CCHPA initiators and grafting of DMAAm from the initiator-modified nanoparticles.

and PDMAAm-ABHA-γ-Fe_2O_3 nanoparticles and relatively high peaks in the spectrum of PDMAAm-CCHPA-γ-Fe_2O_3 nanoparticles. In all cases, the spectra of PDMAAm-modified surfaces differed from those measured before the "grafting-from" modification. To evaluate the efficiency of the "grafting-from" coating, the spectra were compared with those of neat PDMAAm prepared under initiation with ABHA. In the spectrum of neat PDMAAm, the peaks of C–H stretching vibrations at about 2930 cm^{-1}, amide I band at about 1615 cm^{-1}, the peak of CH_3 deformation vibrations and that of amide II at 1496 cm^{-1} were distinguished. Another amide band was observed at 1400 cm^{-1}. These bands can be also distinguished as very weak and slightly shifted bands in the spectra of PDMAAm-AMPA-γ-Fe_2O_3 and PDMAAm-ABHA-γ-Fe_2O_3 nanoparticles. The spectrum of neat PDMAAm was very close to that of PDMAAm-CCHPA-γ-Fe_2O_3 particles. The results of the ATR FTIR analysis and Fe analysis thus confirmed the successful coating of magnetic AMPA-, ABHA- and CCHPA-γ-Fe_2O_3 nanoparticles with PDMAAm by the "grafting-from" method.

Cell Experiments

Engulfment of PDMAAm-coated γ-Fe_2O_3 nanoparticles by murine J774.2 macrophages. The efficiency of engulfment of the PDMAAm-AMPA-γ-Fe_2O_3, PDMAAm-ABHA-γ-Fe_2O_3, PDMAAm-CCHPA-γ-Fe_2O_3 and neat γ-Fe_2O_3 nanoparticles by the murine macrophages J774.2 was preliminarily estimated at 30 min, 1 h, 2 h, 3 h, and 24 h of cell cultivation in the presence of the particles. Figure 7 shows the macrophages treated with the nanoparticles for 1 and 3 h and after staining with fluorescent dyes Acridine Orange and Hoechst 33342. After 30 min treatment of macrophage J774.2 with PDMAAm-AMPA-γ-Fe_2O_3 nanoparticles, most of them remained in the culture medium unengulfed. Visible engulfment of the nanoparticles appeared after 1 h treatment (Fig. 7(a)). After 2 h treatment, granulation of the cytoplasm was observed due to the accumulation of PDMAAm-AMPA-γ-Fe_2O_3 nanoparticles in the peripheral region of the cytoplasm. After 3 h treatment, majority of PDMAAm-AMPA-γ-Fe_2O_3 nanoparticles was engulfed by the macrophages and some cells demonstrated signs of lysosomal activation characterized by red fluorescence of Acridin Orange (Fig. 7(b)). Only a minimal amount of the PDMAAm-AMPA-γ-Fe_2O_3 nanoparticles remained unengulfed, indicating that the engulfment was very efficient. The rapid engulfment of PDMAAm-coated AMPA-γ-Fe_2O_3 nanoparticles by the macrophages contrasted with slow phagocytosis of the heterotelechelic poly(*N*-vinylpyrrolidone) oligoperoxide-coated γ-Fe_2O_3/poly(2-hydroxyethyl methacrylate) nanoparticles by the same cells taking about 20 h.[63] Thus, PDMAAm can be considered superior to poly(2-hydroxyethyl methacrylate) in terms of cell engulfment. This is also in agreement with the earlier observation that PDMAAm-coated γ-Fe_2O_3 nanoparticles efficiently labeled stem cells which was explained by the formation of complexes of PDMAAm chains with charges on the cell surface.[59] In other words, PDMAAm shows the affinity to cell membrane components, which facilitates endocytosis.

The time dependence of the engulfment of PDMAAm-ABHA-γ-Fe_2O_3 nanoparticles by the macrophages was

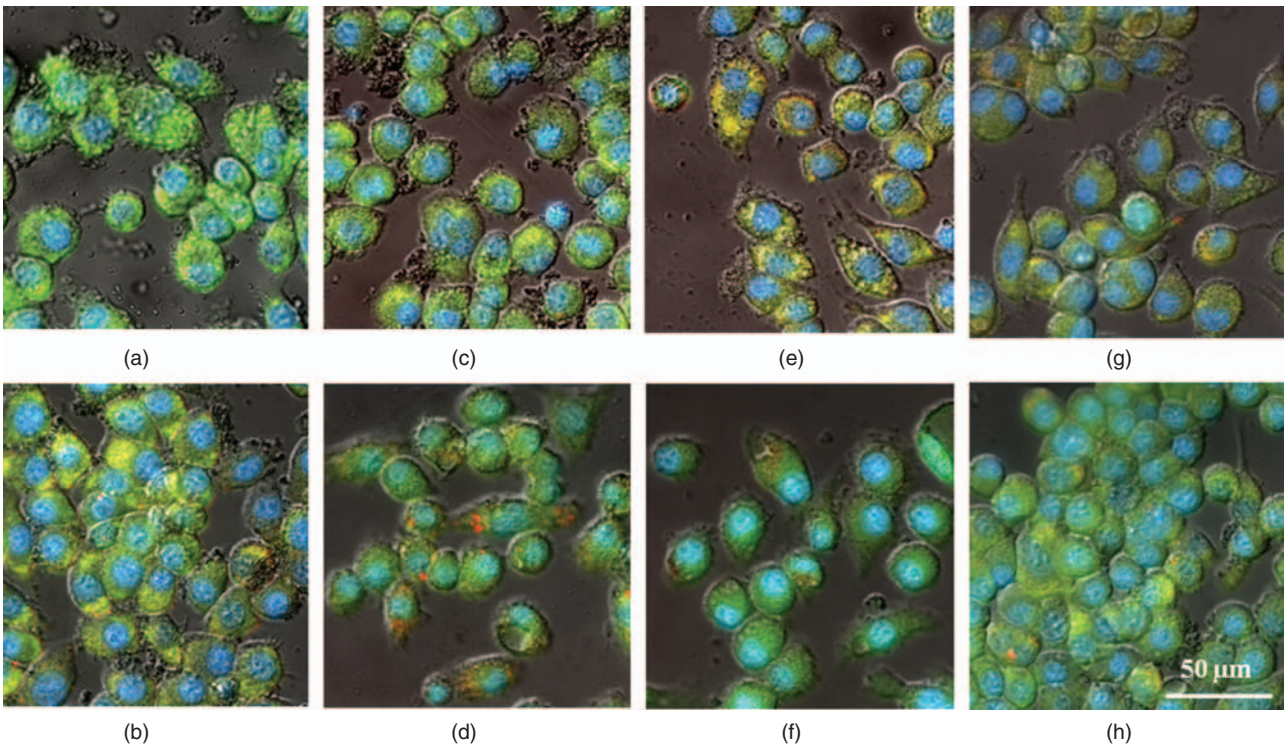

Figure 7. Fluorescence micrographs of murine J774.2 macrophages treated with (a), (b) PDMAAm-AMPA-γ-Fe_2O_3, (c), (d) PDMAAm-ABHA-γ-Fe_2O_3, (e), (f) PDMAAm-CCHPA-γ-Fe_2O_3 and (g), (h) neat γ-Fe_2O_3 nanoparticles for (a), (c), (e), (g) 1 h and (b), (d), (f), (h) 3 h. Double fluorescent staining with Acridine Orange and Hoechst 33342.

similar to that described above for the PDMAAm-AMPA-γ-Fe_2O_3 nanoparticles. After 1 h treatment, phagocytosis was initiated and the particles accumulated in the peripheral region of the cell cytoplasm and lysozymes (red clusters) were apparent (Fig. 7(c)). The main difference was that the number of clusters of activated lysosomes increased with time (1–3 h). Maximum granulation in the cytoplasm and an increase in the number and size of red fluorescent lysosomal clusters was observed after 3 h treatment (Fig. 7(d)). Besides, the size of cells "fed" with nanoparticles increased, few cells treated with the PDMAAm-ABHA-γ-Fe_2O_3 nanoparticles contained small transparent vacuoles in their cytosol (Fig. 7(d)).

The principal peculiarity of the engulfment of PDMAAm-CCHPA-γ-Fe_2O_3 nanoparticles by the J774.2 macrophages was the appearance of intracellular vacuoles as early as 30 min after the start of cell incubation in the presence of the nanoparticles. Figure 7(e) displays a red fluorescence in the lysosomes, transparent vacuoles in cytoplasm formed after 1 h treatment. The diffusive red discoloration within the cytoplasm indicated the beginning of phagocytosis. After 3 h treatment, giant vacuoles occupying most of the intracellular space were observed in some macrophages (Fig. 7(f)). The vacuoles contained associated lysosomal clusters. At the same time, the size of the PDMAAm-CCHPA-γ-Fe_2O_3 treated macrophages increased. Almost no free PDMAAm-CCHPA-γ-Fe_2O_3 nanoparticles remained in the culture medium.

As a control experiment, the engulfment of neat γ-Fe_2O_3 nanoparticles was investigated. The time dependence of the engulfment (Figs. 7(g), (h)) was similar to that for PDMAAm-CCHPA-γ-Fe_2O_3 nanoparticles. Within 1–3 h treatment, the number of vacuoles, their size, as well as the number of lysosomal clusters associated with large vacuoles, increased with time. Numerous unengulfed γ-Fe_2O_3 nanoparticles were accumulated on the surface of treated macrophages, while free γ-Fe_2O_3 nanoparticles were almost absent. The size of cells treated with γ-Fe_2O_3 nanoparticles was also increased.

After detecting significant vacuolization of J774.2 macrophages treated with neat γ-Fe_2O_3 and PDMAAm-CCHPA-γ-Fe_2O_3 nanoparticels, we tried to confirm the vacuolization in other non-phagocytary cells. Therefore, murine transformed fibroblasts of L929 line were cultured with γ-Fe_2O_3 and PDMAAm-CCHPA-γ-Fe_2O_3 nanoparticles and vacuolization of the cytosol was also found (data not shown).

Since morphological changes of treated J774.2 macrophages were best expressed after their 3 h treatment with the nanoparticles, this time period was selected for comparison of the engulfment by macrophages using different nanoparticles (Fig. 8). In the literature,[64, 65] the optimum time for the engulfment of natural objects (yeast cells) was found to be 60–90 min. Thus, the above mentioned cytomorphological changes (vacuole appearance in cytoplasm and/or activation of lysosomes) are probably the

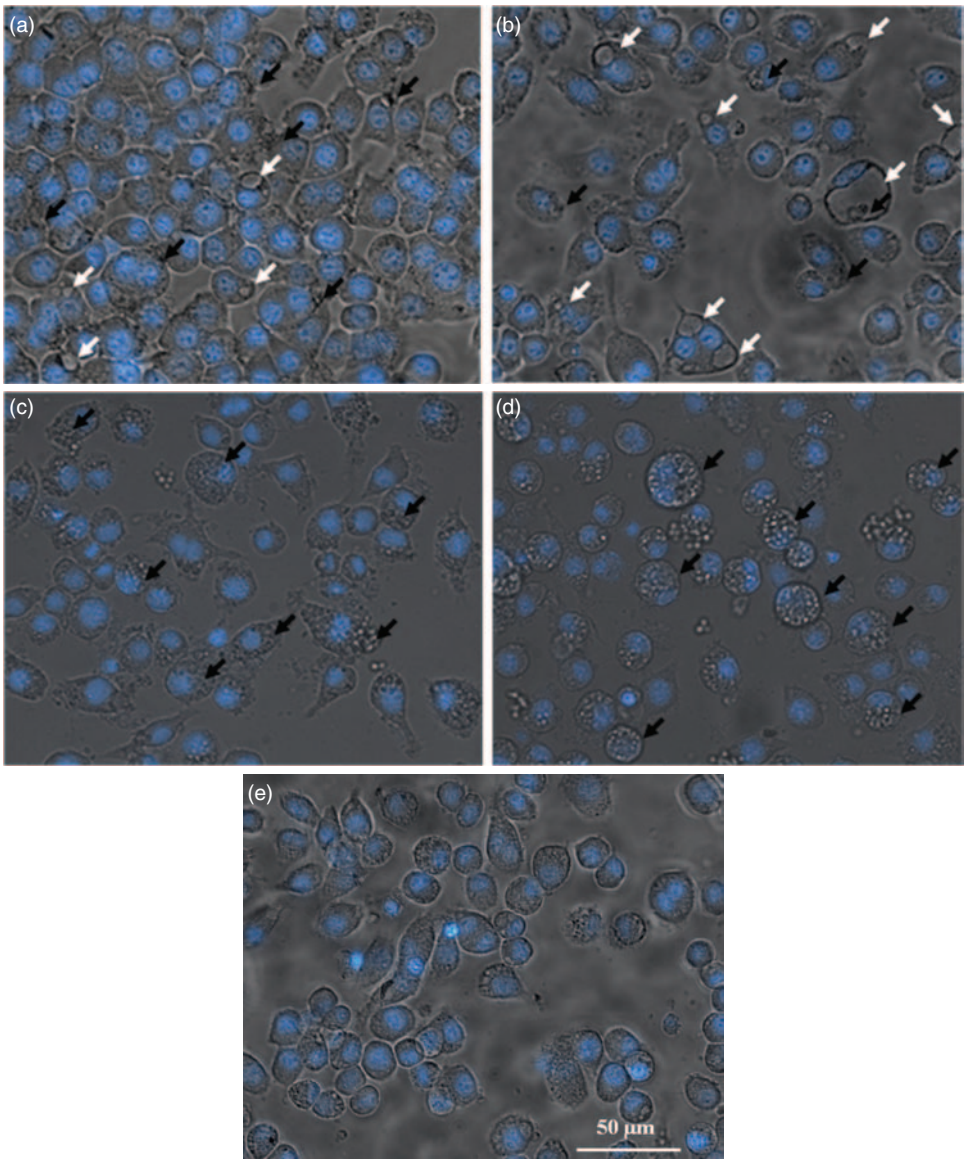

Figure 8. Engulfment of (a) neat γ-Fe_2O_3 nanoparticles, (b) PDMAAm-CCHPA-γ-Fe_2O_3, (c) PDMAAm-AMPA-γ-Fe_2O_3 and (d) PDMAAm-ABHA-γ-Fe_2O_3 by murine macrophages of J774.2 line; (e) control (no particles present). Conditions: 3 h cell incubation in the presence of nanoparticles suspension 1:200, combined light and fluorescence microscopy, staining of cell nuclei with Hoechst 33342. Black and white arrows show engulfed nanoparticles and intracellular vacuoles, respectively.

consequences of the engulfment of specific nanoparticles. Here, we revealed that chemical characteristics of the nanoparticle shell strongly affected the degree of expression of the changes in cell morphology. It was demonstrated that *in vitro* targeting of murine J774.2 macrophages with neat γ-Fe_2O_3 (Fig. 8(a)) and PDMAAm-CCHPA-γ-Fe_2O_3 nanoparticles (Fig. 8(b)), even after their opsonization with fetal bovine serum proteins, induced vacuolization in the cytoplasm of the treated cells and activation of the lysosomes in these cells. At the same time, two other types of superparamagnetic PDMAAm-coated γ-Fe_2O_3 nanoparticles, PDMAAm-AMPA- and PDMAAm-ABHA-γ-Fe_2O_3, were relatively non-toxic for the cultured murine macrophages (Figs. 8(c), (d)). Apparently, for the efficient particle engulfment by the macrophages, the presence of positively charged amidine and amidoxime groups in PDMAAm-AMPA- and PDMAAm-ABHA-γ-Fe_2O_3 nanoparticles, respectively, was superior to that of hydroxamate groups of PDMAAm-CCHPA-γ-Fe_2O_3. The efficiency of engulfment of the PDMAAm-AMPA-γ-Fe_2O_3 and PDMAAm-ABHA-γ-Fe_2O_3 nanoparticles was quite high since after 2 h treatment most cells engulfed the nanoparticles and only few nanoparticles remained in the culture medium. Fluorescence microscopy confirmed only weak activation of lysosomes, which manifested itself by a change in the color of Acridine Orange from green to red. Acridine Orange, a weakly basic amino dye, is known to be a lysosomotropic agent. In its stacked form,

i.e., in lysosomes, it emits red fluorescence, while in the cell nuclei at neutral pH it emits yellow–green fluorescence. Activation of macrophages during the engulfment of foreign extracellular materials is accompanied by an increase in the activity of digestive vacuoles and, thus, it should cause a red fluorescence shift due to accumulation of the dye in lysosomes. Activation of lysosomal compartments accompanies intracellular processing of the engulfed particles (microorganisms, viruses, damaged cells, and foreign macromolecules). Thus, chemical structure of neat (uncoated) γ-Fe_2O_3 and of PDMAAm-CCHPA-γ-Fe_2O_3 superparamagnetic nanoparticles (with hydroxamate groups) provided potential toxicity for the treated cells, which manifested itself by time-dependent evolution of vacuoles in the cell cytosol.

CONCLUSIONS

Superparamagnetic maghemite nanoparticles 9 nm in size have been prepared by coprecipitation of Fe^{2+} and Fe^{3+} salts with aqueous ammonia; the resulting magnetite was then oxidized with sodium hypochlorite to chemically stable maghemite. Three initiators, cationic AMPA and chelating ABHA and CCHPA, were investigated in terms of their ability to be attached to the γ-Fe_2O_3 surface. Due to the attraction of positively charged AMPA to negative charges of iron oxide surface and also due to chelation of γ-Fe_2O_3 with amidoxime and hydroxamate groups, AMPA-, ABHA- and CCHPA-modified nanoparticles were obtained as confirmed by ATR FTIR spectrometry. The morphology, size, polydispersity and zeta-potential of the nanoparticles were investigated by SEM, TEM and DLS measurements. Surface modification with three initiators did not substantially change physicochemical characteristics of the particles. The colloidal particles were stable in aqueous media.

In the next step, polymerization of DMAAm was initiated by surface-modified γ-Fe_2O_3 nanoparticles. The attachment of PDMAAm to AMPA-, ABHA- and CCHPA-γ-Fe_2O_3 particles was confirmed by ATR FTIR spectrometry and Fe analysis.

Since the biotargeting characteristics of engulfed particles are defined mainly by the biomolecules conjugated to their surface, it is desirable that the particle shell contains either membranotropic molecules like phospholipids, poly(ethylene glycol), or macromolecules (proteins) present in biological fluids. In this report, the surface of the formed nanoparticles was opsonized with proteins available in fetal bovine blood serum. As a result, the PDMAAm-AMPA-γ-Fe_2O_3 and PDMAAm-ABHA-γ-Fe_2O_3 nanoparticles were shown to be non-cytotoxic and they were intensively phagocytosized by the mammalian macrophages. The engulfment of superparamagnetic PDMAAm-AMPA-γ-Fe_2O_3, PDMAAm-ABHA-γ-Fe_2O_3 and PDMAAm-CCHPA-γ-Fe_2O_3 nanoparticles by murine J774.2 macrophages was compared with that of neat γ-Fe_2O_3 nanoparticles. While there was no irritation of the cells during effective phagocyting of PDMAAm-AMPA-γ-Fe_2O_3 and PDMAAm-ABHA-γ-Fe_2O_3 nanoparticles, time-dependent vacuolization in cytoplasm of the macrophages treated with neat γ-Fe_2O_3 and PDMAAm-CCHPA-γ-Fe_2O_3 nanoparticles was observed. Chemical properties of neat γ-Fe_2O_3 and PDMAAm-CCHPA-γ-Fe_2O_3 nanoparticles suggest that the negative charges of γ-Fe_2O_3 and anionic hydroxamate groups, which are absent in cationic PDMAAm-AMPA-γ-Fe_2O_3 and PDMAAm-ABHA-γ-Fe_2O_3 nanoparticles, could be responsible for such irritation of the living cells. In contrast, cationic groups in AMPA and ABHA of PDMAAm-AMPA-γ-Fe_2O_3 and PDMAAm-ABHA-γ-Fe_2O_3 did not invoke any cytotoxicity effects.

In summary, a high potential of PDMAAm-AMPA-γ-Fe_2O_3 and PDMAAm-ABHA-γ-Fe_2O_3 nanoparticles in diagnosis of phagocytary activity as well as in delivery of various biomolecules, such as specific proteins, can be predicted. The superparamagnetic γ-Fe_2O_3 nanoparticles are promising in cell applications as the cells labeled with the nanoparticles can be non-invasively monitored and easily magnetically separated and redispersed in water solutions on removing the external magnetic field.

Acknowledgment: The financial support of the Grant Agency of the Czech Republic (project P206/12/0381) and the European Commission (NaDiNe project No. 246513) is gratefully acknowledged.

REFERENCES

1. A. H. Lu, E. L. Salabas, and F. Schüth, Magnetic nanoparticles: Synthesis, protection, functionalization, and application. *Angew. Chem. Int. Ed.* 46, 1222 (**2007**).
2. M. Hofmann-Amtenbrink, H. Hofmann, and X. Montet, Superparamagnetic nanoparticles—A tool for early diagnostics. *Swiss. Med. Weakly* 140, w13081 (**2010**).
3. M. Namdeo, S. Saxena, R. Tankhiwale, M. Bajpai, Y. M. Mohan, and S. K. Bajpai, Magnetic nanoparticles for drug delivery applications. *J. Nanosci. Nanotechnol.* 8, 3247 (**2008**).
4. A. S. Teja and P. Y. Koh, Synthesis, properties, and applications of magnetic iron oxide nanoparticles. *Prog. Cryst. Growth Charact. Mater.* 55, 22 (**2009**).
5. H. J. Lee, Y. T. Nguyen, M. Muthiah, H. Vu-Quang, R. Namgung, W. J. Kim, M. K. Yu, S. Jon, I. K. Lee, Y. Y. Jeong, and I. K. Park, MR traceable delivery of p53 tumor suppressor gene by PEI-functionalized superparamagnetic iron oxide nanoparticles. *J. Biomed. Nanotechnol.* 8, 361 (**2012**).
6. F. Gazeau, M. Lévy, and C. Wilhelm, Optimizing magnetic nanoparticle design for nanothermotherapy. *Nanomedicine* 3, 831 (**2008**).
7. C. Sun, J. S. H. Lee, and M. Q. Zhang, Magnetic nanoparticles in MR imaging and drug delivery. *Adv. Drug Delivery Rev.* 60, 1252 (**2008**).
8. S. A. Corr, Y. P. Rakovich, and Y. K. Gun'Ko, Multifunctional magnetic-fluorescent nanocomposites for biomedical applications. *Nanoscale Res. Lett.* 3, 87 (**2008**).

9. A. Jordan, R. Scholz, P. Wust, H. Fähling, and R. Felix, Magnetic fluid hyperthermia (MFH): Cancer treatment with AC magnetic field induced excitation of biocompatible superparamagnetic nanoparticles. *J. Magn. Magn. Mater.* 201, 413 **(1999)**.

10. P. Baldrian, V. Merhautova, J. Gabriel, F. Nerud, P. Stopka, M. Hruby, and M. J. Benes, Decolorization of synthetic dyes by hydrogen peroxide with heterogeneous catalysis by mixed iron oxides. *Appl. Catal. B* 66, 258 **(2006)**.

11. Z. Roveimiab, A. R. Mahdavian, E. Biazar, and K. S. Heidari, Preparation of magnetic chitosan nanocomposite particles and their susceptibility for cellular separation applications. *J. Colloid Sci. Biotechnol.* 1, 82 **(2012)**.

12. M. A. M. Gijs, F. Lacharme, and U. Lehmann, Microfluidic applications of magnetic particles for biological analysis and catalysis. *Chem. Rev.* 110, 1518 **(2010)**.

13. E. Erdal, D. Kavaz, M. Sam, M. Demirbilek, E. M. Demirbilek, N. Saglam, and E. B. Denkbas, Preparation and characterization of magnetically responsive bacterial polyester based nanospheres for cancer therapy. *J. Biomed. Nanotechnol.* 8, 800 **(2012)**.

14. H. Qu, D. Caruntu, H. Liu, and C. J. O'Connor, Water-dispersible iron oxide magnetic nanoparticles with versatile surface functionalities. *Langmuir* 27, 2271 **(2011)**.

15. A. K. Gupta, R. R. Naregalkar, V. D. Vaidya, and M. Gupta, Recent advances on surface engineering of magnetic iron oxide nanoparticles and their biomedical applications. *Nanomedicine* 2, 23 **(2007)**.

16. Z. L. Zhao, Z. Y. Bian, L. X. Chen, X. W. He, and Y. F. Wang, Synthesis and surface-modifications of iron oxide magnetic nanoparticles and applications on separation and analysis. *Prog. Chem.* 18, 1288 **(2006)**.

17. H. Mouaziz, R. Veyret, A. Theretz, F. Ginot, and A. Elaissari, Aminodextran containing magnetite nanoparticles for molecular biology applications: Preparation and evaluation. *J. Biomed. Nanotechnol.* 5, 172 **(2009)**.

18. W. Yantasee, C. L. Warner, T. Sangvanich, R. S. Addleman, T. G. Carter, R. J. Wiacek, G. E. Fryxell, C. Timchalk, and M. G. Warner, Removal of heavy metals from aqueous systems with thiol functionalized superparamagnetic nanoparticles. *Environ. Sci. Technol.* 41, 5114 **(2007)**.

19. Y. Lalatonne, C. Paris, J. M. Serfaty, P. Weinmann, M. Lecouvey, and L. Motte, Bis-phosphonates-ultra small superparamagnetic iron oxide nanoparticles: A platform towards diagnosis and therapy. *Chem. Commun.* 22, 2553 **(2008)**.

20. K. M. Ho, W. Y. Li, C. H. Wong, and P. Li, Amphiphilic polymeric particles with core–shell nanostructures: Emulsion-based syntheses and potential applications. *Colloid Polym. Sci.* 288, 1503 **(2010)**.

21. S. Edmondson, V. L. Osborne, and W. T. Huck, Polymer brushes via surface-initiated polymerizations. *Chem. Soc. Rev.* 33, 14 **(2004)**.

22. E. Marutani, S. Yamamoto, T. Ninjbadgar, Y. Tsujii, T. Fukuda, and M. Takano, Surface-initiated atom transfer radical polymerization of methyl methacrylate on magnetite nanoparticles. *Polymer* 45, 2231 **(2004)**.

23. S. M. Gravano, R. Dumas, K. Liu, and T. E. Patten, Methods for the surface functionalization of gamma-Fe_2O_3 nanoparticles with initiators for atom transfer radical polymerization and the formation of core–shell inorganic-polymer structures. *J. Polym. Sci., Part A: Polym. Chem.* 43, 3675 **(2005)**.

24. L. J. An, Z. Q. Li, Z. Wang, J. H. Zhang, and B. Yang, Bifunctional Fe_3O_4/CdS nanocomposites synthesized by surface-initiated atom transfer radical polymerization. *Chem. Lett.* 34, 652 **(2005)**.

25. S. J. Ding, Y. C. Xing, M. Radosz, and Y. Q. Shen, Magnetic nanoparticle supported catalyst for atom transfer radical polymerization. *Macromolecules* 39, 6399 **(2006)**.

26. I. Garcia, A. Tercjak, N. E. Zafeiropoulos, M. Stamm, and I. Mondragon, Generation of core/shell iron oxide magnetic nanoparticles with polystyrene brushes by atom transfer radical polymerization. *J. Polym. Sci., Part A: Polym. Chem.* 45, 4744 **(2007)**.

27. Q. L. Fan, K. G. Neoh, E. T. Kang, B. Shuter, and S. C. Wang, Solvent-free atom transfer radical polymerization for the preparation of poly(poly(ethyleneglycol) monomethacrylate)-grafted Fe_3O_4 nanoparticles: Synthesis, characterization and cellular uptake. *Biomaterials* 28, 5426 **(2007)**.

28. A. Kaiser, S. Dutz, and A. M. Schmidt, Kinetic studies of surface-initiated atom transfer radical polymerization in the synthesis of magnetic fluids. *J. Polym. Sci., Part A: Polym. Chem.* 47, 7012 **(2009)**.

29. A. A. H. Abdel-Rahman, A. M. Atta, I. E. El Aassy, F. Y. Ahmed, and M. F. Hamza, Studies on the uptake of uranium(VI) ions on polyacrylamidoxime resins synthesized by free radical polymerization with different crosslinking ratios and pore solvents. *J. Dispersion Sci. Technol.* 32, 224 **(2011)**.

30. L. Tofan, C. Paduraru, I. Crefescu, A. Ceica, and V. Neagu, Chelating sorbent containing two types of functional groups—Hydroxamic acid and amidoxime for lead(II) ions effluent management. *Environ. Eng. Management J.* 9, 113 **(2010)**.

31. B. Gao, Y. Gao, and Y. Li, Preparation and chelation adsorption property of composite chelating material poly(amidoxime)/SiO_2 towards heavy metal ions. *Chem. Eng. J.* 158, 542 **(2010)**.

32. Y. Dong, Z. Han, C. Liu, and F. Du, Preparation and photocatalytic performance of Fe(III)-amidoximated PAN fiber complex for oxidative degradation of azo dye under visible light irradiation. *Sci. Total. Environ.* 408, 2245 **(2010)**.

33. A. H. A. R. Adel, E. E. A. Ibrahim, Y. A. Fadia, and F. H. Mohammed, Studies on the uptake of rare earth elements on polyacrylamidoxime resins from natural concentrate leachate solutions. *J. Dispersion Sci. Technol.* 31, 1128 **(2010)**.

34. W. Ngeontae, W. Aeungmaitrepirom, T. Tuntulani, and A. Imyim, Highly selective preconcentration of Cu(II) from seawater and water samples using amidoamidoxime silica. *Talanta* 78, 1004 **(2009)**.

35. M. J. Haron, M. Tiansih, N. A. Ibrahim, A. Kassim, and W. M. Z. W. Yunus, Sorption of Cu(II) by poly(hydroxamic acid) chelating exchanger prepared from poly(methyl acrylate) grafted oil palm empty fruit bunch (OPEFB). *BioResources* 4, 1305 **(2009)**.

36. S. Das, A. K. Pandey, A. A. Athawale, and V. K. Manchanda, Exchanges of uranium(VI) species in amidoxime-functionalized sorbents. *J. Phys. Chem. B* 113, 6328 **(2009)**.

37. N. Beckmann, C. Cannet, M. Fringeli-Tanner, D. Baumann, C. Pally, C. Bruns, H. G. Zerwes, E. Andriambeloson, and M. Bigaud, Macrophage labeling by SPIO as an early marker of allograft chronic rejection in a rat model of kidney transplantation. *Magn. Reson. Med.* 49, 459 **(2003)**.

38. C. Tassa, S. Y. Shaw, and R. Weissleder, Dextran-coated iron oxide nanoparticles: A versatile platform for targeted molecular imaging, molecular diagnostics, and therapy. *Acc. Chem. Res.* 44, 842 **(2011)**.

39. M. M. Welling, M. Duijvestein, A. Signore, and L. van der Weerd, *In vivo* biodistribution of stem cells using molecular nuclear medicine imaging. *J. Cell Physiol.* 226, 1444 **(2011)**.

40. J. Xie, G. Liu, H. S. Eden, H. Ai, and X. Y. Chen, Surface-engineered magnetic nanoparticle platforms for cancer imaging and therapy. *Acc. Chem. Res.* 44, 883 **(2011)**.

41. L. Zhou, J. Yuan, and Y. Wei, Core–shell structural iron oxide hybrid nanoparticles: From controlled synthesis to biomedical applications. *J. Mater. Chem.* 21, 2823 **(2011)**.

42. C. Tu, T. S. Ng, H. K. Sohi, H. A. Palko, A. House, R. E. Jacobs, and A. Y. Louie, Receptor-targeted iron oxide nanoparticles for molecular MR imaging of inflamed atherosclerotic plaques. *Biomaterials* 32, 7209 **(2011)**.

43. N. Beckmann, C. Gerard, D. Abramowski, C. Cannet, and M. Staufenbiel, Noninvasive magnetic resonance imaging detection of cerebral amyloid angiopathy-related microvascular alterations using superparamagnetic iron oxide particles in app transgenic mouse models of Alzheimer's disease: Application to passive abeta immunotherapy. *J. Neurosci.* 31, 1023 **(2011)**.

44. J. N. Kizhakkedathu and D. E. Brooks, Synthesis of poly(*N*,*N*-dimethylacrylamide) brushes from charged polymeric surfaces by aqueous ATRP: Effect of surface initiator concentration. *Macromolecules* 36, 591 **(2003)**.
45. L. Ma, M. Liu, H. Liu, J. Chen, and D. Cui, *In vitro* cytotoxicity and drug release properties of pH- and temperature-sensitive core–shell hydrogel microspheres. *Int. J. Pharm.* 385, 86 **(2010)**.
46. S. Mornet, S. Vasseur, F. Grasset, and E. Duguet, Magnetic nanoparticle design for medical diagnosis and therapy. *J. Mater Chem.* 14, 2161 **(2004)**.
47. Q. A. Pankhurst, J. Connolly, S. K. Jones, and J. Dobson, Applications of magnetic nanoparticles in biomedicine. *J. Phys. D: Appl. Phys.* 36, R167 **(2003)**.
48. A. S. Lübbe, C. Bergemann, H. Riess, F. Schriever, P. Reichardt, K. Possinger, M. Matthias, B. Dörken, F. Herrmann, R. Gürtler, P. Hohenberger, N. Haas, R. Sohr, B. Sander, A. J. Lemke, D. Ohlendorf, W. Huhnt, and D. Huhn, Clinical experiences with magnetic drug targeting: A phase I study with 4′-epidoxorubicin in 14 patients with advanced solid tumors. *Cancer Res.* 57, 3063 **(1997)**.
49. A. K. Gupta and M. Gupta, Synthesis and surface engineering of iron oxide nanoparticles for biomedical applications. *Biomaterials* 26, 3995 **(2005)**.
50. M. Shinkai, Functional magnetic particles for medical application. *J. Biosci. Bioeng.* 94, 606 **(2002)**.
51. J. Thiele and K. Heuser, Uber Hydrazinderivate der Isobuttersäure. *Justus Liebigs Ann. Chem.* 290, 1 **(1896)**.
52. H. Takeuchi, T. Ito, and Y. Kojima, Polymerization of acrylic acid and derivatives thereof using azoamidoxime salt. U.S. Patent 5,563,276 **(1996)**.
53. Y. Kasai, T. Tanimura, and Z. Tamura, Spectrophotometric determination of carboxylic acids by the formation of hydroxamic acids with dicyclohexylcarbodiimide. *Anal. Chem.* 47, 34 **(1975)**.
54. C. Franzblau, P. M. Gallop, and S. Seifter, The presence in collagen of γ-glutamyl peptide linkages. *Biopolymers* 1, 79 **(1963)**.
55. M. Babič, D. Horák, M. Trchová, P. Jendelová, K. Glogarová, P. Lesný, V. Herynek, M. Hájek, and E. Syková, Poly(L-lysine)-modified iron oxide nanoparticles for stem cell labeling. *Bioconjugate Chem.* 19, 740 **(2008)**.
56. D. E. Koppel, Analysis of macromolecular polydispersity in intensity correlation spectroscopy: The method of cumulants. *J. Chem. Phys.* 57, 4814 **(1972)**.
57. J. Pouchlý, Physical Chemistry of Macromolecular and Colloidal Systems, Institute of Chemical Technology, Prague **(2001)**.
58. L. C. Li and Y. Tian, Encyclopedia of pharmaceutical technology, edited by J. Swarbrick and J. C. Boylan, Marcel Dekker, New York **(2002)**, pp. 3020–3032.
59. M. Babiè, D. Horák, P. Jendelová, K. Glogarová, V. Herynek, M. Trchová, K. Likavèanová, M. Hájek, and E. Syková, Poly(*N*,*N*-dimethylacrylamide)-coated maghemite nanoparticles for stem cell labeling. *Bioconjugate Chem.* 20, 283 **(2009)**.
60. Y. Boguslavsky and S. Margel, Synthesis and characterization of poly(divinylbenzene)-coated magnetic iron oxide nanoparticles as precursor for the formation of air-stable carbon-coated iron crystalline nanoparticles. *J. Colloid Interface Sci.* 317, 101 **(2008)**.
61. D. J. Siegwart, O. J. Kwon, and K. Matyjaszewski, ATRP in the design of functional materials for biomedical applications. *Prog. Polym. Sci.* 37, 18 **(2012)**.
62. L. G. Bach, R. Md Islam, T. J. Kim, S. Seo, and K. T. Lim, Encapsulation of Fe_3O_4 magnetic nanoparticles with poly(methyl methacrylate) via surface functionalized thiol-lactam initiated radical polymerization. *Appl. Surf. Sci.* 258, 2959 **(2012)**.
63. D. Horák, T. Shagotova, N. Mitina, M. Trchová, N. Boiko, M. Babič, R. Stoika, J. Kovářová, O. Hevus, M. Beneš, O. Klyuchivska, P. Holler, and A. Zaichenko, Surface-initiated polymerization of 2-hydroxyethyl methacrylate from heterotelechelic oligoperoxide-coated γ-Fe_2O_3 nanoparticles and their engulfment by mammalian cells. *Chem. Mater.* 23, 2637 **(2011)**.
64. R. S. Stoika, N. I. Kashchak, M. D. Lutsik-Kordovsky, M. Boyko, M. L. Barska, and A. Tsyrulnyk, *In vitro* response of phagocytic cells to immunomodulating agents. *Med. Sci. Monitor* 7, 652 **(2001)**.
65. R. S. Stoika, M. D. Lutsik-Kordovsky, M. L. Barska, and A. O. Tsyrulnyk, *In vitro* studies of activation of phagocytic cells by bioactive peptides. *J. Physiol. Pharmacol.* 53, 675 **(2002)**.

Publication No. 2

Article

Journal of Nanopharmaceutics and Drug Delivery
Vol. 1, 1–11, 2013
www.aspbs.com/jnd

Silica-Coated γ-Fe_2O_3 Nanoparticles: Preparation and Engulfment by Mammalian Macrophages

Beata Anna Zasońska[1], Nataliya Boiko[2], Olga Klyuchivska[2], Miroslava Trchová[1], Eduard Petrovský[3], Rostyslav Stoika[2], and Daniel Horák[1,*]

[1] *Institute of Macromolecular Chemistry, Academy of Sciences of the Czech Republic, Heyrovského Sq. 2, 162 06 Prague 6, Czech Republic*
[2] *Institute of Cell Biology, National Academy of Sciences of Ukraine, Drahomanov St., 14/16, 79005, Lviv, Ukraine*
[3] *Institute of Geophysics, Academy of Sciences of the Czech Republic, Boční II/1401, 141 31 Prague 4, Czech Republic*

Maghemite (γ-Fe_2O_3) nanoparticles were prepared by coprecipitation of Fe(II) and Fe(III) salts followed by oxidation of Fe_3O_4 with sodium hypochlorite. The γ-Fe_2O_3 nanoparticles were then coated by a silica shell using tetramethyl orthosilicate producing γ-Fe_2O_3@SiO_2 particles. In order to introduce amino groups, the surface of the γ-Fe_2O_3@SiO_2 particles was coated with a second silica shell using (3-aminopropyl)triethoxysilane, resulting in γ-Fe_2O_3@SiO_2-NH_2 nanoparticles. The particles were characterized by scanning and transmission electron microscopy (SEM and TEM), dynamic light scattering (DLS) and Fourier-transform infrared (FT-IR) spectroscopy in terms of determination of morphology, particle size, polydispersity and presence of functional groups. Atomic absorption spectroscopy (AAS) was used for determination of the iron content. Moreover, induced magnetization and temperature-dependent magnetic susceptibility were investigated. In the biological experiments, γ-Fe_2O_3@SiO_2 and γ-Fe_2O_3@SiO_2-NH_2 nanoparticles were incubated with murine macrophages of J774.2 line and the uptake of particles by the cells was visualized using both light and fluorescence microscopy. The silica surface coating did not affect the nanoparticle uptake by the cells, however, it decreased induced cytoplasmic vacuolization of macrophages.

KEYWORDS: *Maghemite, Nanoparticles, Silica, Engulfment, Macrophages.*

INTRODUCTION

Recently, nanoparticles find widespread applications, in particular in biomedicine and biotechnology, including cellular therapy, cell labeling,[1] drug delivery,[2] separation and purification of cell populations.[3] Compared with micrometer-sized particles, nanoparticles have an advantage that they possess a large specific surface area available for coupling sufficient amounts of diagnostic or therapeutic agents. Functionalized iron oxide nanoparticles are often used as diagnostic agents and for site-specific drug delivery due to their biocompatibility (non-toxicity) and superparamagnetic behavior.[4] After the intracellular uptake, the iron oxide nanoparticles are metabolized in the lysosomes into a soluble, non-superparamagnetic form of iron that becomes a part of the normal iron pool (e.g., ferritin, hemoglobin).[5] However, neat iron oxide nanoparticles possess relatively low colloidal stability (in particular at higher concentrations, depending on pH), tend to aggregate[6] and have high nonspecific binding, for example, of various proteins, antibodies, and other biomolecules. Moreover, their half-life in blood has to be prolonged to improve the likelihood of reaching target cells. It is therefore important to modify the iron oxide nanoparticle surface by reagents containing carboxyl groups, phosphonates and sulfates to improve both their stability and biocompatibility.[7] Conventional modification agents include dextran,[8] chitosan,[9] starch,[10] poly(ethylene glycol),[11] poly(vinyl alcohol),[12] polyethyleneimine.[9,13–15] Iron oxide nanoparticles can be also coated with inorganic compounds, such as silica.

Silica renders hydrophobic iron oxide nanoparticles with water dispersibility and, moreover, surface silanol groups offer the possibility of additional functionalization. Silica is biocompatible, optically transparent and relatively

*Author to whom correspondence should be addressed.
Email: horak@imc.cas.cz
Received: 7 March 2013
Revisied/Accepted: 5 June 2013

environmentally inert, with minimum non-specific protein adsorption; silica does not tend to be the subject of microbial attacks. Last but not least, silica is highly chemically and thermally stable.[16] Many methods to coat iron oxide nanoparticles with silica include reverse microemulsion,[17] hydrolysis of tetraethoxysilane in the presence of seeds,[17] aerosol pyrolysis[18] and sol–gel processes using organosilanes, such as tetraethyl orthosilicate (TEOS), (3-aminopropyl)triethoxysilane (APTES) or (3-aminopropyl)trimethoxysilane (APTMS).[19–21] Silica-coated iron oxide nanoparticles have advantage of regular spherical shape and also possess a porosity and allow immobilization, e.g., of proteins while reducing diffusional limitations of both reactants and products.

The aim of the present report was to synthesize and characterize unmodified and amino groups-modified γ-Fe_2O_3@SiO_2 nanoparticles, and to test their interaction with the mammalian cells. Macrophages are typically involved in the uptake of various particles, including pathogens, and cell residues. Macrophages are known to contribute to inflammation which plays a central pathophysiological role in a large number of diseases including atherosclerosis, myocardial infarction, pneumonia, bacterial abscess formation, peripheral nerve injury and rejection of donor organs after transplantation.[22] Macrophage imaging thus may identify sub-clinical inflamed lesions, predict future risk, and aid in the assessment of novel therapies.[23] A possibility to track the macrophages *in vivo* will allow monitoring the immune response,[24] as well as getting an insight into the development of different pathological states in the organism.[25] Here, we studied the uptake of the developed silica-coated superparamagnetic nanoparticles by the mammalian macrophages. We have demonstrated that the particles were intensively engulfed by the treated macrophages, and silica coating of the nanoparticles significantly improved their properties decreasing induced cytoplasmic vacuolization of the macrophages. Macrophages labeled with silica-coated iron oxide nanoparticles can be then easily visualized by the magnetic resonance imaging (MRI).

EXPERIMENTAL DETAILS

Materials

Tetramethyl orthosilicate (TMOS) and 3-aminopropyltriethoxysilane (APTES) were from Sigma-Aldrich (Steinheim, Germany). Ammonium hydroxide was from Lach-Ner (Neratovice, Czech Republic), $FeCl_2{\cdot}4H_2O$, $FeCl_3{\cdot}6H_2O$ were purchased from Fluka (Buchs, Switzerland). Sodium hypochlorite (NaClO) solution (5 wt.%) was from Bochemie (Bohumín, Czech Republic). Solvents (2-propanol, ethanol) were from Lach-Ner (Neratovice, Czech Republic). Ultrapure Q-water ultrafiltered on a Milli-Q Gradient A10 system (Millipore, Molsheim, France) was used for preparation of the solutions.

Preparation of Maghemite (γ-Fe_2O_3) Nanoparticles

Iron oxide nanoparticles were prepared by modification of previously described method[26] from iron (III) chloride and iron (II) chloride. 0.2 M aqueous $FeCl_3$ solution (100 ml), 0.2 M aqueous $FeCl_2$ solution (50 ml) and 0.5 M aqueous NH_4OH solution (100 ml) were sonicated (Sonicator W-385; Heat Systems-Ultrasonics; Farmingdale, USA) for 5 min. The mixture was added to 3.3 wt.% NH_4OH solution (460 ml) and stirred at 23 °C for 1 h (200 rpm). Magnetite was magnetically separated and washed by Q-water until peptization and sonicated with 5 wt.% sodium hypochlorite solution (16 ml) for 5 min. Again, the precipitate was magnetically separated and repeatably washed with Q-water until formation of γ-Fe_2O_3 colloid. The final concentration of γ-Fe_2O_3 was fixed to 50 mg of γ-Fe_2O_3 per ml.

Preparation of γ-Fe_2O_3@SiO_2 Nanoparticles

Silica shell on the particles was prepared by modification of an earlier published procedure[27] based on Stöber method[28] using hydrolysis and condensation of TMOS. In a typical experiment, solution containing 2-propanol (24 ml), water (6 ml) and 25 wt.% ammonia (1.5 ml) was mixed with a γ-Fe_2O_3 colloid (1 ml; 50 mg γ-Fe_2O_3) for 5 min. TMOS (0.2 ml) was added and the mixture stirred (400 rpm) at 50 °C for 16 h. The resulting colloidal solution (γ-Fe_2O_3@SiO_2) was then three times washed with ethanol using magnetic separation. If the γ-Fe_2O_3@SiO_2 particles were analyzed by analytical methods, they were dried in an oven at 100 °C for 3 h; for modification reactions and biological experiments, the particles were stored as a colloid.

Preparation of γ-Fe_2O_3@SiO_2-NH_2 Nanoparticles

Amino group-functionalized particles were prepared by modification of γ-Fe_2O_3@SiO_2 nanoparticles with APTES. Briefly, γ-Fe_2O_3@SiO_2 nanoparticles were dispersed in ethanol (50 ml) under sonication for 15 min and solution of APTES (0.15 ml) in ethanol (20 ml) and water (1 ml) was added. The mixture was stirred using an anchor-type stirrer (400 rpm) at 50 °C for 7 h. After completion of the reaction, the resulting γ-Fe_2O_3@SiO_2-NH_2 particles were washed as described above.

Characterization of the Nanoparticles

The synthesized nanoparticles were characterized by a Quanta 200 F scanning (SEM; FEI Brno, Czech Republic) and a Tecnai Spirit G2 transmission electron microscope (TEM; FEI) and number- (D_n) and weight-average particle diameter (D_w) and polydispersity index (PDI = D_w/D_n) calculated. The hydrodynamic particle size (D_h) of γ-Fe_2O_3 and γ-Fe_2O_3@SiO_2 and polydispersity PI was also determined by dynamic light scattering (DLS) using a Zetasizer Nano-ZS Model ZEN3600 instrument

(Malvern Instruments; Malvern, UK). Fourier-transform infrared measurement (FT-IR) was performed in an attenuated total reflection (ATR) mode using a Thermo Nicolet NEXUS 870 FT-IR Spectrometer (Madison, WI, USA). Spectra of the powdered samples were measured with Golden Gate™ Heated Diamond ATR Top-Plate (MKII single reflection ATR system; Specac; Orpington, UK). Nitrogen content was determined on a Perkin-Elmer 2400 CHN elemental analyzer (Waltham, MA, USA). Magnetization curves were measured at room temperature using an EV9 vibrating-sample magnetometer (DSM Magnetics; ADE Corporation, Lowell, MA, USA) with the maximum magnetic field of 2 T. The temperature dependence of magnetic susceptibility, κ, was measured from liquid nitrogen temperature (77 K) to *ca*. 1000 K using a KLY-4S/CS-3 kappabridge (AGICO; Brno, Czech Republic) according to a previously described procedure.[29] The measurements were carried out in an ambient atmosphere; the heating rate was 8.5 K min^{-1}.

Cell Experiments

Cell Culture

Murine macrophages of J774.2 line were obtained from the William Harvey Institute (London, UK). Cells were cultured in Dulbecco's modified Eagle's medium (DMEM; Sigma, St. Louis, USA) supplemented with 10% fetal bovine serum (FBS; Sigma). Cells were kept in incubator in 5% CO_2 atmosphere at 37 °C and 100% humidity.

Phagocytosis of Magnetic Nanoparticles by Macrophages

Murine macrophages J774.2 were seeded for 24 h on the glass microscope slides and allowed to attach. Suspension of the neat γ-Fe_2O_3, γ-Fe_2O_3@SiO_2 and γ-Fe_2O_3@SiO_2-NH_2 nanoparticles was then added to the DMEM medium in which macrophages of J774.2 line were cultured to reach concentration 0.005 mg γ-Fe_2O_3@SiO_2/ml. To engulf the particles by macrophages, the cultures were kept at 37 °C for 3 h in the incubator under 5% CO_2 atmosphere. The engulfment of neat γ-Fe_2O_3 nanoparticles and the culture medium without particles were used as controls.

Light and Fluorescence Microscopy

Cells were stained with Acridine Orange and Hoechst 33342 and observed under a Carl Zeiss AxioImager A1 light and fluorescence microscope (Carl Zeiss, Germany). Final concentration of both fluorescent dyes equaled to 0.3 μg/ml and the staining time was 15 min. For Hoechst 33342, the excitation and emission wavelengths were 365–395 nm and 445–450 nm, respectively. The excitation and emission wavelengths for Acridine Orange were 470–495 nm and 525–550 nm, respectively, with green filter and 546–560 nm and 575–640 nm, respectively, with red filter. Cells were photographed in microscope with a digital camera (Carl Zeiss, Germany).

Statistically significant differences ($P < 0.05$) were determined using a two-sided Student's *t*-test.

RESULTS AND DISCUSSION

Preparation and Characterization of γ-Fe_2O_3@SiO_2-NH_2 Nanoparticles

As magnetite (Fe_3O_4) nanoparticles in biological solutions are known to be prone to uncontrolled oxidation resulting in non-magnetic iron oxides,[30] in this report, maghemite (γ-Fe_2O_3) was preferred for biological experiments since it is chemically more stable in air or water and does not change its properties as easily as Fe_3O_4. However, in the synthesis of the nanoparticles, Fe_3O_4 nanoparticles were obtained first by modification of conventional coprecipitation of Fe(II) and Fe(III) salts with ammonia[27] which was followed by fast controlled oxidation of Fe_3O_4 with a commonly used oxidant, such as NaClO, to obtain γ-Fe_2O_3 nanoparticles. Magnetic behavior of neat γ-Fe_2O_3 at room temperature was evaluated by vibrating sample magnetometer (VSM). Saturation magnetization (M_s) of γ-Fe_2O_3 nanoparticles was found to be 56.5 emu/g (Fig. 1), which was lower than that of bulk maghemite ($M_s = 74$ emu/g).[31] This may be explained by the fact that the material is not pure maghemite due to various surface effects and imperfections in the crystal structure that are typical for nanoparticles.[32] The presence of imperfections is supported also by subtle values of coercivity (1.1 mT) and remanent magnetization (1.15 emu/g). Presence of maghemite was confirmed by the thermomagnetic curve (Fig. 2), which was, upon heating, completely transformed to poorly magnetic (antiferromagnetic) hematite (low susceptibility during cooling and anomaly corresponding to Neel temperature at about 760 °C).

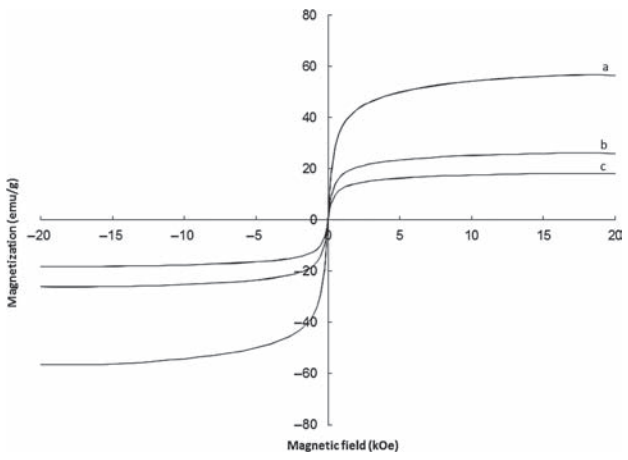

Figure 1. Magnetization curves of (a) initial γ-Fe_2O_3, (b) γ-Fe_2O_3@SiO_2 C and (c) γ-Fe_2O_3@SiO_2-NH_2 particles; measured at room temperature.

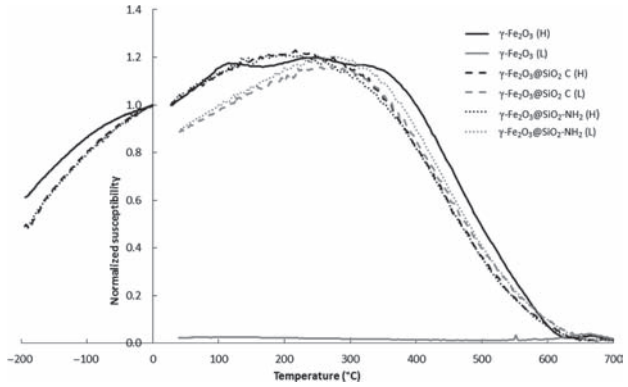

Figure 2. Temperature dependence of magnetic susceptibility of γ-Fe_2O_3, γ-Fe_2O_3@SiO_2 C and γ-Fe_2O_3@SiO_2-NH_2 nanoparticles. "H" and "L" stand for high and low temperature analysis, respectively.

For modification of γ-Fe_2O_3 nanoparticles with alkoxysilanes, TMOS was selected as a silica precursor, since it is more reactive than TEOS,[33] and 2-propanol as a solvent.[34] Optionally, γ-Fe_2O_3@SiO_2 nanoparticles were further modified with APTES to introduce amino groups available for prospective attachment of the required target biomolecules. In the presence of γ-Fe_2O_3 nanoparticles, the condensation occurred between the silanol group and the iron hydroxyl groups present on the surface of the oxide particles (Fig. 3). Formation of silica-coated γ-Fe_2O_3 (γ-Fe_2O_3@SiO_2) nanoparticles depended on pH, concentrations of γ-Fe_2O_3, 2-propanol and ammonia and on the amount and the rate of TMOS addition. At acidic conditions (pH = 3), mostly neat silica was precipitated and γ-Fe_2O_3 particles remained uncoated. Moreover, iron oxide had a tendency to be dissolved at low pH. At optimal pH range (7–11), γ-Fe_2O_3@SiO_2 nanoparticles were obtained. Zeta potential of neat γ-Fe_2O_3 and γ-Fe_2O_3@SiO_2 nanoparticles was −37.3 mV and −33.1 mV (pH = 7), respectively. After addition of APTES, zeta potential changed to −10.3 mV (pH = 7) thus compromising the stability of the colloid. γ-Fe_2O_3@SiO_2-NH_2 nanoparticles contained 0.23 mmol NH_2 groups per g according to analysis of nitrogen.

γ-Fe_2O_3/SiO_2 ratio was investigated in the range 0.1–0.8 w/w in order to determine optimal conditions to control morphology and size of the nanoparticles. The morphology and the size of the γ-Fe_2O_3@SiO_2 nanoparticles was observed by SEM (Fig. 4) and TEM (Fig. 5). Rather aggregated γ-Fe_2O_3@SiO_2 particles were seen in the dry state in SEM (Figs. 4(b–c)). All particles had spherical shape. While neat γ-Fe_2O_3 nanoparticles had size ~ 10 nm (PDI = 1.15), size of γ-Fe_2O_3@SiO_2 particles ranged from *ca.* 12 to 192 nm depending on γ-Fe_2O_3/SiO_2 ratio. When comparing morphology of neat γ-Fe_2O_3 (Fig. 5(a)) and γ-Fe_2O_3@SiO_2 A nanoparticles (Table I) on TEM micrographs, a hallo was visible in γ-Fe_2O_3@SiO_2 A particles (γ-Fe_2O_3/SiO_2 = 0.8 w/w) suggesting the presence of a silica shell *ca.* 0.6 nm thick (Fig. 5(b)); it should be noted that unbound SiO_2 was removed by washing. γ-Fe_2O_3@SiO_2 B nanoparticles (γ-Fe_2O_3/SiO_2 = 0.4 w/w) were 11.9 nm in size with a quite narrow size distribution (PDI = 1.07) and 2.2 nm thick shell. With increasing amounts of silica relative to iron oxide, exemplified by γ-Fe_2O_3@SiO_2 C (γ-Fe_2O_3/SiO_2 = 0.2 w/w) and γ-Fe_2O_3@SiO_2-NH_2 nanoparticles, D_n was 19 and 192 nm, respectively (Table I). It was difficult to avoid aggregation of silica-coated particles. Hydrodynamic diameter D_h was therefore generally much larger than D_n, increasing from ~100 nm for neat γ-Fe_2O_3 nanoparticles to ~500 nm for double silica-coated particles. Polydispersity PI of the nanoparticles indicated their broad particle size distribution. According to AAS, the content of iron decreased from 66.1 wt.% in γ-Fe_2O_3 to 27.7 and 19.8 wt.% in γ-Fe_2O_3@SiO_2 C and γ-Fe_2O_3@SiO_2-NH_2 nanoparticles, respectively. This was obviously associated with increasing thickness of silica shell surrounding the γ-Fe_2O_3 particles. Nevertheless, this amount of iron was sufficient to render the particles with good magnetic properties.

The surface of the neat γ-Fe_2O_3, γ-Fe_2O_3-SiO_2 C and γ-Fe_2O_3@SiO_2-NH_2 nanoparticles was analyzed by a surface-sensitive ATR FT-IR spectroscopy (Fig. 6). After functionalization of γ-Fe_2O_3 nanoparticles with TMOS, the spectrum of γ-Fe_2O_3@SiO_2 C particles confirmed presence of SiO_2 shell around the iron oxide. Shift of the maximum of Si-O-C asymmetric stretching vibration at about 1050 cm^{-1} was ascribed to the interaction of SiO_2 with γ-Fe_2O_3 (Fig. 6(a)). After addition of APTES, the spectrum of γ-Fe_2O_3@SiO_2-NH_2 nanoparticles only slightly differed from the spectrum of γ-Fe_2O_3@SiO_2 C.

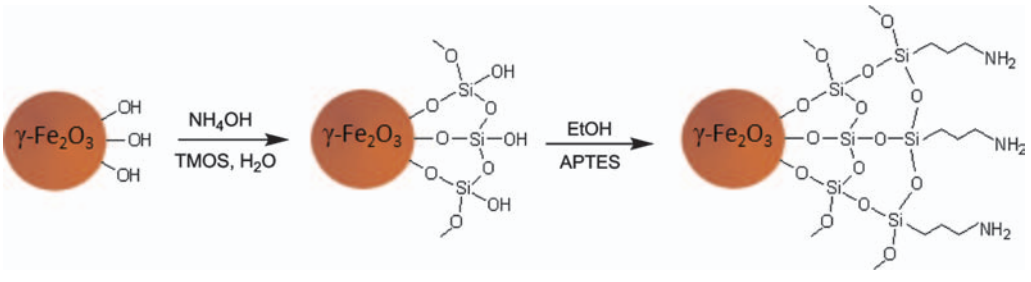

Figure 3. Scheme of silanization of γ-Fe_2O_3 with TMOS and modification of γ-Fe_2O_3@SiO_2 nanoparticles with APTES.

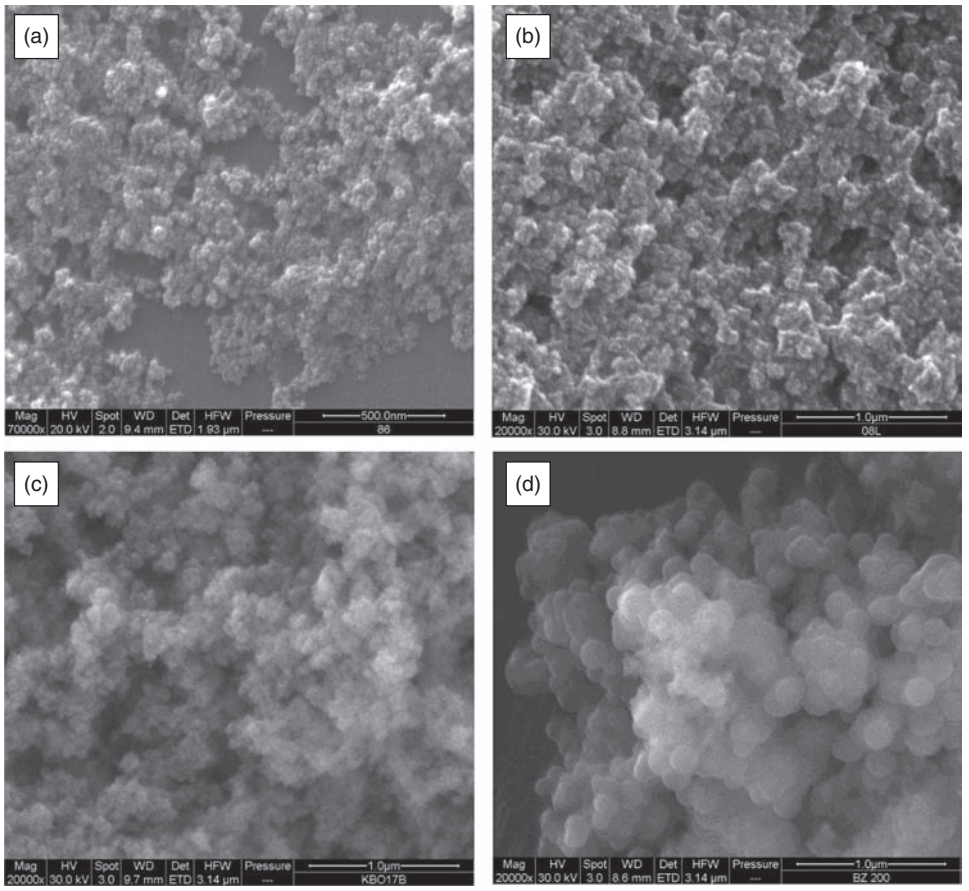

Figure 4. SEM micrographs of (a) neat γ-Fe_2O_3, (b) γ-Fe_2O_3@SiO_2 A (Table I; γ-Fe_2O_3/TMOS = 0.8 w/w), (c) γ-Fe_2O_3@SiO_2 C (γ-Fe_2O_3/TMOS = 0.2 w/w) and (d) γ-Fe_2O_3@SiO_2-NH_2 nanoparticles (γ-Fe_2O_3/[TMOS + APTES] = 0.1 w/w).

The peaks at 1070 cm^{-1} (Si-O-C asymmetric stretching vibrations), 940 cm^{-1} (Si-OH stretching vibrations) and 796 cm^{-1} (O-H deformation vibrations) were well distinguished in both spectra. To confirm the presence of amino groups on the surface of γ-Fe_2O_3@SiO_2-NH_2 nanoparticles, the spectra were multiplied by the factor 5 and presented in two different regions. In the region from 4000 to 2500 cm^{-1} (Fig. 6(b)), the broad band of O-H stretching vibrations was situated at about 3400 cm^{-1}. The shift of the peaks at 2981 versus 2951 cm^{-1} (CH_3 asymetric and symetric stretching vibrations) and disappearence of the peak at 2850 cm^{-1} (CH_2 stretching vibrations) in the spectrum of γ-Fe_2O_3@SiO_2 C again support the interaction of SiO_2 with γ-Fe_2O_3. The peaks at 3344 and 3278 cm^{-1} (NH_2 stretching vibrations) in the spectrum of neat silica obtained by a reaction of APTES with water (SiO_2-NH_2) overlapped in the spectrum of γ-Fe_2O_3@SiO_2-NH_2. The peak at 2981 cm^{-1} almost disappeared and intensity of the peak at 2928 cm^{-1} (CH_2 stretching vibrations) increased in the spectrum of γ-Fe_2O_3@SiO_2-NH_2 nanoparticles. In the region from 1800 to 1350 cm^{-1} (Fig. 6(c)), the shift of the peak at 1470 cm^{-1} in the spectrum of SiO_2 to 1450 cm^{-1} in the spectrum of γ-Fe_2O_3@SiO_2 C again support the interaction of SiO_2 with γ-Fe_2O_3 (Fig. 6(c)). The peaks at 1630 cm^{-1} (OH bending vibrations), 1485, 1450 and 1395 cm^{-1} (CH_3 deformation vibrations) were present in the spectra of both γ-Fe_2O_3@SiO_2 C and γ-Fe_2O_3@SiO_2-NH_2 nanoparticles. A slight enhancement of the absorption in the spectrum of γ-Fe_2O_3@SiO_2-NH_2 in the region of the peaks with maxima at 1570 cm^{-1} (Si-NH_2 bending vibrations), 1473 cm^{-1} (Si-CH_2 bending vibrations) and 1408 cm^{-1} (NH deformation vibrations), which were observed also in the spectrum of SiO_2-NH_2, indicate the presence of amino groups on the particle surface. We can conclude from the FT-IR spectrum of γ-Fe_2O_3@SiO_2 C particles that SiO_2 shell is present around the iron oxide (Fig. 6). From the comparison of the spectrum of γ-Fe_2O_3@SiO_2 C with the spectra of γ-Fe_2O_3@SiO_2-NH_2 and SiO_2-NH_2 follows that only a moderate amount of amino groups was present on the particle surface. This finding is in agreement with biological experiments.

In order to determine magnetic properties of silica-modified particles and to compare them with initial γ-Fe_2O_3, magnetization curves and temperature dependence of magnetic susceptibility of γ-Fe_2O_3@SiO_2 C and γ-Fe_2O_3@SiO_2-NH_2 particles were measured. As expected, saturation magnetization of the silica-coated

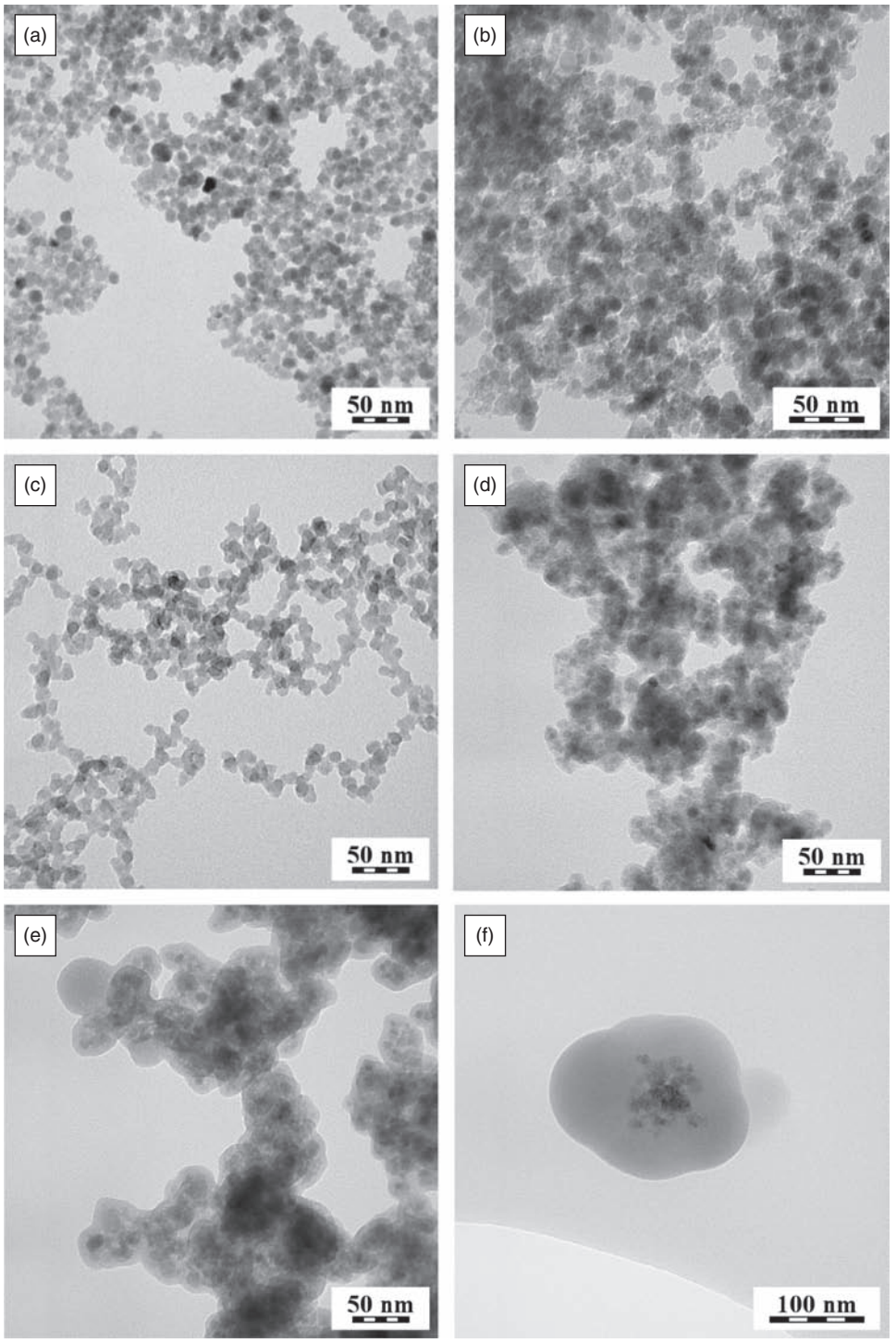

Figure 5. **TEM micrographs of (a) neat γ-Fe_2O_3, (b) γ-Fe_2O_3@SiO_2 A (Table 1; γ-Fe_2O_3/TMOS = 0.8 w/w), (c) γ-Fe_2O_3@SiO_2 B (γ-Fe_2O_3/TMOS = 0.4 w/w), (d) γ-Fe_2O_3@SiO_2 C (γ-Fe_2O_3/TMOS = 0.2 w/w) and (e, f) γ-Fe_2O_3@SiO_2-NH_2 nanoparticles (γ-Fe_2O_3/[TMOS + APTES] = 0.1 w/w).**

nanoparticles was substantially lower than that of initial neat γ-Fe_2O_3 (56.5 emu/g) (Fig. 1). The saturation magnetizations of γ-Fe_2O_3@SiO_2 C and γ-Fe_2O_3@SiO_2-NH_2 nanoparticles were 25 and 17.4 emu/g, respectively. The decrease in magnetization can be explained by a lower concentration of iron oxide substance in a sample due to the silica coating. The magnetic measurements enabled estimation of iron oxide content in the composite particles by comparing the saturation magnetization of composite particles and neat γ-Fe_2O_3. The calculated contents of maghemite in the particles were slightly higher than the amount of γ-Fe_2O_3 according to AAS. This might

Table I. Characterization of γ-Fe_2O_3@SiO_2 nanoparticles.

Run	γ-Fe_2O_3/ TMOS (w/w)	D_n (nm)	PDI	D_h(nm)	PI	γ-Fe_2O_3 (wt.%) AAS	γ-Fe_2O_3 (wt.%) VSM
γ-Fe_2O_3	–	9.7	1.15	108	0.12	– – –	– – –
γ-Fe_2O_3@SiO_2 A	0.8	10.3	1.09	148	0.2	64.8	– – –
γ-Fe_2O_3@SiO_2 B	0.4	11.9	1.07	239	0.12	43.9	– – –
γ-Fe_2O_3@SiO_2 C	0.2	19.2	1.14	294	0.2	39.6	44.2
γ-Fe_2O_3@SiO_2-NH_2*	0.1	192	1.02	494	0.3	28.3	30.8

Note. *γ-Fe_2O_3/(TMOS + APTES) = 0.1 w/w; TMOS-tetramethyl orthosilicate, D_n - number average particle diameter, PDI-polydispersity index, D_h-hydrodynamic diameter, PI-polydispersity, AAS-according to atomic absorption spectroscopy, VSM-according to vibrating sample magnetometer.

be explained by inaccuracies in AAS analysis. Hysteresis curves of the neat and both modified γ-Fe_2O_3 particles (i.e., γ-Fe_2O_3@SiO_2 C and γ-Fe_2O_3@SiO_2-NH_2) suggest that the nanoparticles consisted of pure maghemite with a very narrow grain size distribution. However, a small remanence was found in γ-Fe_2O_3@SiO_2 C and γ-Fe_2O_3@SiO_2-NH_2 nanoparticles which can be partly attributed to a high concentration of ferrimagnetic. The γ-Fe_2O_3@SiO_2 C and γ-Fe_2O_3@SiO_2-NH_2 particles, although superparamagnetic, can interact with each other and show certain collective behavior. Temperature dependence of magnetic susceptibility of γ-Fe_2O_3@SiO_2 C and γ-Fe_2O_3@SiO_2-NH_2 showed that the material was thermally stable. In our previous studies,[35,36] iron oxides coated by organic polymers were transformed during heating to a magnetically weaker substance with a much lower final susceptibility. No changes during heating of γ-Fe_2O_3@SiO_2 C and γ-Fe_2O_3@SiO_2-NH_2 naoparticles upon 700 °C, i.e., and no reduction to magnetite, were observed (Fig. 2). The maghemite seemed to be pure, with no traces of magnetite. Curie temperature was difficult to estimate, but was close to about 500 °C, which agreed with the one theoretically proposed for nano-sized maghemite[37] and observed 617 °C in natural maghemite. In the coated nanoparticles, no indication of transformation to hematite was also observed, which is in agreement with the literature,[38] although a certain decrease in final susceptibility compared to the initial value would suggest so. Contrary to that, magnetic susceptibility of the neat γ-Fe_2O_3 decreased significantly after the heating-cooling run, suggesting practically complete oxidation to hematite (Fig. 2). Our observation confirms the thermal stability of silica. Consequently, this coating prevents maghemite nanoparticles from surface redox reactions to a less magnetic substance.

Coating of γ-Fe_2O_3 particles with a thin silica shell hindered particle aggregation and made them hydrophilic; as a result, the particles were well dispersible in water. Secondary coating obtained by reaction of γ-Fe_2O_3@SiO_2 particles with APTES makes prospective attachment of a target biomolecule (e.g., protein, antibody, enzyme, drug) possible. However, γ-Fe_2O_3@SiO_2-NH_2 nanoparticles formed aggregates (Fig. 4(d)) at neutral pH suggesting that the initial γ-Fe_2O_3@SiO_2 particles agglomerated during the reaction with APTES.

Uptake of γ-Fe_2O_3@SiO_2 and γ-Fe_2O_3@SiO_2-NH_2 Nanoparticles by Murine J774.2 Macrophages

Conventional treatment of inflammatory diseases based on administration of high doses of immune-suppressant or anti-inflammatory drugs is often complicated by serious adverse effects. Thus, a carrier system that delivers the drug specifically to the inflamed region and exhibits a prolonged drug release is highly desirable.[39] Such a site-specific delivery could be achieved by the macrophages. For example, highly porous silica particles were made magnetic by the inclusion of superparamagnetic iron oxide nanoparticles (30 nm). They were then capable of accommodating nanogram quantities of a model molecular load (e.g., easy detectable enzyme such as horseradish peroxidase or pronase E) that was released under experimental conditions.[40] The realization that blood-borne delivery systems must overcome several biological barriers has led to the development of multi-stage delivery systems designed to successive release of doses of particles or agents to cross sequential barriers.[41] The goal was to enhance delivery of therapeutic and diagnostic agents to the target site.

An understanding of the interaction of the nanoparticle surface with various biological components is of key importance for prospective biological applications. Therefore, the interaction of γ-Fe_2O_3@SiO_2 and γ-Fe_2O_3@SiO_2-NH_2 nanoparticles with murine J774.2 macrophages was investigated. Engulfment of γ-Fe_2O_3@SiO_2 A, γ-Fe_2O_3@SiO_2-NH_2 and neat γ-Fe_2O_3 nanoparticles (Table I) at a concentration 0.005 mg/ml by the murine macrophages J774.2 was almost completed after 3 h of cell cultivation. Quantitative analysis of macrophages that engulfed synthesized nanoparticles showed that most of cells contained the nanoparticles (Table II).

Within the macrophages, neat γ-Fe_2O_3 particles were larger in size (due to aggregation) than γ-Fe_2O_3@SiO_2 and γ-Fe_2O_3@SiO_2-NH_2 nanoparticles. Although the neat

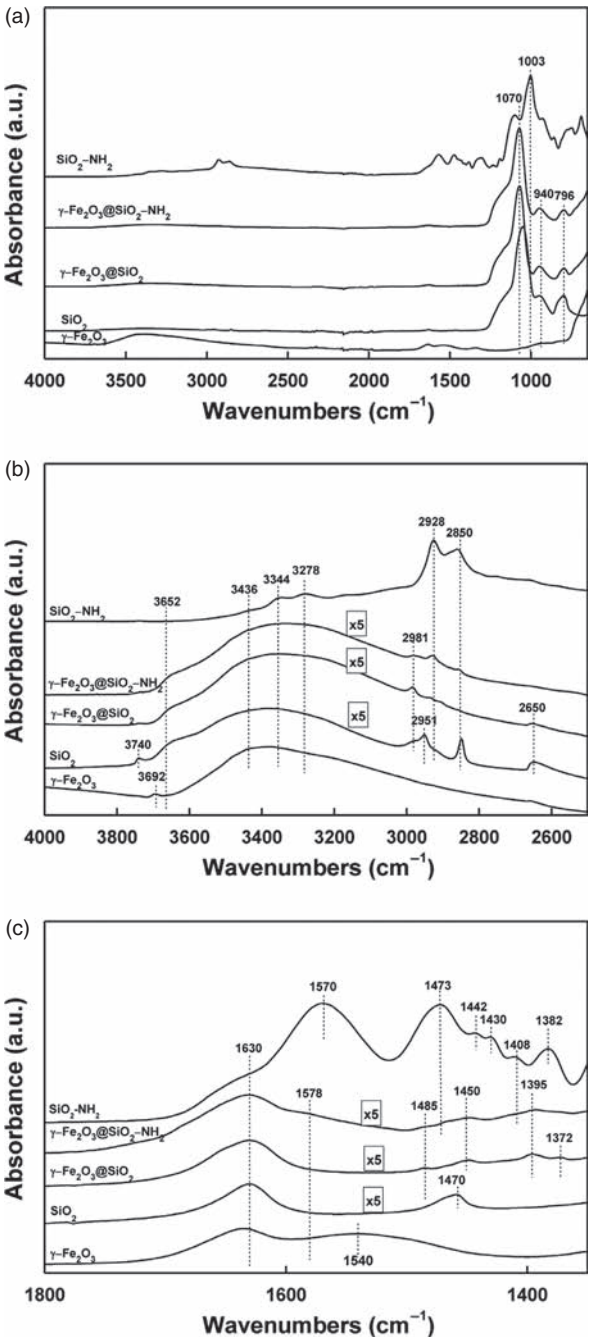

Figure 6. ATR FT-IR spectra of γ-Fe_2O_3 nanoparticles before and after silanization; Spectrum of neat SiO_2 is shown for comparison.

γ-Fe_2O_3 particles were relatively efficiently engulfed by the macrophages (Figs. 7(a, b)), number of active lysosomes (measured by the intensity of intracellular red fluorescence after Acridin orange staining of cells) was comparable with that in the control experiment (Fig. 7(e)). However, the uptake was much lower than the engulfment of the γ-Fe_2O_3@SiO_2 and γ-Fe_2O_3@SiO_2-NH_2 nanoparticles (Figs. 7(c, d); for details see.[42])

In the experiment with neat γ-Fe_2O_3 nanoparticles, 27.3% of cells (12.8 $\pm$ 3.2 of 46.8 $\pm$ 7.1) demonstrated intense vacuolization of the cytoplasm (2% in the untreated cells) (Table II; white arrows in Fig. 7(b)) while vacuoles were absent if γ-Fe_2O_3@SiO_2 and γ-Fe_2O_3@SiO_2-NH_2 nanoparticles were engulfed. That suggests certain destructive processes developed in the macrophages fed with the neat maghemite nanoparticles. The presence of SiO_2 shell caused a considerable activation of treated macrophages measured by the appearance of lysosomal signal (Table II). That was especially distinctly expressed in γ-Fe_2O_3@SiO_2-NH_2 particles. It should be noted that the neat γ-Fe_2O_3 particles acted oppositely and decreased lysosomal activation (1.8 $\pm$ 1.5 versus 15 $\pm$ 4.1 in the control). We suggest that a significant lysosomal activation (33.3% of observed cells) in control experiment (no treatment of cells with the nanoparticles) was caused by cellular contact with the glass surface of the microscopic slides. The macrophages responded thus more to both γ-Fe_2O_3@SiO_2 and γ-Fe_2O_3@SiO_2-NH_2 than to neat γ-Fe_2O_3 nanoparticles.

Neither neat γ-Fe_2O_3 or γ-Fe_2O_3@SiO_2 and γ-Fe_2O_3@SiO_2-NH_2 nanoparticles demonstrated a significant toxic effect towards J774.2 macrophages during 1–4 days of incubation (data not shown). It is not surprising that no difference in the engulfment of γ-Fe_2O_3@SiO_2 and γ-Fe_2O_3@SiO_2-NH_2 nanoparticles by the macrophages was observed due to the low content of amino groups on the latter particles. Nevertheless, the fact that high cellular labeling efficiency of γ-Fe_2O_3@SiO_2-NH_2 nanoparticles was achieved in the absence of a transfection agent which is often toxic to the cells is very convenient.[43]

γ-Fe_2O_3@SiO_2 and γ-Fe_2O_3@SiO_2-NH_2 nanoparticles displayed thus good efficiency of uptake by the macrophages. Such efficiency was slightly lower than for poly(*N*, *N*-dimethylacrylamide)-coated-γ-Fe_2O_3 nanoparticles that were very rapidly (within 1 h) engulfed

Table II. Quantitative analysis of the engulfment of the particles by murine macrophages J774.2.

Run	Number of cells in microscopic field	Cells with lysosome activation	Cells with intense vacuolization
Control	45 $\pm$ 7.4	15 $\pm$ 4.1	1 $\pm$ 1.4
γ-Fe_2O_3	46.8 $\pm$ 7.1	1.8 $\pm$ 1.5*	12.8 $\pm$ 3.2**
γ-Fe_2O_3@SiO_2 C	48 $\pm$ 8.0	25 $\pm$ 9.6	0.3 $\pm$ 0.2
γ-Fe_2O_3@SiO_2-NH_2	47 $\pm$ 4.8	43.3 $\pm$ 5.2**	0.3 $\pm$ 0.2

Note: One microscopic field of view contained approximately 50 cells; totally 4 fields were counted. *$P < 0.05$, **$P < 0.01$.

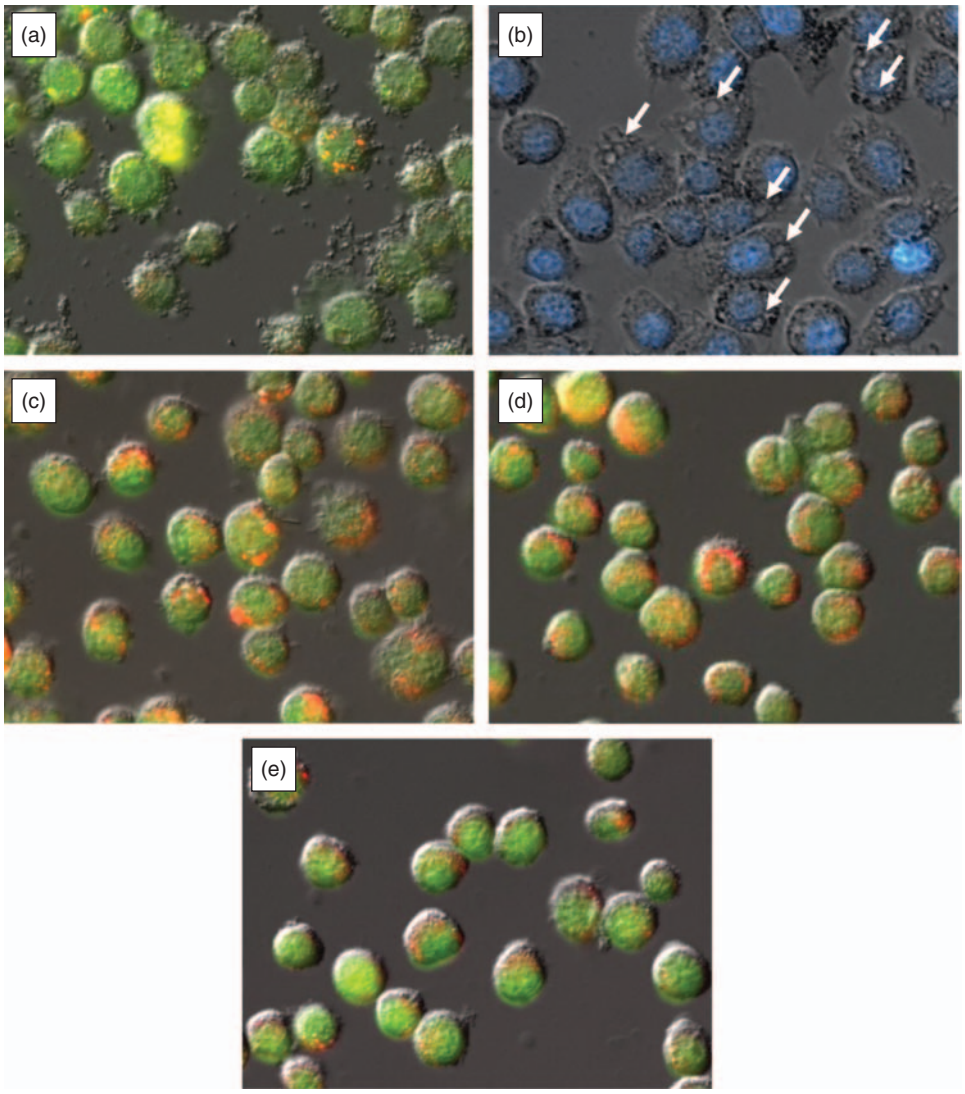

Figure 7. **Murine J774.2 macrophages treated with neat γ-Fe_2O_3 (a, b), γ-Fe_2O_3@ SiO_2 (c), γ-Fe_2O_3@ SiO_2-NH_2 (d) nanoparticles for 3 h and control experiment (e; no treatment). Micrographs of cells were taken after their staining with Acridine Orange (a, c-e; combined differential interference contrast and fluorescence microscopy) or cell nuclei staining with Hoechst 33342 (b; combined light and fluorescence microscopy).**

by the macrophages under similar conditions.[43] In contrast, rater slow phagocytosis lasting for about 20 h was observed for heterotelechelic poly(*N*-vinylpyrrolidone) oligoperoxide-coated γ-Fe_2O_3/poly(2-hydroxyethyl methacrylate) nanoparticles.[44] Different engulfment efficiencies may be explained by differences in a composition of coating materials. Moreover, different surface charges could in turn affect binding of proteins from culture media.[45]

CONCLUSIONS

Magnetic γ-Fe_2O_3@SiO_2 nanoparticles were reproducibly prepared by a two-stage reaction: (i) synthesis of γ-Fe_2O_3 nanoparticles via coprecipitation and oxidation, and (ii) preparation of silica-coated γ-Fe_2O_3 particles through condensation with tetramethyl orthosilicate and eventually with 3-(aminopropyl)triethoxysilane. The latter particles contained amino groups on the surface which is important for intracellular delivery of exogenous materials.[46] The particles were spherical with relatively narrow particle size distributions (PDI = 1.07 – 1.15). In the literature, cationic surfaces have been shown to facilitate cellular internalization.[47] Silica is an inert coating that prevents aggregation of particles and enhances chemical stability. Magnetic measurements showed that due to its thermal stability, silica prevents the maghemite nanoparticles from surface oxidation/reduction. As a result, the magnetic properties of these nanoparticles are resistant to temperatures up to 700 °C. Moreover, silica is susceptible to chemical modifications which make synthesis of particles for combined diagnosis and therapy possible. Our biolog-

ical experiments demonstrated that both γ-Fe_2O_3@SiO_2 and γ-Fe_2O_3@SiO_2-NH_2 core/shell nanoparticles were recognized and engulfed by the macrophages. It can be thus supposed that following intravenous injection, silica-coated iron oxide nanoparticles are incorporated into macrophages via phagocytosis. The uptake of silica-coated iron oxide nanoparticles by phagocytic monocytes and macrophages could provide a valuable *in vivo* tool by which magnetic resonance imaging (MRI) can be used to monitor involvement of macrophages in inflammatory processes[48] that can develop in multiple sclerosis, traumatic nerve injury, stroke, brain tumors, and vulnerable plaque in carotid artery. Silica-coated γ-Fe_2O_3 nanoparticles seem to be thus promising for cell imaging and tracking and for other biomedical applications. Moreover, magnetic field can be used to steer and concentrate magnetically labeled cells inside the body.

Acknowledgments: The financial support of the Europeans Union (grant DiaTools No. 259796) and Grant Agency of the Czech Republic (grant P207/12/J013) is gratefully acknowledged.

REFERENCES

1. A. S. Arbab, L. A. Bashaw, B. R. Miller, E. K. Jordan, B. K. Lewis, H. Kalish, and J. A. Frank, Characterization of biophysical and metabolic properties of cells labeled with superparamagnetic iron oxide nanoparticles and transfection agent for cellular MR imaging. *Radiology* 229, 838 **(2003)**.
2. C. Alexiou, R. J. Schmid, R. Jurgons, M. Kremer, G. Wanner, C. Bergemann, E. Huenges, T. Nawroth, W. Arnold, and F. G. Parak, Targeting cancer cells: Magnetic nanoparticles as drug carriers. *Eur. Biophys. J.* 35, 446 **(2006)**.
3. A. K. Gupta and M. Gupta, Synthesis and surface engineering of iron oxide nanoparticles for biomedical applications. *Biomaterials* 26, 3995 **(2005)**.
4. S. Laurent and M. Mahmoudi, Superparamagnetic iron oxide nanoparticles: Promises for diagnosis and treatment of cancer. *Int. J. Mol. Epidemiol. Genet.* 2, 367 **(2011)**.
5. Y. X. Wang, S. M. Hussain, and G. P. Krestin, Superparamagnetic iron oxide contrast agents: Physicochemical characteristics and applications in MR imaging. *Eur. Radiol.* 11, 2319 **(2001)**.
6. M. Chorny, B. Polyak, I. S. Alferiev, K. Walsh, G. Friedman, and R. J. Levy, Magnetically driven plasmid DNA delivery with biodegradable polymeric nanoparticles. *Faseb. J.* 21, 2510 **(2007)**.
7. Y. Gong, M. Fan, F. Gao, J. Hong, S. Liu, S. Luo, J. Yu, and J. Huang, Preparation and characterization of amino-functionalized magnetic nanogels via photopolymerization for MRI applications. Colloid Surf. *B-Biointerfaces* 71, 243 **(2009)**.
8. S. Dutz, W. Andrä, R. Hergt, R. Müller, C. Oestreich, C. Schmidt, J. Töpfer, M. Zeisberger, and M. E. Bellemann, Influence of dextran coating on the magnetic behaviour of iron oxide nanoparticles. *J. Magn. Magn. Mater.* 311, 51 **(2007)**.
9. F. M. Kievit, O. Veiseh, N. Bhattarai, C. Fang, J. W. Gunn, D. Lee, R. G. Ellenbogen, JM J. M. Olson, and M. Zhang, PEI-PEG-chitosan-copolymer-coated iron oxide nanoparticles for safe gene delivery: Synthesis, complexation, and transfection. *Adv. Funct. Mater.* 19, 2244 **(2009)**.
10. D. K. Kim, M. Mikhaylova, F. Wang, J. Kehr, B. Bjelke, Y. Zhang, T. T. Sakalakos, and M. Muhammed, Starch-coated superparamagnetic nanoparticles as MR contrast agents. *Chem. Mat.* 15, 4343 **(2003)**.
11. C. Barrera, A. P. Herrera, and C. Rinaldi, Colloidal dispersions of monodisperse magnetite nanoparticles modified with poly(ethylene glycol). *J. Colloid. Interface Sci.* 329, 107 **(2009)**.
12. M. Chastellain, A. Petri, and H. Hofmann, Particle size investigations of a multistep synthesis of PVA coated superparamagnetic nanoparticles. *J. Colloid. Interface Sci.* 278, 353 **(2004)**.
13. S. C. McBain, H. H. P. Yiu, A. El Haj, and J. Dobson, Polyethyleneimine functionalized iron oxide nanoparticles as agents for DNA delivery and transfection. *J. Mater. Chem.* 17, 2561 **(2007)**.
14. C. M. Jewell, J. Zhang, N. J. Fredin, and D. M. Lynn, Multilayered polyelectrolyte films promote the direct and localized delivery of DNA to cells. *J. Control. Release* 106, 214 **(2005)**.
15. P. A. Jarzyna, T. Skajaa, A. Gianella, D. P. Cormode, D. D. Samber, S. D. Dickson, W. Chen, A. W. Griffioen, Z. A. Fayad, and W. J. Mulder, Iron oxide core oil-in-water emulsions as a multifunctional nanoparticle platform for tumor targeting and imaging. *Biomaterials* 30, 6947 **(2009)**.
16. D. Knopp, D. Tang, and R. Niessner, Bioanalytical applications of biomolecule-functionalized nanometer-sized doped silica particles. *Anal. Chim. Acta.* 647, 14 **(2009)**.
17. M. Shi, Y. Liu, M. Xu, H. Yang, Ch. Wu, and H. Miyoshi, Core/shell Fe_3O_4@SiO_2 nanoparticles modified with PAH as a vector for EGFP plasmid DNA delivery into HeLa Cells. *Macromol. Biosci.* 11, 1563 **(2011)**.
18. B. Guo, H. Yim, A. Khasanov, and J. Stevens, Formation of magnetic Fe_xO_y/silica core-shell particles in a one-step flame aerosol process. *Aerosol. Sci. Technol.* 44, 281 **(2010)**.
19. X. M. Zhu, Y. X. Wang, K. C. Leung, S. F. Lee, F. Zhao, D. W. Wang, J. M. Lai, C. Wan, C. H. Cheng, and A. T. Ahuja, Enhanced cellular uptake of aminosilane-coated superparamagnetic iron oxide nanoparticles in mammalian cell lines. *Int. J. Nanomedicine* 7, 953 **(2012)**.
20. M. Yamaura, R. L. Camilo, L. C. Sampaio, M. A. Macedo, M. Nakamura, and H. E. Toma, Preparation and characterization of (3-aminopropyl)triethoxysilane-coated magnetite nanoparticles. *J. Magn. Magn. Mater.* 279, 210 **(2004)**.
21. K. S. Rao, K. El-Hami, T. Kodaki, K. Matsushige, and K. Makino, A snovel method for synthesis of silica nanoparticles. *J. Colloid Interface Sci.* 289, 125 **(2005)**.
22. G. Stoll, T. Basse-Lüsebrink, G. Weise, and P. Jakob, Visualization of inflammation using (19) F-magnetic resonance imaging and perfluorocarbons. *Wiley Interdiscip. Rev-Nanomed. Nanobiotechnol.* 4, 438 **(2012)**.
23. K. Morishige, D. F. Kacher, P. Libby, L. Josephson, P. Ganz, R. Weissleder, and M. Aikawa, High-resolution magnetic resonance imaging enhanced with superparamagnetic nanoparticles measures macrophage burden in atherosclerosis. *Circulation* 122, 1707 **(2010)**.
24. G. Fleige, F. Seeberger, D. Laux, M. Kresse, M. Taupitz, H. Pilgrim, and C. Zimmer, *In vitro* characterization of two different ultrasmall iron oxide particles for magnetic resonance cell tracking. *Invest. Radiol.* 37, 482 **(2002)**.
25. U. Flogel, Z. Ding, H. Hardung, S. Jander, G. Reichmann, C. Jacoby, R. Schubert, and J. Schrader, *In vivo* monitoring of inflammation after cardiac and cerebral ischemia by fluorine magnetic resonance imaging. *Circulation* 118, 140 **(2008)**.
26. M. Babiè, D. Horák, M. Trchová, P. Jendelová, K. Glogarová, P. Lesný, V. Herynek, M. Hájek, and E. Syková, Poly(L-lysine)-modified iron oxide nanoparticles for stem cell labeling. *Bioconjugate Chem.* 19, 740 **(2008)**.
27. S. Kralj, D. Makovec, S. Čampelj, and M. Drofenik, Producing ultrathin silica coatings on iron-oxide nanoparticles to improve their surface reactivity. *J. Magn. Magn. Mater.* 322, 1847 **(2010)**.
28. W. Stöber and A. Fink, Controlled growth of monodisperse silica spheres in the micron size range. *J. Colloid Interface Sci.* 26, 62 **(1968)**.

29. F. Hrouda, A technique for the measurement of thermal changes of magnetic susceptibility of weakly magnetic rocks by the CS-2 apparatus and KLY-2 Kappabridge. *Geophys. J. Int.* 118, 604 **(1994)**.

30. A. A. Maich, E. Y. Erdem, and F. M. Doyle, Characterization of magnetic and non-magnetic iron oxide nanoparticles synthesized by different routes. Characterization of Minerals, Metals, and Materials, edited by J. Y. Hwang, S. N. Monteiro, C. G. Bai, J. Carpenter, M. Cai, D. Firrao, B. G. Kim, Wiley **(2012)**, pp. 99–106.

31. D. J. Dunlop and Ö. Özdemir, Rock magnetism: Fundamentals and frontiers, Cambridge University Press, Cambridge **(1997)**, pp. 56–60.

32. C. J. Goss, Saturation magnetisation, coercivity and lattice parameter changes in the system $Fe_3O_4 - \gamma$-Fe_2O_3, and their relationship to structure. *Phys. Chem. Miner.* 16, 164 **(1988)**.

33. B. Tan and S. E. Rankin, Study of the effects of progressive changes in alkoxysilane structure on sol-gel reactivity. *J. Phys. Chem. B* 110, 22353 **(2006)**.

34. H. H. P. Yiu, H. Niu, E. Biermans, G. van Tendeloo, and M. J. Rosseinsky, Designed multifunctional nanocomposites for biomedical applications. *Adv. Funct. Mater.* 20, 1599 **(2010)**.

35. H. Macková, D. Horák, E. Petrovský, and J. Kovářová, Magnetic hollow poly(*N*-isopropylacrylamide-*co*-*N*, *N*′-methylenebisacrylamide-*co*-glycidyl acrylate) particles prepared by inverse emulsion polymerization. *Colloid. Polym. Sci.* 291, 205 **(2013)**.

36. P. Šálek, L. Korecká, D. Horák, E. Petrovský, J. Kovářová, R. Metelka, M. Čadková, and Z. Bílková, Immunomagnetic sulfonated hypercrosslinked polystyrene microspheres for electrochemical detection of proteins. *J. Mater. Chem.* 21, 14783 **(2011)**.

37. A. U. Gehring, H. Fischer, M. Louvel, K. Kunze, and P. G. Weidler, High temperature stability of natural maghemite: A magnetic and spectroscopic study. *Geophys. J. Int.* 179, 1361 **(2009)**.

38. O. Ozdemir and S. K. Banerjee, High temperature stability of maghemite (γ-Fe_2O_3). *Geophys. Res. Lett.* 11, 161 **(1984)**.

39. E. M. Collnot, H. Ali, and C. M. Lehr, Nano- and microparticulate drug carriers for targeting of the inflamed intestinal mucosa. *J. Control. Release* 161, 235 **(2012)**.

40. J. C. Thomas, C. Pacholski, and M. J. Sailor, Delivery of nanogram payloads using magnetic porous silicon microcarriers. *Lab. Chip.* 6, 782 **(2006)**.

41. R. E. Serda, A. Mack, M. Pulikkathara, A. M. Zaske, C. Chiappini, J. R. Fakhoury, D. Webb, B. Godin, J. L. Conyers, X. W. Liu, J. A. Bankson, and M. Ferrari, Cellular association and assembly of a multistage delivery system. *Small* 6, 1329 **(2010)**.

42. B. A. Zasonska, N. Boiko, D. Horák, O. Klyuchivska, H. Macková, M. Beneš, M. Babič, M. Trchová, J. Hromádková, and R. Stoika, The use of hydrophilic poly(*N*, *N*-dimethylacrylamide) grafted from magnetic γ-Fe_2O_3 nanoparticles to promote engulfment by mammalian cells. *J. Biomed. Nanotechnol.* 9, 479 **(2013)**.

43. B. L. Strand, T. L. Ryan, P. Veld, B. Kulseng, A. M. Rokstad, G. Skjåk-Braek, and T. Espevik, Poly-L-lysine induces fibrosis on alginate microcapsules via the induction of cytokines. *Cell Transplant* 10, 263 **(2001)**.

44. D. Horák, T. Shagotova, N. Mitina, M. Trchová, N. Boiko, M. Babič, R. J. Stoika, Kovářová, O. Hevus, M. Beneš, O. Klyuchivska, P. Holler, and A. Zaichenko, Surface-initiated polymerization of 2-hydroxyethyl methacrylate from heterotelechelic oligoperoxide-coated γ-Fe_2O_3 nanoparticles and their engulfment by mammalian cells. *Chem. Mat.* 23, 2637 **(2011)**.

45. A. Kunzmann, B. Andersson, C. Vogt, N. Feliu, F. Ye, S. Gabrielsson, M. S. Toprak, T. Buerki-Thurnherr, S. Laurent, M. Vahter, H. Krug, M. Muhammed, A. Scheynius, and B. Fadeel, Efficient internalization of silica-coated iron oxide nanoparticles of different sizes by primary human macrophages and dendridic cells. *Toxicol. Appl. Pharmacol.* 253, 81 **(2011)**.

46. X. M. Zhu, Y. X. Wang, K. C. Leung, S. F. Lee, F. Zhao, D. W. Wang, J. M. Lai, C. Wan, C. H. Cheng, and A. T. Ahuja, Enhanced cellular uptake of aminosilane-coated superparamagnetic iron oxide nanoparticles in mammalian cell lines. *Int. J. Nanotechnol.* 7, 953 **(2012)**.

47. D. L. J. Thorek and A. Tsourkas, Size, charge and concentration dependent uptake of iron oxide particles by non-phagocyting cells. *Biomaterials* 29, 3583 **(2008)**.

48. Y. X. Wang and W. W. Lam, Characterisation of brain disorders and evaluation of therapy by functional and molecular magnetic resonance techniques. *Hong Kong Med. J.* 14, 469 **(2008)**.

Publication No. 3

Croat Med J. 2016;57:
doi: 10.3325/cmj.2016.57.

Functionalized porous silica&maghemite core-shell nanoparticles for applications in medicine: design, synthesis, and immunotoxicity

Beata A. Zasońska[1], Aurélia Líšková[2], Miroslava Kuricová[2], Jana Tulinská[2], Ognen Pop-Georgievski[1], Fedor Čiampor[3], Ivo Vávra[4], Mária Dušinská[5], Silvia Ilavská[2], Mira Horváthová[2], Daniel Horák[1]

[1]Institute of Macromolecular Chemistry, Academy of Sciences of the Czech Republic, Prague, Czech Republic

[2]Medical Faculty, Slovak Medical University, Bratislava, Slovakia

[3]Institute of Virology, Slovak Academy of Sciences, Bratislava, Slovakia

[4]Institute of Electrical Engineering, Slovak Academy of Sciences, Bratislava, Slovakia

[5]Health Effects Laboratory, Department of Environmental Chemistry, NILU-Norwegian Institute for Air Research, Kjeller, Norway

Aim To determine cytotoxicity and effect of silica-coated magnetic nanoparticles (MNPs) on immune response, in particular lymphocyte proliferative activity, phagocytic activity, and leukocyte respiratory burst and *in vitro* production of interleukin-6 (IL-6) and 8 (IL-8), interferon-gamma (IFN-γ), tumor necrosis factor-alpha (TNF-α), and granulocyte macrophage colony stimulating factor (GM-CSF).

Methods Maghemite was prepared by coprecipitation of iron salts with ammonia, oxidation with NaOCl and modified by tetramethyl orthosilicate and aminosilanes. Particles were characterized by transmission electron microscopy (TEM), dynamic light scattering (DLS), Fourier-transform infrared (FTIR), and x-ray photoelectron spectroscopy (XPS). Cytotoxicity and lymphocyte proliferative activity were assessed using [^{3}H]-thymidine incorporation into DNA of proliferating human peripheral blood cells. Phagocytic activity and leukocyte respiratory burst were measured by flow cytometry; cytokine levels in cell supernatants were determined by ELISA.

Results γ-Fe_2O_3&SiO_2-NH_2 MNPs were 13 nm in size. According to TEM, they were localized in the cell cytoplasm and extracellular space. Neither cytotoxic effect nor significant differences in T-lymphocyte and T-dependent B-cell proliferative response were found at particle concentrations 0.12-75 μg/cm^2 after 24, 48, and 72 h incubation. Significantly increased production of IL-6 and 8, and GM-CSF cytokines was observed in the cells treated with 3, 15, and 75 μg of particles/cm^2 for 48 h and stimulated with pokeweed mitogen (PHA). No significant changes in TNF-α and IFN-γ production were observed. MNPs did not affect phagocytic activity of monocytes and granulocytes when added to cells for 24 and 48 h. Phagocytic respiratory burst was significantly enhanced in the cultures exposed to 75 μg MNPs/cm^2 for 48 h.

Conclusions The cytotoxicity and *in vitro* immunotoxicity were found to be minimal in the newly developed porous core-shell γ-Fe_2O_3&SiO_2-NH_2 magnetic nanoparticles.

Received: January 13, 2016

Accepted: March 24, 2016

Correspondence to:
Daniel Horák
Department of Polymer Particles
Institute of Macromolecular Chemistry
Academy of Sciences of the Czech Republic
Heyrovského Sq. 2
162 06 Prague 6, Czech Republic
horak@imc.cas.cz

Superparamagnetic nanoparticles containing both nonporous and porous shells have been intensively investigated in recent years with respect to their potential applications in separation of molecules (1), sensors (2), as contrast agents in magnetic resonance imaging (MRI) (3), as well as carriers of drugs and biomolecules (4) for diagnostic (5) and therapeutic purposes (6).

Magnetic nanoparticles (MNPs), such as magnetite (Fe_3O_4) or maghemite (γ-Fe_2O_3), received considerable attention for their small size, spherical shape, strong magnetic properties enabling targeting to a specific organ using an external magnetic field (7), and rather low toxicity (8). However, neat (uncoated) iron oxide particles showed toxicity at high doses, tendency to aggregate, and high nonspecific adsorption of biomolecules, which is inacceptable for *in vitro* or *in vivo* medical applications (9). This can be avoided by surface modifications, such as grafting (coating) and/or encapsulation of MNPs by polymers, which are the most frequently used materials to improve biocompatibility and stability of the iron oxide nanoparticles in aqueous media. Some examples of polymers include dextran, poly(vinyl alcohol) (10), chitosan (11), poly(methyl methacrylate) (12), poly(ethylene glycol) (13), or poly(L-lysine). One of the universal agents to modify the iron oxide surface is also silica (14). This chemically inert inorganic material has a lot of advantages for biomedical applications compared to other materials. It is porous, biocompatible, modifiable with various functional agents, and has no toxicity at moderate concentrations (15); however silica dust is harmful if inhaled, and induces silicosis. Silica derivatives can introduce functional groups, eg, NH_2, COOH, SH, on the iron oxide surface to enable immobilization of target biomolecules. Mesoporous silica nanoparticles are thus attractive for drug loading and controlled release (16).

The aim of this research was to synthesize γ-Fe_2O_3, γ-Fe_2O_3&SiO_2, and γ-Fe_2O_3&SiO_2-NH_2 MNPs and thoroughly characterize them. We also aimed to investigate *in vitro* cytotoxicity and immunotoxicity of the γ-Fe_2O_3&SiO_2-NH_2 nanoparticles.

MATERIALS AND METHODS

Materials

$FeCl_2 \cdot 4H_2O$ and $FeCl_3 \cdot 6H_2O$ were purchased from Fluka (Buchs, Switzerland). Sodium hypochlorite solution (5 wt.%) was from Bochemie (Bohumín, Czech Republic). Tetramethyl orthosilicate (TMOS), (3-aminopropyl)triethoxysilane (APTES), (3-aminopropyl)dimethylethoxysilane (APDMES), RPMI-1640 medium, phytohemagglutinin (PHA), concanavalin A (Con A), pokeweed mitogen (PWM), L-glutamine, and hydroethidine were purchased from Sigma-Aldrich (Steinheim, Germany). Anti-CD3 monoclonal antibody was purchased from Beckman Coulter and fetal calf serum (FCS) from PAA. Fluorescein-labeled *Staphylococcus aureus* bacteria and opsonizing reagent were purchased from Molecular Probes (Eugene, OR, USA). Cationic surfactant, cetyltrimethylammonium bromide (CTAB) was purchased from Lachema (Brno, Czech Republic). Ammonium hydroxide solution (25%) and ethanol were purchased from Lach-Ner (Neratovice, Czech Republic). Gentamycin was purchased from Sandoz (Bratislava, Slovakia), cyclophosphamide (Cyf) from Baxter (Deerfield, IL, USA), and [^{3}H]-thymidine from Moravek Biochemicals (Brea, CA, USA). Scintillation fluid was purchased from Perkin Elmer (Waltham, MA, USA). Ultrapure Q-water ultrafiltered on a Milli-Q Gradient A10 system (Millipore, Molsheim, France) was used for preparation of the solutions. ELISA sets were purchased from Affymetrix e-Biosciences.

Preparation of γ-Fe_2O_3 nanoparticles

Iron oxide nanoparticles were prepared from iron(III) chloride and iron(II) chloride by a standard procedure (17). Aqueous 0.2 M $FeCl_3$ (100 mL), 0.2 M $FeCl_2$ (50 mL), and 0.5 M NH_4OH (100 mL) solutions were sonicated (Sonicator W-385; Heat Systems-Ultrasonics; Farmingdale, USA) for 5 min. The mixture was added to 3.3 wt.% NH_4OH (460 mL) and stirred at 23°C for 1 h (200 rpm). Magnetite was magnetically separated and washed by Q-water until peptization. Then, 5 wt.% sodium hypochlorite solution (16 mL) was added and the system sonicated for 5 min. The precipitate was magnetically separated and repeatedly washed with Q-water until formation of γ-Fe_2O_3 colloid.

Synthesis of porous core-shell γ-Fe_2O_3&SiO_2-NH_2 nanoparticles

First, silica shell was introduced on the particles by modification of Stöber method using hydrolysis and condensation of TMOS (18). In a typical experiment, ethanol (60 mL), water (3 mL), and 25 wt.% ammonia (0.3 mL) were mixed with γ-Fe_2O_3 (150 mg) for 5 min. TMOS (0.1 mL) was added and the mixture stirred (400 rpm) at 50°C for 16 h. The resulting γ-Fe_2O_3&SiO_2 colloid was three times washed with ethanol using magnetic separation.

The second (porous) shell containing amino groups on the surface was introduced by modification of γ-Fe_2O_3&SiO_2

nanoparticles with APTES/APDMES mixture (Figure 1). Briefly, γ-Fe_2O_3&SiO_2 nanoparticles were dispersed in ethanol (60 mL) and CTAB (0.15 g), APTES (0.05 mL), APDMES (0.05 mL), and water (1 mL) were added. The mixture was stirred using an anchor-type stirrer (400 rpm) at 50°C for 24 h. After completion of the reaction, the resulting porous γ-Fe_2O_3&SiO_2-NH_2 particles were washed using magnetic separation (5 times with ethanol and 3 times with water) and centrifugation (3 times).

Characterization of nanoparticles

The synthesized nanoparticles were characterized by a Tecnai Spirit G2 transmission electron microscope (TEM; FEI) and number- (D_n) and weight-average particle diameter (D_w) and polydispersity index (PDI = D_w/D_n) were calculated by analyzing ca. 400 particles. The hydrodynamic particle size (D_h) of γ-Fe_2O_3 and γ-Fe_2O_3&SiO_2 and polydispersity PI (0-1) was determined by dynamic light scattering (DLS) using a Zetasizer Nano-ZS Model ZEN3600 instrument (Malvern Instruments; Malvern, UK). Fourier-transform infrared (FTIR) spectra were recorded in an attenuated total reflection (ATR) mode using a Thermo Nicolet NEXUS 870 FT-IR Spectrometer (Madison, WI, USA). Specific surface area (S_{BET}) of the nanoparticles was determined by dynamic nitrogen adsorption using a Gemini VII 2390 Analyzer (Micromeritics; Norcross, GA, USA). x-ray photoelectron spectroscopy (XPS) was carried out with a K-Alpha+ spectrometer (ThermoFisher Scientific) equipped with a micro-focused monochromated Al Kα x-ray source (400 μm spot size). The kinetic energy of the electrons was measured using a 180° hemispherical energy analyzer operated in the constant energy mode at 200 and 50 eV pass energy for survey and high resolution spectra, respectively. Data acquisition and processing were performed using Thermo Advantage software. The XPS spectra were fitted with one or more Voigt profiles (binding energy BE, uncertainty ±0.2 eV). The analyzer transmission function, Scofield sensitivity factors, and effective attenuation lengths for photoelectrons were calculated using the standard TPP-2M formalism. All spectra were referenced to the C 1s peak of hydrocarbons at 285 eV of BE controlled by means of the well-known photoelectron peaks of metallic Cu, Ag, and Au.

Participants

Ten healthy male volunteers participating in the study signed an informed consent approved by the Ethics Committee of the Slovak Medical University in Bratislava. Blood was collected by venepuncture using heparinized tubes.

Preparation of MNPs for cell treatment

Porous γ-Fe_2O_3&SiO_2-NH_2 core-shell nanoparticles were vortex-shaken in the tubes for a few minutes before use and diluted with the RPMI 1640 medium containing 10% FCS to obtain a stock solution (75 μg/cm^2). Serial dilutions of this solution in the cell culture medium were prepared to obtain the full concentration range of MNP dispersions: 0.12, 0.6, 3, 15, and 75 μg/cm^2 corresponding to 0.17, 0.85, 4.24, 21.2, and 106 μg of particles/mL, respectively. In all assays, MNPs were added to the cell cultures in a volume of 25 μL.

Interaction of nanoparticles with peripheral blood cells according to TEM

Human heparinized whole blood (diluted 1:1 with phosphate buffered saline, PBS) was layered on Lymphosep (MP Biomedicals) and centrifuged for 30 min (700 *g*). Mononuclear cells were collected from interphase and washed in PBS and Roswell Park Memorial Institute medium (RPMI 1640) with 10% fetal calf serum (FCS). Cells were adjusted to 2.5×10^6 cells/mL in RPMI, 10% FCS, and pipetted in six-plicates in a volume of 180 μL to the microplates. MNPs in concentrations 0.12, 3, and 75 μg/cm^2 were added in a vol-

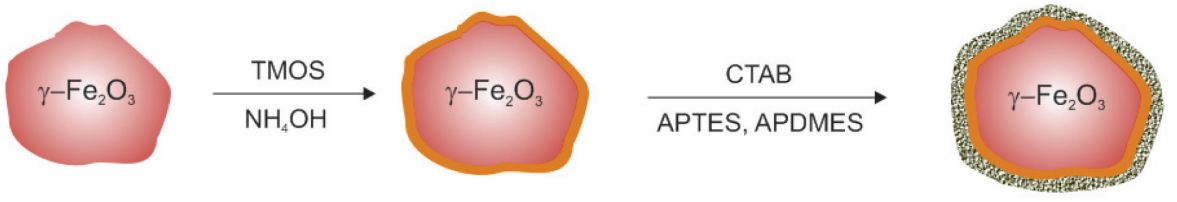

FIGURE 1. Scheme of silanization of γ-Fe_2O_3 with tetramethyl orthosilicate (TMOS) and (3-aminopropyl)triethoxysilane/(3-aminopropyl)dimethylethoxysilane (APTES/APDMES) to introduce NH_2 groups on the particle surface.

ume of 20 µL. The plates were incubated at 37°C for 24 h under 5% CO_2 atmosphere. Then the cells were two times washed with saline, centrifuged, saline was decanted, and the cells were fixed with 2.5% glutaraldehyde in PBS (pH 7.2) at room temperature for 60 min. Subsequently, the cells were washed with PBS and dehydrated with increasing concentration of ethanol (30, 50, 70, 90, 2×100%) in the solution. The cell pellet was embedded in London Resin White (Polysciences; Warrington, PA, USA) and polymerized at 60°C for 24 h. Ultrathin sections were prepared using LKB ultramicrotome and captured on EM mesh without the support membrane without staining. Ultrathin sections were evaluated using a JEOL 1200 EX TEM microscope with 100 kV accelerating voltage.

Assessment of cytotoxicity and immunotoxicity of γ-Fe_2O_3&SiO_2-NH_2 nanoparticles

Cytotoxicity and proliferative activity of lymphocytes. Cytotoxicity and proliferative activity of lymphocytes were assessed by ^{3}H-thymidine incorporation into DNA of proliferating cells using a liquid scintillation. Human heparinized whole blood (150 µL) diluted 1:15 in complete RPMI 1640 medium containing 10% FCS, L-glutamine, and gentamycin was dispensed in triplicate wells of a 96-well microtiter culture plate under sterile conditions. Mitogens were added to obtain the following final concentrations: concanavalin A (Con A) (25 µg/mL), phytohemagglutinin (PHA) (25 µg/mL), pokeweed mitogen (PWM) (2.5 µg/mL), and antigen CD3 (3 µg/mL). γ-Fe_2O_3&SiO_2-NH_2 nanoparticles (25 µL) were added in different exposure intervals (24, 48, and 72 h) before the end of whole 72 h incubation period. Cyf (40 mg/mL) was used as a suppressive control in unstimulated and PHA-stimulated cultures. The plates were incubated at 37°C for 48 h under 5% CO_2 atmosphere; then wells were pulsed with 1 µCi [^{3}H]-thymidine diluted in medium (20 µL) and incubated at 37°C for additional 24 h. After the whole 72 h incubation period, cell cultures were harvested onto glass filter paper, which was placed into a scintillation fluid. Radioactivity was measured using a Microbeta 2 scintillation counter (Perkin Elmer). Additionally, interference of the nanoparticles with the assay was tested, when the particles were added to the control cultures (unstimulated or stimulated with mitogens and antigen) few minutes before harvesting of the cells. Counts per minute (cpm)/per culture were calculated in triplicate for each variable.

In vitro production of interlekin-6 (IL-6), interleukin-8 (IL-8), interferon-gamma (IFN-γ), tumor necrosis factor-alpha (TNF-α), and granulocyte macrophage colony-stimulating factor (GM-CSF). Human heparinized blood diluted in complete RPMI-1640 medium (10% FCS) with PHA mitogen and the nanoparticles were cultivated for 72 h as described above. The nanoparticles were added 24 h after the beginning of the 72 h incubation period. After the incubation, cell culture supernatants were removed and frozen at -70°C. The levels of cytokines IL-6, IL-8, IFN-γ, TNF-α, and GM-CSF in the cell supernatants were analyzed by ELISA according to the manufacturer's procedure.

Phagocytic activity and respiratory burst of leukocytes. Phagocytic activity and respiratory burst of leukocytes were examined by an Epics XL flow cytometer. Briefly, 150 µL of human heparinized blood (diluted 1:1 in RPMI-1640 consisting of 10% FCS, L-glutamine, and gentamycin) was distributed into wells of 96-well culture microplate under a sterile conditions, γ-Fe_2O_3&SiO_2-NH_2 nanoparticles (25 µL) were added, and the mixture incubated for 24 and 48 h. Cyf (5 mg/mL) was used as a suppressive control. After the incubation, blood (30 µL) from each well was pipetted into the tube and hydroethidine solution (10 µL) was added. First, the samples were incubated at 37°C for 15 min and 3 µL of fluorescein-labeled *Staphylococcus aureus* bacteria (1.4×10^6 per test) was added. Second, all tubes were incubated at 37°C for another 15 min, the samples were put on an ice, and cold lysis solution (700 µL) was added. In the control tubes, *S. aureus* was added after the lysis solution. The samples were tested in duplicates and analyzed by flow cytometry within 30 min as before. Phagocytic activity of granulocytes and monocytes and respiratory burst of phagocytes were measured. Interference of particles with the assay was tested by measuring the same control tubes without particles and few seconds after addition of particles.

Statistical analysis

SPSS 16.0 software (Chicago, IL, USA) was used for statistical analysis. Triplicates or duplicates from each human subject were averaged and used as a single value for statistical analysis. Normality was determined by Shapiro-Wilk test. The paired-sample *t* test and the Mann-Whitney U-test (or Wilcoxon's test) were used to estimate significant differences between groups for normally and non-normally distributed data, respectively. Data were expressed as the mean values with a standard deviation. Differences at $P<0.05$ were considered to be statistically significant.

RESULTS

Maghemite nanoparticles (γ-Fe_2O_3) were prepared according to the following reactions:

$$FeCl_2 + 2\,FeCl_3 + 8\,NH_4OH \longrightarrow Fe_3O_4 + 8\,NH_4Cl + 4\,H_2O$$

$$2\,Fe_3O_4 + NaOCl \longrightarrow 3\,\gamma\text{–}Fe_2O_3 + NaCl$$

where magnetite (Fe_3O_4) was obtained by coprecipitation of $FeCl_2$ and $FeCl_3$ by ammonia, which was followed by oxidation. The final product (γ-Fe_2O_3) was brownish with high absolute value of ζ-potential (-41 mV) and exhibiting strong magnetization under magnetic field (19). Morphology of the resulting products was investigated by TEM, which images the dry particles (Figure 2). However, drying of aqueous colloids always leads to an aggregation. Nevertheless, potentially individual almost spherical particles can be distinguished and their diameters were measured for size statistics. Diameter of the γ-Fe_2O_3 particles was 9 nm and the particle size distribution was rather narrow (PDI = 1.21). After hydrolysis and condensation of TMOS, APTES and APDMES, size of the γ-Fe_2O_3&SiO_2-NH_2 particles increased to 13 nm (Table 1) due to formation of 2 nm-thick silica shell seen as a low-contrast layer (Figure 2B). Silica shell increased also the hydrodynamic particle diameter from 176 (γ-Fe_2O_3) to 474 nm (γ-Fe_2O_3&SiO_2-NH_2), while the PI increased from ~0.1 to 0.2. The reason for such large differences between D_n and D_h is that the DLS provides information about the particle dimers and clusters in water, while TEM shows individual particles in the dry state. DLS measurements of γ-Fe_2O_3&SiO_2-NH_2 nanoparticles incubated with serum at 37.7°C for 24 h showed even larger hydrodynamic size ~ 600 nm and size distribution PI ~ 0.3-0.4. The γ-Fe_2O_3&SiO_2-NH_2 particle colloids were stable; a tendency to aggregation was observed up to few months of storage. The results from dynamic adsorption of nitrogen are presented in Table 1. The specific surface area increased from 65.9 (neat γ-Fe_2O_3) to 206 m^2/g for γ-Fe_2O_3&SiO_2-NH_2 documenting thus porous character of the silica shell. Porosity was obviously induced by CTAB present in the silanization mixture; after completion of the reaction,

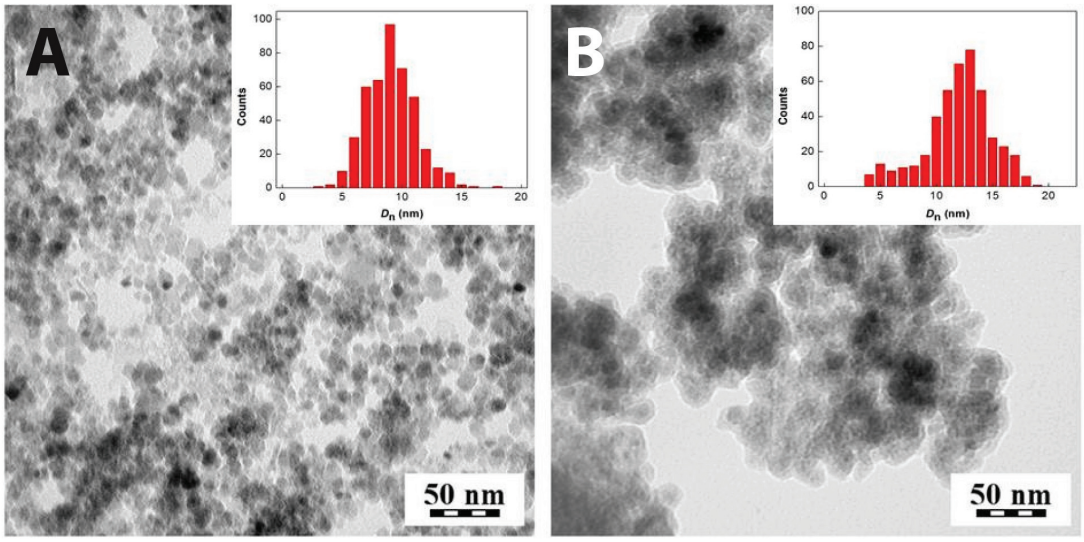

FIGURE 2. Transmission electron micrographs of (**A**) γ-Fe_2O_3 and (**B**) γ-Fe_2O_3&SiO_2-NH_2 nanoparticles.

TABLE 1. Properties of the developed nanoparticles*

					Mixed with blood serum after incubation		
Nanoparticles	D_n (nm)	PDI	D_h (nm)	PI	D_h (nm)	PI	S_{BET} (m^2/g)
γ-Fe_2O_3	9	1.21	176	0.09	623	0.43	66
γ-Fe_2O_3&SiO_2	10	1.28	260	0.08	-	-	167
γ-Fe_2O_3&SiO_2-NH_2	13	1.34	474	0.2	598	0.34	206

*D_n – number average particle diameter (TEM), PDI – polydispersity index (TEM), D_h – hydrodynamic diameter (DLS), PI – polydispersity (DLS), S_{BET} – specific surface area.

CTAB was removed from the silica by washing with ethanol and water using magnetic separation and centrifugation.

FTIR analysis confirmed successful coating of the neat γ-Fe_2O_3 particles with the silica modification agents (Figure 3). The spectrum of the γ-Fe_2O_3 showed absorption bands at 3372, 1558, 1418, 896, and 542 cm^{-1}. The range of 3600-3100 cm^{-1} was attributed to antisymmetric and symmetric O–H stretching, which can suggest the presence of adsorbed water on the particle surface (20). Wide peak at 542 cm^{-1} is characteristic for the metal oxygen stretching vibrations. After the first modification of γ-Fe_2O_3 nanoparticles with TMOS, the spectrum of γ-Fe_2O_3&SiO_2 confirmed the presence of SiO_2 shell around the iron oxide cores (Figure 3B). Shift of the maximum of Si-O-C asymmetric stretching vibration at ~1054 cm^{-1} was ascribed to the interaction of SiO_2 with γ-Fe_2O_3. When the γ-Fe_2O_3&SiO_2 was modified with APTES, the spectrum of γ-Fe_2O_3&SiO_2-NH_2 nanoparticles was shifted and the presence of NH_2 groups was well visible at 1638 and 1472 cm^{-1}; N-H stretching vibration at ~3300 cm^{-1} was only slightly noticeable. The peaks at 1480, 1450, and 1395 cm^{-1} (CH_3 deformation vibrations) were present in spectra of both γ-Fe_2O_3&SiO_2 and γ-Fe_2O_3&SiO_2-NH_2 particles.

x-ray photoelectron spectroscopy (XPS)

The XPS results confirmed that the neat γ-Fe_2O_3 nanoparticles contained Fe and O with Fe/O ratio=0.55, which is close to the theoretically expected value of 0.67 (Table 2; Figure 4). The Fe 2p spectrum showed two main peaks at 710.8 and 724.4 eV corresponding to Fe $2p_{3/2}$ and Fe $2p_{1/2}$, respectively (Figure 4A). These peaks were accompanied by weakly pronounced satellite peaks. Importantly, the Fe $2p_{3/2}$ satellite peak (719.0 eV) appeared at separation energy of 8.2 eV, thus verifying the presence of Fe^{3+} species. The absence of satellite peaks at 716.0 eV characteristic for Fe^{2+} confirmed the absence of Fe_3O_4 in the nanoparticles. The O 1s spectrum of the neat nanoparticles showed two contributions at 530.0 and 531.3 eV arising from γ-Fe_2O_3 lattice oxygen and surface hydroxyls (Figure 4B). The latter band had contributions from the adventitious organic carbon contaminants originating from alcohol contaminants as further evidenced by the peak at 285.0 eV. The Si 2p spectrum of the neat nanoparticles also showed a minute contribution of Si at 101.2 eV (Figure 4C). The low intensity of this band made the exact identification of the silicon binding state difficult.

The formation of SiO_2 shell on the γ-Fe_2O_3 nanoparticle surface was clearly confirmed by decrease of the Fe and increase of Si and O content in the γ-Fe_2O_3&SiO_2 (Table 2). The O 1s and Si 2p regions were characterized by new dominating bands at 533.1 and 104.1 eV, respectively, which are typical of pure silica (Figure 4C). Concomitantly, the initially observed contributions of γ-Fe_2O_3 lattice oxygen and surface hydroxyls were significantly lowered.

Introduction of aminosilica (using APTES and APDMES) on the nanoparticle surface did not change the O 1s spectra. The Si 2p region of the γ-Fe_2O_3&SiO_2-NH_2 nanoparticles was characterized by a stronger contribution at 102.6 eV arising from the Si-C bonds of APTES and APDMES. Importantly, the high-resolution XPS spectrum in the C 1s and N 1s region clearly showed the silane coating containing amino terminal groups (Figure 4 D, E). The C 1s envelope of

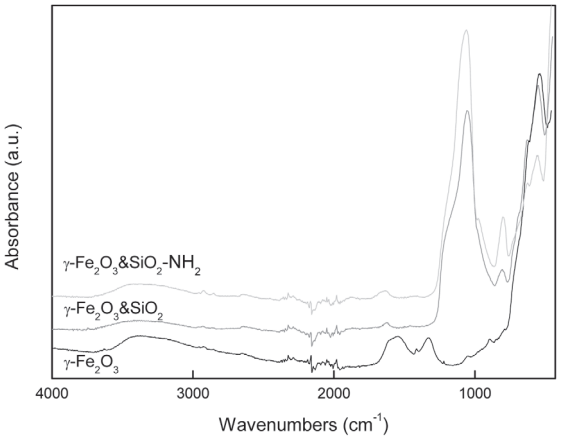

FIGURE 3. Attenuated total reflection Fourier-transform infrared spectra of γ-Fe_2O_3, γ-Fe_2O_3&SiO_2, and γ-Fe_2O_3&SiO_2-NH_2 nanoparticles.

TABLE 2. Surface atomic percentages for γ-Fe_2O_3, γ-Fe_2O_3&SiO_2, and γ-Fe_2O_3&SiO_2-NH_2 nanoparticles determined by x-ray photoelectron spectroscopy

	Atomic concentration (%)						
Nanoparticles	Fe 2p	O 1s	C 1s	Si 2p	N 1s	Na 1s	Cl 2p
γ-Fe_2O_3	27.7	50.5	17.6	0.8	-	2.5	0.9
γ-Fe_2O_3&SiO_2	8.1	58.1	10.2	23.6	-	-	-
γ-Fe_2O_3&SiO_2-NH_2	12.5	55.9	10.6	20.6	0.4	-	-

the silane layer could be resolved into contributions centered at 284.2, 285.0, 285.7, and 286.5 eV arising from C-Si, sp^3 carbon (C-C and C-H functionalities), C-N species of amines, and C-O contribution of hydroxyls present in the non-hydrolyzed ethoxy groups of APTES, respectively. We assigned the peak at 288.7 eV to carbamates formed by reaction of amino groups with atmospheric CO_2.

TEM assessment of interaction of γ-Fe_2O_3&SiO_2-NH_2 nanoparticles with peripheral blood cells

TEM micrograph of ultrathin section of peripheral blood mononuclear cells treated with the γ-Fe_2O_3&SiO_2-NH_2 nanoparticles showed that they were localized within the cytoplasm and in the extracellular space (Figure 5). Micro-

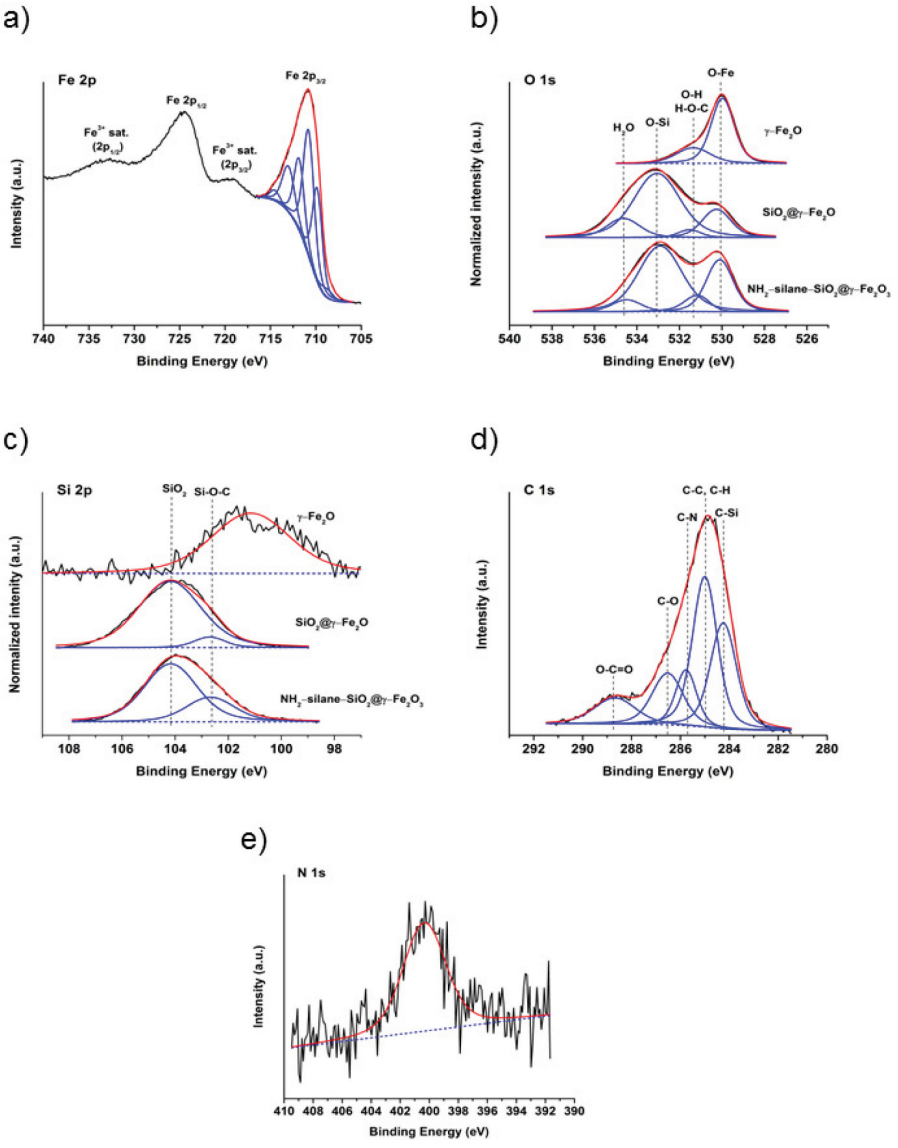

FIGURE 4. Measured high resolution (**A**) Fe 2p, (**B**) O 1s, (**C**) Si 2p, (**D**) C 1s, and (**E**) N 1s x-ray photoelectron spectra (XPS; black) fitted (red) by resolving the individual components (blue). Simulated Fe $2p_{3/2}$ spectrum was obtained by considering Gupta-Sen multiplets and satellite peaks of high and low binding energy (26). O 1s high-resolution XPS spectra of neat γ-Fe_2O_3, γ-Fe_2O_3&SiO_2, and γ-Fe_2O_3&SiO_2-NH_2 nanoparticles showed the presence of surface oxides, hydroxyls, and adsorbed water. Si 2p spectra confirmed the formation of SiO_2 and SiO_2-NH_2 shell on the γ-Fe_2O_3 surface. The presence of amino groups on the γ-Fe_2O_3&SiO_2-NH_2 surface was further verified by the detailed analysis of the C 1s and N 1s spectra.

photograph did not display any preferential localization of nanoparticles in the cells. Majority of the nanoparticles was localized on the cell surface and in cell surroundings.

Assessment of immunotoxicity of γ-Fe_2O_3&SiO_2-NH_2 nanoparticles

Cytotoxicity of γ-Fe_2O_3&SiO_2-NH_2 nanoparticles to peripheral blood cells and the effect of particles on proliferative activity of lymphocytes. In these experiments, cytotoxicity and proliferative activity of lymphocytes incubated with γ-Fe_2O_3&SiO_2-NH_2 nanoparticles was assessed using ^{3}H-thymidine incorporation into DNA of proliferating peripheral blood cells. Since the particles showed interference with the assay (data not shown), cultures with the nanoparticles added few minutes before cell harvesting were used as controls for statistical analysis and graphic display of the results.

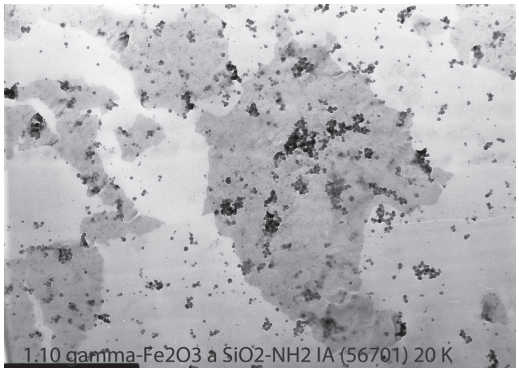

FIGURE 5. Transmission electron micrograph of ultrathin section of blood cells treated with γ-Fe_2O_3&SiO_2-NH_2 nanoparticles. They are localized within the cytoplasm of treated cells and in the extracellular space. There is no preferential localization in the cells, majority of the nanoparticles is localized on the cell surface and in cell surroundings. Magnification: 20 000×.

No cytotoxic effect of the newly developed γ-Fe_2O_3&SiO_2-NH_2 core-shell particles on human peripheral blood cells was found when the cells were exposed to the whole range of particle concentrations (0.12-15 μg/cm^2) during several time intervals (24, 48, and 72 h). No significant differences in basic proliferative activity of cells were observed (Figure 6).

Since no generally accepted nanoparticle positive and negative controls for immune assays are available at the moment, Cyf (well-known cytotoxic immunosuppressive agent) was used in three assays. They included assessment of cytotoxicity, proliferative activity of lymphocytes, and phagocytic activity of leukocytes. Appropriate doses were tested in previous experiments. Cyf (suppressive control) exposed to unstimulated peripheral blood cells for 48 and 72 h displayed a significant cytotoxicity.

In vitro proliferative response of γ-Fe_2O_3&SiO_2-NH_2-treated human peripheral blood T-lymphocytes and T-dependent B-cells after 24, 48 and 72 h exposure was assessed by their stimulation with a panel of mitogens and CD3 antigen (Figures 7A-D). Incorporation of [^{3}H]-thymidine into DNA of

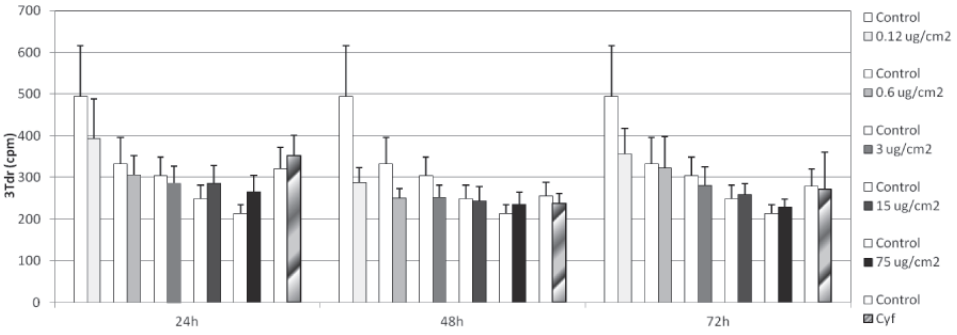

FIGURE 6. Cytotoxicity of γ-Fe_2O_3&SiO_2-NH_2 nanoparticles for human peripheral blood cells determined with [^{3}H]-thymidine incorporation assay. Results are expressed as counts/min/culture (cpm). Bars indicate mean cpm group values (+ standard deviation) in non-stimulated cell cultures. Blood cultures were treated with 0 (control), 0.12, 0.6, 3, 15, and 75 μg of γ-Fe_2O_3&SiO_2-NH_2/cm^2. The assay was performed after 24, 48, and 72 h of *in vitro* exposure of the peripheral blood cells (n = 10 human volunteers) with γ-Fe_2O_3&SiO_2-NH_2 nanoparticles. Cyf (40 mg/mL) served as a suppressive control. Statistical analysis was performed by comparing cpm in particle-exposed cultures vs control cultures using Mann-Whitney test, $P < 0.001$.

proliferating cells was highest (~30 000 cpm) in cultures stimulated *in vitro* with PHA mitogen, as expected (Figure 7 B). Statistical analysis revealed no significant effect of γ-Fe_2O_3&SiO_2-NH_2 particle concentration ranging 0.12-15 μg/cm^2 on proliferative activity of lymphocytes stimulated with this mitogen in all time intervals. Moreover, regardless of the other mitogen and antigen used (Con A, PWM, and CD3), no significant changes in proliferative response of lymphocytes were found in cultures exposed to the whole concentration range of γ-Fe_2O_3&SiO_2-NH_2 particles (Figure 7 A,C,D). A non-significant increase in proliferative response of T-cells stimulated through the T-cell receptor with CD3 antigen was found in the cell cultures treated with low doses of nanoparticles (0.12 μg/mL) for 24, 48, and 72 h (Figure 7D). Similarly, non-significant increase in proliferation was induced by middle concentrations of γ-Fe_2O_3&SiO_2-NH_2 particles (0.6-15 μg/cm^2) in cell cultures stimulated with Con A (Figure 7A). Non-significant decrease was found also in cell cultures containing high dose of particles (75 μg/cm^2) stimulated with PWM mitogen (Figure 7C). The effect of suppressive control (Cyf) on PHA-stimulated cell cultures was observed as a significant decrease in proliferative response of lymphocytes in all time intervals.

In vitro production of cytokines IL-6, IL-8, IFN-γ, TNF-α, and GM-CSF. *In vitro* production of cytokines IL-6, IL-8, TNF-α, IFN-γ, and GM-CSF in cells stimulated with PHA or PWM mitogens and treated for 48 h with whole range of particle concentrations is displayed on Figures 8 A-E. Significant increase in production of IL-6 without clear dose-dependence was found in cell cultures *in vitro* stimulated with PHA mitogen and exposed to middle and high particle doses (3 and 75 μg/cm^2). Similarly, significantly enhanced production of IL-8 without clear dose-dependence was observed in cells *in vitro* simulated with the same mitogen (PHA) exposed to middle γ-Fe_2O_3&SiO_2-NH_2 doses (3 and 15 μg/cm^2). On the other hand, production of IL-8 in PWM mitogen-stimulated cultures was significantly suppressed in almost all cells exposed to the particles. Levels of IFN-γ were significantly elevated in cells *in vitro* stimulated with PWM mitogen treated with two low γ-Fe_2O_3&SiO_2-NH_2 doses (0.12 and 0.6 μg/cm^2). Regardless of the particle dose and mitogen used, production of TNF-α did not differ in all experiments. Production of GM-CSF cytokine was significantly increased in supernatants derived from cultures stimulated with PWM mitogen exposed to the high dose of γ-Fe_2O_3&SiO_2-NH_2 (75 μg/cm^2).

Phagocytic activity and respiratory burst of leukocytes. While the phagocytic activity was evaluated by ingestion of fluorescein-labeled *Staphylococcus aureus*, respiratory burst of phagocytes was measured using hydroethidine in

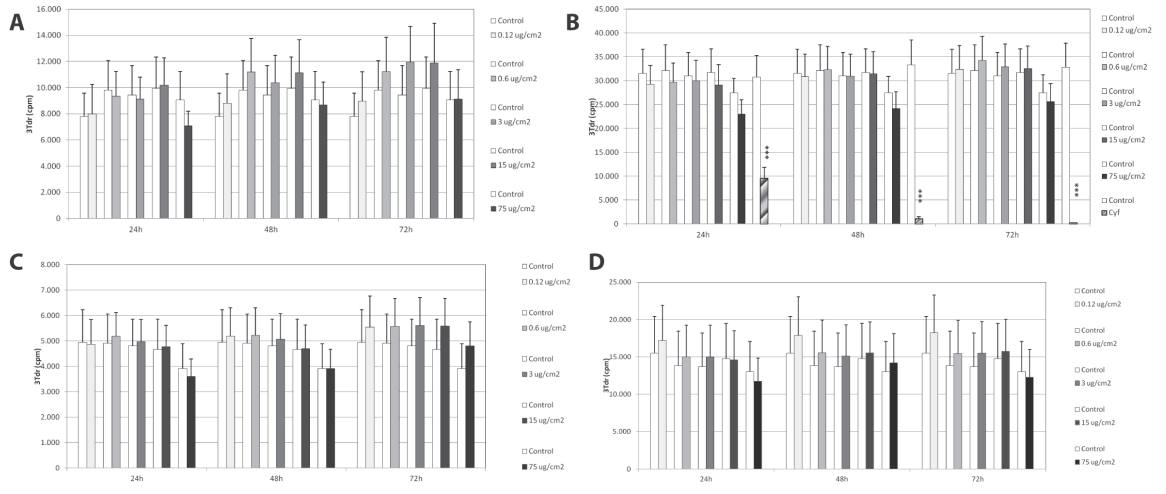

FIGURE 7. Proliferative response of human peripheral blood T-lymphocytes and T-dependent B-cells measured as incorporation of [^{3}H]-thymidine (^{3}Tdr) into replicating cells. Results are expressed as counts/min/culture (cpm). Bars indicate mean cpm group values (+ standard deviation) in cell cultures *in vitro* stimulated with (**A**) concanavalin, (**B**) phytohemagglutinin, (**C**) pokeweed mitogen, and (**D**) monoclonal anti-CD3 antigen. Blood cultures were treated with 0 (Control), 0.12, 0.6, 3, 15, and 75 μg of γ-Fe_2O_3&SiO_2-NH_2/cm^2. The assay was performed after 24, 48, and 72 h of *in vitro* exposure of the peripheral blood cells (n = 10 human volunteers) to particles. Cyf (40 mg/mL) was used as a suppressive control. Statistical analysis was performed by comparing cpm in particle-exposed cell cultures vs control cultures using Mann-Whitney test. Significance: *** $P < 0.001$.

the peripheral blood cells *in vitro* exposed to γ-Fe_2O_3&SiO_2-NH_2 for 24 and 48 h (Figures 9 A-C). No interference of particles with the assay was observed. Phagocytic activity of monocytes in γ-Fe_2O_3&SiO_2-NH_2-treated cell cultures did not show significant changes compared to the control cultures after both 24 and 48 h exposure (Figure 9A). A similar situation was observed also for the granulocytes (Figure 9B). Respiratory burst of phagocytes increased with increasing γ-Fe_2O_3&SiO_2-NH_2 concentration and was significantly enhanced after exposure to high dose of particles (75 μg/cm^2) after 48 h exposure. Suppressive control agent (Cyf) significantly decreased phagocytic activity of granulocytes and respiratory burst of phagocytes in both time exposure intervals (24 and 48 h; Figure 9 B,C).

DISCUSSION

The core-shell γ-Fe_2O_3&SiO_2-NH_2 nanoparticles were prepared by chemical coprecipitation, which was followed by oxidation and silanization. The coprecipitation technique belongs to the most convenient methods for production of iron oxide particles, which find many biological applications, such as in cell imaging and tracking, drug and gene delivery, hyperthermia, and capture of various cells and biomolecules (21). Morphology including shape, size, and its distribution depend on various reaction parameters, eg, type of salt, Fe(II)/Fe(III) ratio, temperature, pH, ionic strength, stirring, etc. Big advantage of these particles consists in their superparamagnetic behavior, which

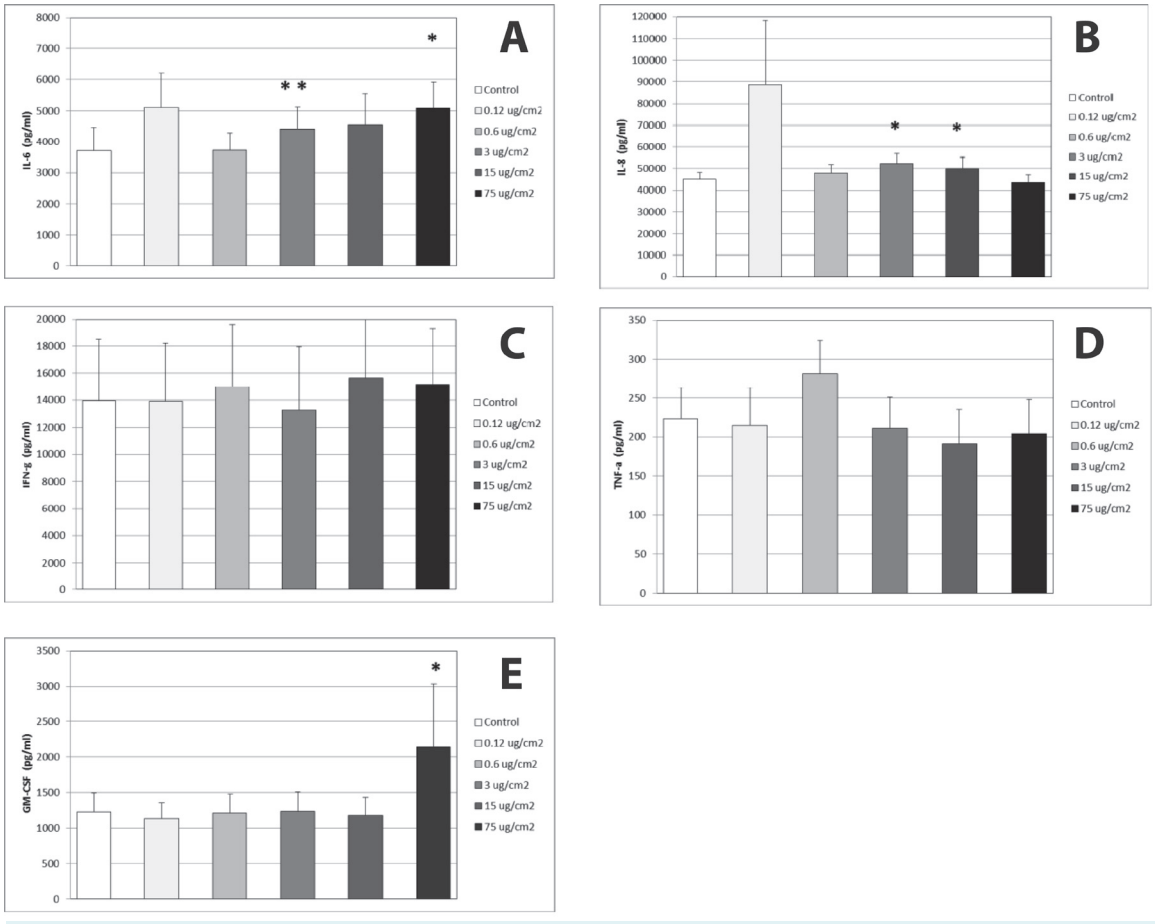

FIGURE 8. *In vitro* production of (**A**) interleukin-6, (**B**) interleukin-8, (**C**) interferon-gamma, (**D**) tumor necrosis factor-alpha, and (**E**) granulocyte macrophage colony stimulating factor cytokines in blood cells (n = 8 human volunteers) stimulated with phytohemagglutinin and for 48 h exposed to various concentrations of γ-Fe_2O_3&SiO_2-NH_2 nanoparticles: 0 (control), 0.12, 0.6, 3, 15, and 75 μg of γ-Fe_2O_3&SiO_2-NH_2/cm^2. Results are expressed as pg/mL. Bars indicate mean group values (+ standard deviation). Statistical analysis was performed by comparing cytokine levels in particle-exposed and non-exposed (control) cell culture supernatants using paired *t* test. Significance: * $P < 0.05$, ** $P < 0.01$.

means that below certain size (<20 nm) the particles have no hysteresis and are attracted by a magnet, however, they are easily redispersed in water when the magnetic field is removed (22). In this paper, optimal reaction conditions led to formation of 9 nm γ-Fe_2O_3 particles. After their modification with silica and aminosilica, diameter of the particles increased to 13 nm. Properties of the starting and modified particles were determined by a range of physico-chemical methods including TEM, DLS, and XPS measurements. The coating on the iron oxide nanoparticle surface was confirmed by TEM, ATR FTIR spectroscopy, and XPS analysis. Silica coating of the γ-Fe_2O_3 prevented aggregation of the particles in water and enhanced their chemical stability to several months.

In the biological *in vitro* experiments, the cytotoxicity and the effect of particles on the immune response were examined. Five different particle concentrations, which are typically used in analogous works, were selected ranging 0.12-75 μg/cm^2, which corresponded to 0.17-106 μg of particles/mL (calculated Fe content was from 21.25 ng/mL to 13.25 μg/mL). In our experimental setup, γ-Fe_2O_3&SiO_2-NH_2 particles displayed no cytotoxic effect on human peripheral blood cells. The newly synthesized particles can be therefore considered as a nanomaterial with very low *in vitro* cytotoxicity. However, *in vivo* experiments will be needed to confirm the results. Although *in vitro* and *in vivo* comparison of particle doses is very inaccurate even almost impossible; in human clinical diagnostics, the recommended dose for liver imaging is 15 μmol of Fe per kg if dextran-coated iron oxide (Endorem) is used.

With the aim to gain an overview on concentrations required for MR imaging, capacity of human monocytes to phagocyte iron oxide of different particle sizes, concentrations, and incubation times was investigated (23). The intracellular iron content was measured by atomic emission absorption spectrometry. A significantly higher cellular iron oxide uptake was found after incubation with large compared to small particles. It means that the former par-

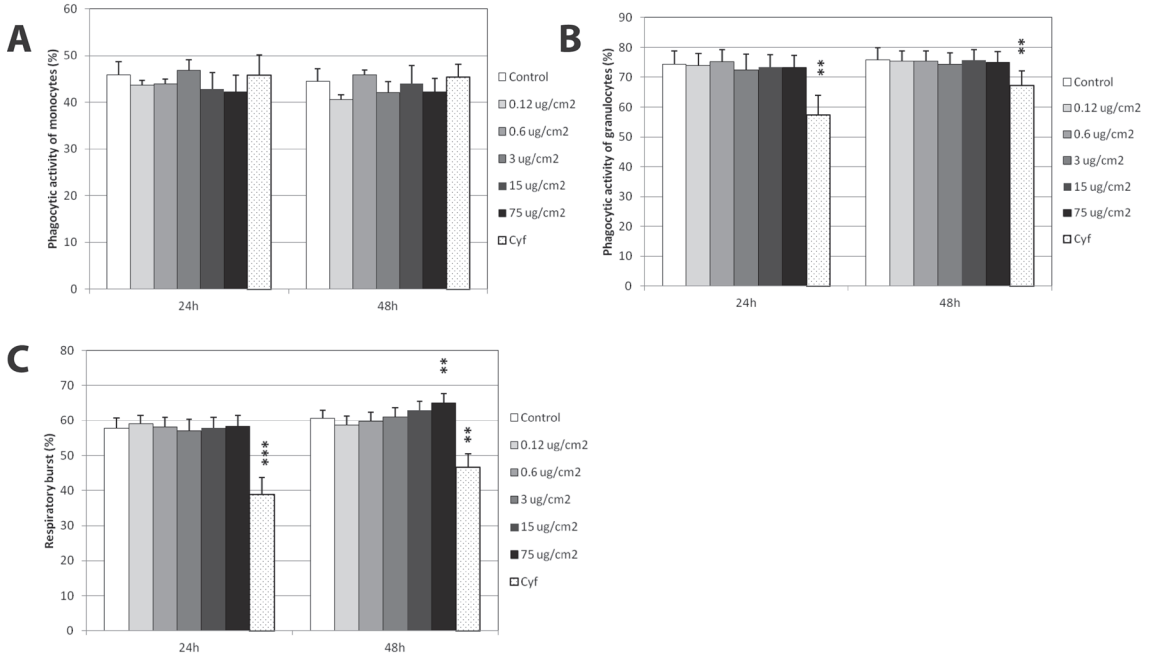

FIGURE 9. Phagocytic activity of (**A**) monocytes and (**B**) granulocytes evaluated by ingestion of fluorescein-labeled *Staphylococcus aureus,* and (**C**) respiratory burst of phagocytes monitored by flow cytometry using hydroethidine. Bars indicate mean group activity (+ standard deviation) in peripheral blood cultures treated *in vitro* with different concentrations of γ-Fe_2O_3&SiO_2-NH_2: 0 (control), 0.12, 0.6, 3, 15, and 75 μg/cm^2; Cyf (5 mg/mL) served as a suppressive control. The assay was performed after 24 and 48 h of *in vitro* exposure of the peripheral blood cells (n = 10 human volunteers) to magnetic particles. Statistical analysis was performed by comparing phagocytic activity and respiratory burst in particle-containing samples with control using paired *t* test. Significance: ** $P < 0.01$, *** $P < 0.001$.

ticles were better suited for MRI than the latter ones for *ex vivo* labeling of human monocytes prior to injection (23).

Function of lymphocytes was examined in cultures derived from human peripheral blood and *in vitro* treated either with stimulators of T-cells (PHA, Con A mitogens, and CD3 antigen) or stimulator of T-dependent B-cell response (PWM mitogen). In mitogen-stimulated cultures, differences in proliferative activity between the particle-exposed and unexposed lymphocytes might become more visible. This can be attributed to the increased sensitivity of the assay due to higher counts per minute per culture. Nevertheless, no significant differences in proliferative response of T-lymphocytes, as well as T-dependent B-cells, treated with all γ-Fe_2O_3&SiO_2-NH_2 concentrations compared to the control untreated cells were found at all time intervals.

Significantly increased production of IL-6, IL-8, and GM-CSF cytokines by human blood cells treated with middle and high doses of γ-Fe_2O_3&SiO_2-NH_2 particles (3, 15, and 75 μg/cm^2) were observed in cell cultures stimulated with PHA mitogen. However, elevated productions were without clear dose-dependence. This phenomenon can be partially explained by different nanoparticle dispersibility in the wells resulting in partial agglomeration and variable nanoparticle/cell ratios. Absence of γ-Fe_2O_3&SiO_2-NH_2 dose dependence in stimulation of IL-6, IL-8, and GM-CSF production has to be taken into consideration in future investigations. IL-6 is a pro-inflammatory cytokine secreted by T-cells, which stimulates immune response, eg, during infection and after tissue damage leading to inflammation. IL-6 is known to stimulate the inflammatory and auto-immune processes in many diseases, such as diabetes or atherosclerosis. IL-8 is a chemokine produced by macrophages and other cell types. IL-8 has two primary functions: induction of phagocytosis and chemotaxis, primarily neutrophils, but also other granulocytes causing their migration toward the site of infection. GM-CSF is a white blood cell growth factor, which stimulates stem cells to produce granulocytes and monocytes. GM-CSF is part of the immune/inflammatory cascade, by which activation of small number of macrophages can rapidly lead to an increase in their numbers for fighting infection (24).

Results of the effect of γ-Fe_2O_3&SiO_2-NH_2 particles on phagocytic activity and respiratory burst of phagocytes in human peripheral blood cultures are in agreement with studies on the interactions of Ferumoxtran-10 (F-10) iron oxide with human monocyte-macrophages *in vitro*, where lack of pro-inflammatory activity were assessed (25). After 72 h incubation, F-10 (1 mg/mL) was not toxic and only mildly toxic at high concentrations (10 mg/mL). Viability of the cells was not affected during 14 days. F-10 did not stimulate cytokines (interleukin-12, interleukin-6, tumor necrosis factor-α, and interleukin-1β), superoxide anion production, or Fc-receptor-mediated phagocytosis. Similarly, amino-poly(vinyl alcohol)-coated magnetic particles did not affect viability of human immune cells, but cytokine secretion (26). At the same time, percentage of viable macrophages increased, especially when the particles were added very early in the differentiation process.

On the other hand, magnetic nanoparticles induced formation of membranous ferroportin and incited secretion of ferritin, TNF-α, and IL-10 in human histiocytic lymphoma cells (U937) and human monocyte leukemia cells without any decrease of cell viability (27). A dose- and time-dependent cytotoxicity increase of oleate- or oleate/poly(ethylene glycol)/poly(lactic-*co*-glycolic acid)-coated magnetic particles was found in human lung adenocarcinoma epithelial (A549) and human embryo lung cells (HEL 12469) (28).

Animal experiments showed that iron oxide particles administered in mice in successive intratracheal instillations modulated the pulmonary immune response to ovalbumin (OVA) depending on the particle dose and size. At high and intermediate doses (4×250 or 4×500 μg of nanoparticles/mouse), the OVA-induced allergic response was significantly inhibited, as evidenced by the decrease in eosinophil cell influx and specific IgE levels. However, the low dose (4×100 μg of nanoparticles/mouse) had no significant effect on the OVA allergic response, while the same nanoparticle dose had an adjuvant effect on the Th2 response to OVA (29).

In conclusion, superparamagnetic γ-Fe_2O_3 nanoparticles were successfully developed and modified with two silica precursors. Assessment of interaction of γ-Fe_2O_3&SiO_2-NH_2 nanoparticles with human peripheral blood cells using TEM showed that the particles were localized within the cytoplasm of treated cells and in the extracellular space. No preferential localization in the cells was observed. The γ-Fe_2O_3&SiO_2-NH_2 particles proved to be non-toxic even at high dose (75 μg/cm^2) and after long-time incubation period (72 h). No significant differences in proliferative response of T-lymphocytes, as well as T-dependent B-cells treated with γ-Fe_2O_3&SiO_2-NH_2 particles in all concentrations and time exposures were found. Significantly increased production of IL-6, IL-8, and GM-CSF cytokines

by human blood cells treated with middle and high doses of γ-Fe_2O_3&SiO_2-NH_2 particles (3, 15, and 75 μg/cm^2) was observed without clear dose-dependence. No significant changes in production of TNF-α and IFN-γ was observed. Magnetic nanoparticles did not affect phagocytic activity of monocytes and granulocytes. Respiratory burst of phagocytes was significantly enhanced in cell cultures exposed to high particle dose (75 μg/cm^2) for 48 h. Cytotoxicity and *in vitro* immunotoxicity of new porous γ-Fe_2O_3&SiO_2-NH_2 core-shell nanoparticles were minimal, however, more assessments will be needed before possible use in human medicine, eg, in cell labeling, MRI, and drug delivery.

Acknowledgment The authors thank Helena Nagyová and Edita Mrvíková for technical help.

Funding This work was financially supported by the Czech Science Foundation (No. 16-01128J), the European Commission 7th Framework Programme (QualityNano project INFRA-2010-1.1.31, No. 214547-2, SMU-TAF 227), the Slovak Research and Development Agency (No. APVV-0401-11), the ITMS (No. 26240120033, Operational research and development program from the European Regional Development Fund), Cedars Sinai Medical Center's International Research and Innovation in Medicine Program, the Association for Regional Cooperation in the Fields of Health, Science and Technology (RECOOP HST Association) and the participating Cedars-Sinai Medical Center – RECOOP Research Centers (CRRC).

Ethical approval received from the Ethics Committee of the Slovak Medical University in Bratislava.

Declaration of authorship BAZ prepared the silica-modified magnetic nanoparticles. AL and MK determined toxicity. JT coordinated biological experiments. OPG measured XPS spectra. FČ provided TEM micrograph of blood cells. IV, MD, SI, and MH determined immunotoxicity. DH coordinated the research and writing of the manuscript.

Competing interests All authors have completed the Unified Competing Interest form at www.icmje.org/coi_disclosure.pdf (available on request from the corresponding author) and declare: no support from any organization for the submitted work; no financial relationships with any organizations that might have an interest in the submitted work in the previous 3 years; no other relationships or activities that could appear to have influenced the submitted work.

References

1 Gupta AK, Gupta M. Synthesis and surface engineering of iron oxide nanoparticles for biomedical applications. Biomaterials. 2005;26:3995-4021. Medline:15626447 doi:10.1016/j.biomaterials.2004.10.012

2 Li J, He X, Wu Z, Wang K, Shen G, Yu R. Piezoelectric immunosensor based on magnetic nanoparticles with simple immobilization procedures. Anal Chim Acta. 2003;481:191-8. doi:10.1016/S0003-2670(03)00089-8

3 Arbab AS, Bashaw LA, Miller BR, Jordan EK, Lewis BK, Kalish H, et al. Characterization of biophysical and metabolic properties of cells labeled with superparamagnetic iron oxide nanoparticles and transfection agent for cellular MR imaging. Radiology. 2003;229:838-46. Medline:14657318 doi:10.1148/radiol.2293021215

4 Xing Z-C, Chang Y, Kang I-K. Immobilization of biomolecules on the surface of inorganic nanoparticles for biomedical applications. Sci Technol Adv Mater. 2010;11:014101. doi:10.1088/1468-6996/11/1/014101

5 Mahmoudi M, Sahraian MA, Shokrgozar MA, Laurent S. Superparamagnetic iron oxide nanoparticles: promises for diagnosis and treatment of multiple sclerosis. ACS Chem Neurosci. 2011;2:118-40. Medline:22778862 doi:10.1021/cn100100e

6 Schleich N, Sibret P, Danhier P, Ucakar B, Laurent S, Muller RN, et al. Dual anticancer drug/superparamagnetic iron oxide-loaded PLGA-based nanoparticles for cancer therapy and magnetic resonance imaging. Int J Pharm. 2013;447:94-101. Medline:23485340 doi:10.1016/j.ijpharm.2013.02.042

7 Cornell RM, Schwertmann U. The iron oxides: structure, properties, reactions, occurrences and uses. 2nd Ed., Wiley, Darmstadt 2000.

8 Liu G. ·, Gao J, Ai H, Chen X. Applications and potential toxicity of magnetic iron oxide nanoparticles. Small. 2013;9:1533-45. Medline:23019129 doi:10.1002/smll.201201531

9 Baalousha M, Manciulea A, Cumberland S, Kendall K, Lead JR. Aggregation and surface properties of iron oxide nanoparticles: Influence of pH and natural organic matter. Environ Toxicol Chem. 2008;27:1875-82. Medline:19086206 doi:10.1897/07-559.1

10 Chastellain M, Petri A, Hofmann H. Particle size investigations of a multistep synthesis of PVA coated superparamagnetic nanoparticles. J Colloid Interface Sci. 2004;278:353-60. Medline:15450454 doi:10.1016/j.jcis.2004.06.025

11 Kaushik A, Khan R, Solanki PR, Pandey P, Alam J, Ahmad S, et al. Iron oxide nanoparticles–chitosan composite based glucose biosensor. Biosens Bioelectron. 2008;24:676-83. Medline:18692384 doi:10.1016/j.bios.2008.06.032

12 Garcia I, Zafeiropoulos NE, Janke A, Tercjak A, Eceiza A, Stamm M, et al. Functionalization of iron oxide magnetic nanoparticles with poly(methyl methacrylate) brushes via grafting-from atom transfer radical polymerization. J Polym Sci A Polym Chem. 2007;45:925-32. doi:10.1002/pola.21854

13 Barrera C, Herrera AP, Rinaldi C. Colloidal dispersions of monodisperse magnetite nanoparticles modified with poly(ethylene glycol). J Colloid Interface Sci. 2009;329:107-13. Medline:18930466 doi:10.1016/j.jcis.2008.09.071

14 Zasonska BA, Boiko N, Klyuchivska O, Trchová M, Petrovský E, Stoika R, et al. Silica-coated γ-Fe2O3 nanoparticles: preparation and engulfment by mammalian macrophages. J Nanopharmaceutics Drug Delivery. 2013;1:182-92. doi:10.1166/jnd.2013.1020

15 Lin W, Hung Y-W, Zhou X-D, Ma Y. In vitro toxicity of silica nanoparticles in human lung cancer cells. Toxicol Appl Pharmacol. 2006;217:252-9. Medline:17112558 doi:10.1016/j.taap.2006.10.004

16 Kayal S, Ramanujan RV. Anti-cancer drug loaded iron–gold core–shell nanoparticles (Fe@Au) for magnetic drug targeting. J Nanosci Nanotechnol. 2010;10:1-13. Medline:21133071 doi:10.1166/jnn.2010.2461

17 Zasonska BA, Boiko N, Horák D, Klyuchivska O, Macková H, Beneš

M, et al. The use of hydrophilic poly(N,N-dimethylacrylamide) grafted from magnetic γ-Fe2O3 nanoparticles to promote engulfment by mammalian cells. J Biomed Nanotechnol. 2013;9:479-91. Medline:23621005 doi:10.1166/jbn.2013.1552

18 Stöber W, Fink A. Controlled growth of monodisperse silica spheres in the micron size range. J Colloid Interface Sci. 1968;26:62-9. doi:10.1016/0021-9797(68)90272-5

19 Wahajuddin AS. Superparamagnetic iron oxide nanoparticles: magnetic nanoplatforms as drug carriers. Int J Nanomedicine. 2012;7:3445-71. Medline:22848170 doi:10.2147/IJN.S30320

20 Miller FA, Wilkins CH. Infrared spectra and characteristic frequencies of inorganic ions. J Anal Chem. 1952;24:1253-94. doi:10.1021/ac60068a007

21 Tong L, Zhao M, Zhu S, Chen J. Synthesis and application of superparamagnetic iron oxide nanoparticles in targeted therapy and imaging of cancer. Frontiers of Medicine. 2011;5:379-87. Medline:22198749 doi:10.1007/s11684-011-0162-6

22 Hofmann-Amtenbrink M, von Rechenberg B, Hofmann H. Superparamagnetic nanoparticles for biomedical applications. Adv Drug Deliv Rev. 2013;65:119-49.

23 Metz MD. Optimized labelling of human monocytes with iron oxide MR contrast agents. Radiological Society of North America, Scientific Assembly and Annual Meeting, Chicago 2003. http://archive.rsna.org/2003/3105866.html

24 Francisco-Cruz A, Aguilar-Santelises M, Ramos-Espinosa O, Mata-Espinosa D, Marquina-Castillo B, Barrios-Payan J, et al. Granulocyte-macrophage colony-stimulating factor: not just another haematopoietic growth factor. Med Oncol. 2014;31:774. Medline:24264600 doi:10.1007/s12032-013-0774-6

25 Müller K, Skepper JN, Posfai M, Trivedi R, Howarth S, Corot C, et al. Effect of ultrasmall superparamagnetic iron oxide nanoparticles (Ferumoxtran-10) on human monocyte-macrophages in vitro. Biomaterials. 2007;28:1629-42. Medline:17178155 doi:10.1016/j.biomaterials.2006.12.003

26 Strehl C, Gaber T, Maurizi L, Hahne M, Rauch R, Hoff P, et al. Effects of PVA coated nanoparticles on human immune cells. Int J Nanomedicine. 2015;10:3429-45. Medline:26056442 doi:10.2147/IJN.S75936

27 Laskar A, Ghosh M, Khattak SI, Li W, Yuan XM. Degradation of superparamagnetic iron oxide nanoparticle-induced ferritin by lysosomal cathepsins and related immune response. Nanomedicine (Lond). 2012;7:705-17. Medline:22500704 doi:10.2217/nnm.11.148

28 Mesarosova M, Ciampor F, Zavisova V, Koneracka M, Ursinyova M, Kozics K, et al. The intensity of internalization and cytotoxicity of superparamagnetic iron oxide nanoparticles with different surface modifications in human tumor and diploid lung cells. Neoplasma. 2012;59:584-97. Medline:22668025 doi:10.4149/neo_2012_075

29 Ban M, Langonné I, Huguet N, Guichard Y, Goutet M. Iron oxide particles modulate the ovalbumin-induced Th2 immune response in mice. Toxicol Lett. 2013;216:31-9. Medline:23147377 doi:10.1016/j.toxlet.2012.11.003

Publication No. 4

Colloids and Surfaces B: Biointerfaces 141 (2016) 382–389

Contents lists available at ScienceDirect

Colloids and Surfaces B: Biointerfaces

journal homepage: www.elsevier.com/locate/colsurfb

Magnetoconductive maghemite core/polyaniline shell nanoparticles: Physico-chemical and biological assessment

Zasońska Beata Anna[a,b], Bober Patrycja[a], Jošt Petr[c], Eduard Petrovský[d], Boštík Pavel[c], Horák Daniel[a,*]

[a] Institute of Macromolecular Chemistry, The Czech Academy of Sciences, Heyrovský Sq. 2, 162 06 Prague 6, Czech Republic
[b] Faculty of Science, Department of Physical and Macromolecular Chemistry, Charles University in Prague, Hlavova 2030, 128 40 Prague 2, Czech Republic
[c] Faculty of Military Health Sciences, University of Defense, Třebešská 1575, 500 01 Hradec Králové, Czech Republic
[d] Institute of Geophysics, The Czech Academy of Sciences, Boční II/1401, 141 31 Prague 4, Czech Republic

ARTICLE INFO

Article history:
Received 18 December 2015
Received in revised form 28 January 2016
Accepted 29 January 2016
Available online 1 February 2016

Keywords:
Maghemite
Nanoparticles
Core–shell
Polyaniline
Cytotoxicity

ABSTRACT

Nanoparticles of various compositions are increasingly being used in many areas of medicine. The aim of this study was to develop nanoparticles, which would possess both magnetic and conductive properties and, thus improve their suitability for a wider range of biomedical applications. Namely, it would enable both the particle manipulation and imaging using their magnetic properties and simultaneous stimulation of electro-sensitive cell types using their magnetic properties, which can be used in tissue therapy, engineering and as biosensors. Maghemite (γ-Fe_2O_3) particles were prepared by the co-precipitation of Fe^{2+} and Fe^{3+} salts with ammonium hydroxide, followed by the controlled oxidation with NaOCl. The polyaniline (PANI) shell on the γ-Fe_2O_3 nanoparticles was obtained by the polymerization of aniline hydrochloride with ammonium peroxydisulfate in an aqueous solution of poly(*N*-vinylpyrrolidone) at two reaction temperatures (0 and 25 °C). The resulting γ-Fe_2O_3&PANI particles were characterized by both the light and transmission electron microscopies, dynamic light scattering, magnetic measurements, UV–vis and energy dispersive X-ray (EDAX) spectroscopy. The size of the starting γ-Fe_2O_3 particles was 11 nm, that increased to 25 nm after the modification with PANI. The incubation of both the γ-Fe_2O_3 and γ-Fe_2O_3&PANI nanoparticles with the human neuroblastoma derived SH-SY5Y cells for 8 days showed neither significant decrease in the cell viability, nor detectable changes in the cell morphology. This indicates, that the particles have no detectable cytotoxicity in cell culture and represent a promising tool for further use in biomedical applications.

1. Introduction

Hybrid nanoparticles containing an inorganic iron oxide core and a conducting polymer shell have been recently widely investigated due to their unique combination of magnetic and electrical properties [1,2]. While the former property enables both the *in vitro* and *in vivo* manipulation and/or imaging of the particles in an external magnetic field, the latter can be utilized to electrochemically stimulate tissues and cells [3]. The interest in conductive polymers is increasing due to their attractive features, such as combined ionic and electric conductivities making them well suited for the use in neural tissue engineering [4], or as bioactuators [5] and biosensors [6]. The best-known conductive polymer polyaniline (PANI) has been found useful in diverse areas, including molecular electronics, batteries [7], ion-separation membranes [8] and solid-state ion-selective electrodes [9,10]. Nanoparticles with magnetic properties are being utilized or tested in various biomedical applications, such as in immunoassays [11], drug delivery [12,13], hyperthermic treatment [14,15], tissue repair [16,17], cell labeling [18,19] and as contrast agents in magnetic resonance imaging [20]. In these applications, an encapsulation of inorganic nanoparticles with polymers is necessary to improve their colloidal stability preventing the undesirable particle aggregation, reduce their toxicity and attach reactive groups for the subsequent binding of bioactive ligands [21,22].

Polyaniline-coated iron oxide particles have become a subject of an intensive research for their use in a broad spectrum of various fields, such as a corrosion protection [23], removal of toxic dyes from waste water [24], biosensing [25,26], detection of specific bacteria [27], actuators, adsorption of DNA [28] and electrically

* Corresponding author.
E-mail address: horak@imc.cas.cz (H. Daniel).

http://dx.doi.org/10.1016/j.colsurfb.2016.01.059
0927-7765/

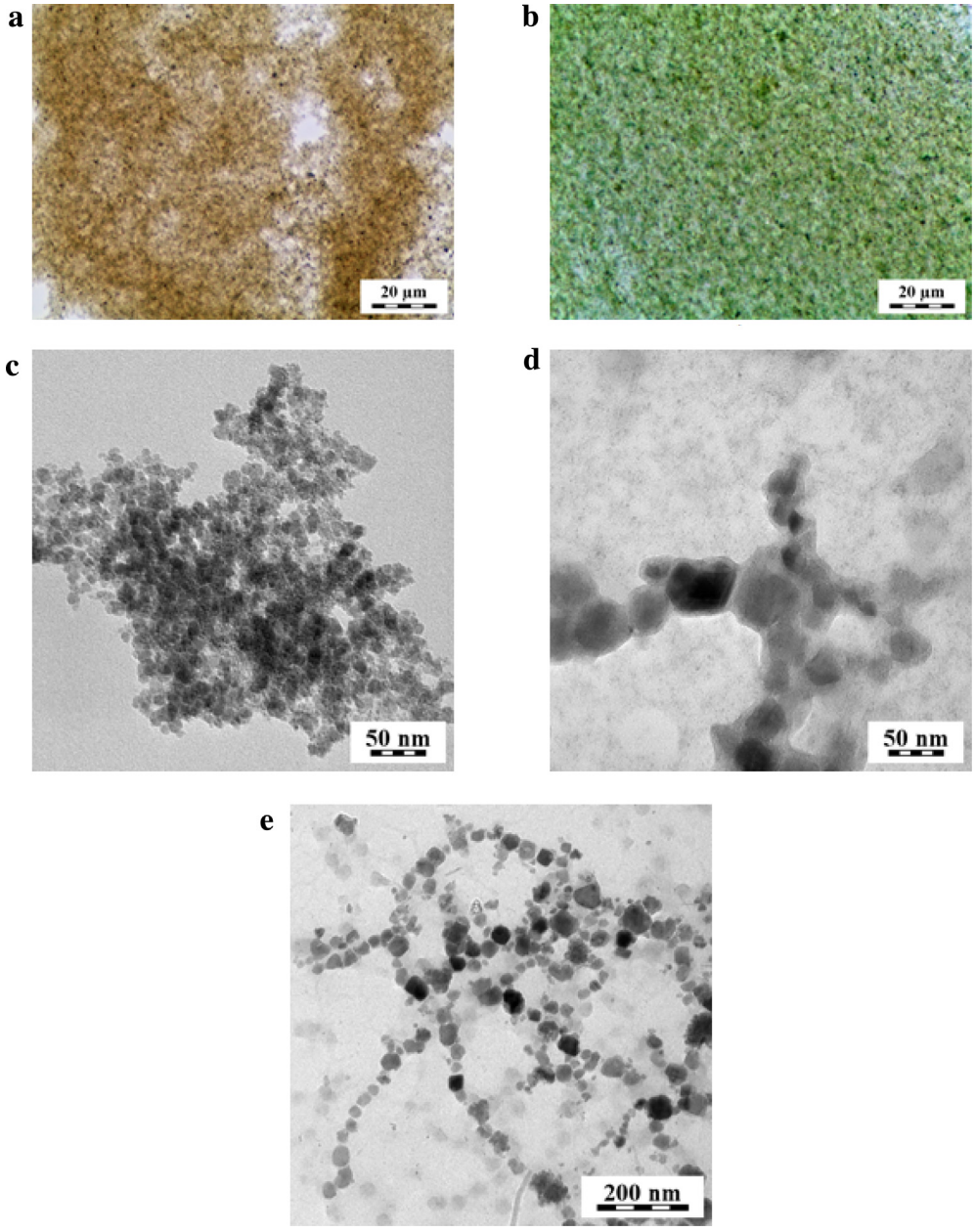

Fig. 1. (a, b) Light and (c–e) TEM micrographs and of (a, c) γ-Fe_2O_3 and (b, d) γ-Fe_2O_3&PANI nanoparticles No. 1 and (e) No. 2.

conductive fibers [29]. The PANI itself has been shown to support a formation of reactive oxygen species and thus to increase the antibacterial activity of the nanocomposites against *Escherichia coli* [30]. Different synthetic approaches of such composites in the forms of nanoparticles, nanowires or nanotubes have been already described [31–38]. In these systems, the magnetic properties were affected by the PANI content and size of the particles [39]. The most widely used synthetic method consists of the *in situ* polymerization of aniline in an aqueous dispersion of Fe_3O_4 nanoparticles using sodium dodecylbenzenesulfonate as a surfactant [40–45]. The potential for the utilization of such nanoparticles with both the (electro) magnetic and conductive properties as the means of drug delivery to the central nervous system or malignant tissues is one of the challenging fields for a pharmaceutical research and development. However, potential adverse effects associated with cytotoxicity and other parameters, such as tissue distribution profiles must be well defined and are essential for risk assessment [46,47].

In this report, the polyaniline shell was selected for coating of new maghemite (γ-Fe_2O_3) nanoparticles not only due to its electrical conductivity, but also due to the good environmental stability, low ionization potential, and excellent optical properties. In order to estimate biocompatibility of the new hybrid iron oxide core/PANI shell particles, cytotoxicity was determined using a real-time cytotoxicity-monitoring assay.

2. Experimental

2.1. Materials

$FeCl_2 \cdot 4H_2O$, $FeCl_3 \cdot 6H_2O$ and poly(*N*-vinylpyrrolidone) (PVP; M_w = 360,000 Da) were purchased from Fluka (Buchs, Switzerland), sodium hypochlorite (NaOCl) solution (5 wt%) was from Bochemie (Bohumín, Czech Republic). Ammonium peroxydisulfate and aqueous ammonia were obtained from Lachner (Neratovice, Czech

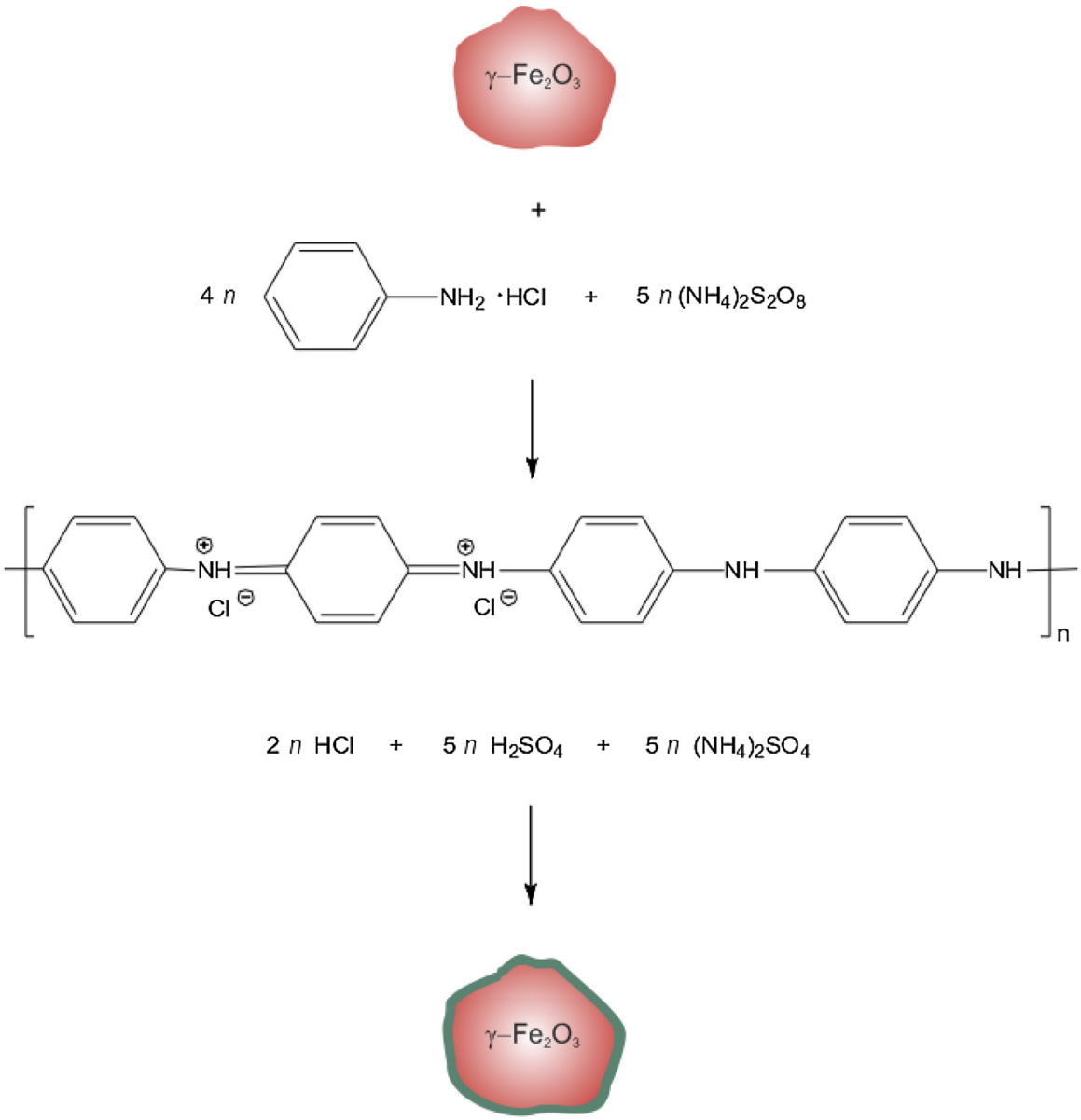

Fig. 2. Scheme of aniline hydrochloride oxidation with ammonium peroxydisulfate in the presence of poly(*N*-vinylpyrrolidone) in aqueous γ-Fe_2O_3 dispersion.

Republic). Aniline hydrochloride was purchased from Penta (Prague, Czech Republic). Ultrapure Q-water ultrafiltered in a Milli-Q Gradient A10 system (Millipore; Molsheim, France) was used for preparations of all solutions.

2.2. Synthesis of the γ-Fe_2O_3 nanoparticles

The γ-Fe_2O_3 nanoparticles were prepared as described previously [48]. Briefly, 0.2 M aqueous iron(III) chloride (100 ml) and 0.2 M iron(II) chloride (50 ml) solutions were mixed with the 0.5 M aqueous ammonia (100 ml) under sonication (5 min). The resulting solution was then added to the 0.5 M aqueous ammonia solution (400 ml) and stirred for 1 h (200 rpm) at a room temperature. The resulting precipitate was magnetically separated and washed with the Q-water (5–7 times). Then the 5 wt% NaOCl aqueous solution (16 ml) was added and the mixture sonicated for 5 min. The product (γ-Fe_2O_3) was again magnetically separated and washed with water.

2.3. Preparation of γ-Fe_2O_3&PANI nanoparticles

γ-Fe_2O_3&PANI colloid was prepared by the oxidation of aniline hydrochloride with ammonium peroxydisulfate in the presence of PVP stabilizer (2 wt%) dissolved in an aqueous γ-Fe_2O_3 dispersion (10 mg γ-Fe_2O_3/ml) at 0 or 25 °C and the resulting particles were denoted as γ-Fe_2O_3&PANI Nos. 1 and 2, respectively. The volume of the reaction mixture was 50 ml and ammonium peroxydisulfate/aniline hydrochloride and aniline hydrochloride/γ-Fe_2O_3 ratios were 1.25 mol/mol and 0.2 w/w, respectively. The reaction mixture was stirred (150 rpm) for five hours and then left to stand for 24 h. The resulting dark-green colloidal dispersion was dialyzed against the Q-water to reach pH 7 or against 0.2 M hydrochloric acid to remove reaction by-products, as well as residual monomers and oxidants; optionally, pH of this product was adjusted to 3.

2.4. Characterization of the nanoparticles

The size and morphology of the particles before and after modification was determined by the Tecnai Spirit G2

Table 1
Characteristics of prepared nanoparticles.

Run	D_n[a] (nm)	PDI[b]	D_h[c] (nm)	PD[d]	γ-Fe_2O_3[e] (wt%)	ζ-potential (mV)	M_s[f] (A m^2/kg)
γ-Fe_2O_3	11 ± 2	1.3	192 ± 40	0.1	100	−51 ± 3	49
γ-Fe_2O_3&PANI No. 1[g]	25 ± 8	1.4	257 ± 31	0.3	33.1	1 ± 4	16.2
γ-Fe_2O_3&PANI No. 2[h]	16 ± 5	1.4	234 ± 21	0.3	28.4	−0.35 ± 3	13.9

[a] Number-average diameter (TEM).
[b] Polydispersity index (D_w/D_n).
[c] Hydrodynamic diameter (DLS).
[d] Polydispersity (DLS).
[e] Content according to VSM.
[f] Saturation magnetization.
[g] PANI prepared at 0 °C.
[h] 25 °C.

transmission electron micrographs (TEM; FEI; Brno, Czech Republic). The number-average diameter (D_n), as well as the weight-average diameter (D_w), and the uniformity (polydispersity index PDI = D_w/D_n) were calculated from at least 400 individual nanoparticles on the micrographs using the Atlas software (Tescan Digital Microscopy Imaging; Brno, Czech Republic). The PANI shell thickness was estimated from the difference between D_n of starting and modified γ-Fe_2O_3 particles. The composition of the nanoparticles was analyzed using the Quanta 200 FEG scanning electron microscope (SEM; FEI) equipped with the energy dispersive X-ray spectrometer (EDAX; Mahwah, NJ, USA). Light micrographs were obtained using the Nikon ECLIPSE 80i microscope. The hydrodynamic diameter (D_h) of particles in water and the polydispersity (PD), as well as the ζ-potential and conductivity, were determined using the Zetasizer Nano-ZS Model ZEN3600 instrument (Malvern Instruments; Malvern, UK). PD is generally in the range 0–1, where 0 and 1 represent the monodisperse and highly polydisperse particles, respectively. The colloidal dispersions were diluted with water and mean D_h, PD and ζ-potential were calculated from at least 5 measurements. The Fourier-transform infrared measurement (FT-IR) was achieved in the attenuated total reflection (ATR) mode using the Thermo Nicolet NEXUS 870 FT-IR spectrometer (Madison, WI, USA). The magnetization was measured using the EV9 vibrating sample magnetometer (VSM; DSM Magnetics ADE Corporation; Lowell, MA, USA) at a room temperature. Ultraviolet–visible spectra (UV–vis) of γ-Fe_2O_3 and γ-Fe_2O_3&PANI colloids were recorded in buffer solutions (pH 3 and 7) using the PerkinElmer Lambda 950 spectrometer. The buffer solutions providing a constant ionic strength and no light absorption at 340–900 nm utilized for these measurements consisted of 0.0225 M citric acid (monohydrate), 0.0225 M Tris, 0.0225 M KCl (all from Fluka), 0.0225 M KH_2PO_4 and 0.0225 M $NaB_4O_7 \cdot 10\,H_2O$ (Merck; Kenilworth, NJ, USA) [49].

2.5. Real-time cytotoxicity assay

Cytotoxicities of the developed γ-Fe_2O_3 and γ-Fe_2O_3&PANI particles were tested using the human neuroblastoma SH-SY5Y (ATCC® CRL-2266™) cell line (ATCC; Rockvile, MD, USA). Changes of the cell viability were monitored in the real time using the xCELLigence system (Roche). This system uses specially designed 96-well microtiter plates (E-plate 96) with an array of gold microelectrodes on the bottom of each well. The cell growth in each well is monitored as changes in the electric impedance. The E-plate 96 was first filled with 50 μl of Dulbecco's Modified Eagle Medium (DMEM) per well to measure a background signal. The 100 μl of cell suspension containing 15,000 cells was then added to each well and the E-plate was left at a room temperature for 20 min to allow the cells to spread evenly. The E-plate was then placed in the incubator at 37 °C, connected with the monitoring device and cell proliferation was monitored overnight. Subsequently, 50 μl of cell media was then removed from each well and replaced with 100 μl of dispersions containing 1 or 100 μg/ml of γ-Fe_2O_3 nanoparticles in DMEM. The electrical impedance signal expressed as a normalized cell index (NCI) was automatically recorded every 60 min for next 192 h (8 days) to obtain a time dependent cell-response curve. Each measurement was carried out in quadruplicates and mean values with standard deviations were calculated.

The morphology of cells was observed using the Olympus CKX41 inverted light microscope (Tokyo, Japan) at the 200× magnification and photographed using the Olympus SP-350 digital camera after 72 h incubation of cells with particles.

3. Results and discussion

3.1. Physicochemical characterization

Multifunctional magnetic iron oxide nanoparticles are recently attracting a great deal of attention in medical diagnostics and treatment. There is thus need to design and develop new and efficient procedures for synthesis and surface modifications of such particles. In this report, the two-stage synthetic approach consisted of a synthesis of neat γ-Fe_2O_3 nanoparticles, which were subsequently coated with PANI. The PANI modification adds the electrical conductivity to the particle properties enabling them to be used to stimulate cells and tissues when an electrical field is applied.

The core iron oxide particles were prepared by a simplified two-step procedure involving the precipitation of iron chlorides in the alkaline medium (aqueous ammonia) and the subsequent NaOCl oxidation of magnetite (Fe_3O_4) to γ-Fe_2O_3. The reason for the introduction of the oxidation step was to achieve a higher chemical stability of γ-Fe_2O_3 compared to Fe_3O_4 [50]. Fig. 1a shows the brownish color of the prepared γ-Fe_2O_3 particles, which had the number-average diameter D_n = 11 nm, with PDI = 1.3 suggesting their polydisperse character (Fig. 1c). The particles were colloidally stable due to low value of ζ-potential (−51 mV; Table 1).

At the second stage of the synthesis, a conductive shell was formed on the surface of the γ-Fe_2O_3 core by the oxidation of aniline hydrochloride with ammonium persulfate at 0 or 25 °C in the presence of the PVP stabilizer (2 wt%) to prevent the particles from the aggregation (Fig. 2). PANI is known to be physically adsorbed on the iron oxide surface [51]. While a high-molecular-weight product is expected to be formed at the lower reaction temperature (0 °C), a low-molecular-weight PANI should be the result of the reaction at the higher temperature (25 °C). The reaction temperature thus affects the thickness of the PANI shell. The color of the originally brownish colloid (Fig. 1a) changed during the reaction to blue, indicating the formation of pernigraniline, and, finally, to green, representing emeraldine salt [52] (Fig. 1b). It should be noted that freshly prepared γ-Fe_2O_3&PANI colloids are acidic, but the pH during the dialysis was adjusted to 7, which supports a transformation of a conducting PANI salt to non-conducting PANI base (conductivity σ of powder $\sim 10^{-9}$ S/cm). In some cases, pH of γ-

Fe_2O_3&PANI was adjusted to 3 to achieve high conductivity of the powder PANI salt (~4 S/cm). The coating at two different reaction temperatures (0 and 25 °C) yielded two kinds of the γ-Fe_2O_3&PANI nanoparticles Nos. 1 and 2 with the average sizes of 25 and 16 nm (PDI = 1.4; Table 1), respectively. This corresponds to the previously reported observation that a decrease in the polymerization temperature leads to an increase in the shell thickness of films [53]. The shell thicknesses of γ-Fe_2O_3&PANI particles Nos. 1 and 2 were estimated to be ~5–7 and 2 nm, respectively (Fig. 1d,e). This temperature control of the PANI shell thickness can be considered as one of the novel and original aspects of the presented work. Moreover, the composite maghemite/polyaniline nanoparticles seen in Fig. 1d,e to the best of our knowledge were not yet described. The hydrodynamic diameters D_h of the particles measured in water also increased after the aniline polymerization from 192 nm to 257 and 234 nm for the γ-Fe_2O_3&PANI Nos. 1 and 2, respectively. The big discrepancy between the number-average and hydrodynamic diameters is attributed to the fact, that the former represents the dry particle size measured using TEM, while the latter value is obtained from DLS of an aqueous colloid. DLS does not measure the number-average, but the z-average size that is sensitive to a presence of large particles and, moreover, the particles are measured in doublets, triplets and small groups. At the same time, ζ-potential of the γ-Fe_2O_3&PANI particles approached zero. Similarly to the TEM analysis, the particle size distribution of the γ-Fe_2O_3&PANI particles according to DLS was rather broad (PD = 0.3). It should be noted that the polydispersity PD (DLS) estimated from the correlation function, which represents an assemble-averaged product of a scattered intensities at the beginning and a given time of the experiment, differed from the polydispersity index PDI (TEM) obtained from the analysis of dry particles. For monodisperse particles, the correlation function is single exponential [54] and PD thus indicates a deviation of the correlation function from the exponential behavior. The PANI coating thus improved the colloidal stability of the particles that therefore had a low tendency to aggregate (Fig. 1e) compared to the uncoated γ-Fe_2O_3 (Fig. 1c).

The additional physico-chemical characterization of the γ-Fe_2O_3 and γ-Fe_2O_3&PANI particles consisted in the determination of magnetic hysteresis curves (Fig. 3). The nanoparticles showed a superparamagnetic behavior, although a slight remanent magnetization and coercivity could be still observed. This behavior can be attributed to interactions between the particles resulting in a kind of collective behavior. In biomedical applications, the superparamagnetic behavior is preferred as it ensures, that the particles can be dispersed in an aqueous media in the absence of magnet (the magnetization appears to be zero). However, when an external magnetic field is applied, it magnetizes the nanoparticles, which are attracted by the magnet. As expected, the magnetic behavior of the nanoparticles was different from the bulk material due to the nano-size effect, inter-particle interactions and other surface effects. The γ-Fe_2O_3&PANI particles showed a lower concentration of maghemite than the original γ-Fe_2O_3, according to the magnetic measurements (Table 1). The γ-Fe_2O_3&PANI particles No. 2 (synthesized at 25 °C) exhibited lower magnetization than the γ-Fe_2O_3&PANI No. 1 (prepared at 0 °C) due to the thicker shell of the particles No. 1 (Fig. 3a). Hysteresis loops presented in this chart, which depict the dependence of the induced magnetization on the applied magnetic field, provide three important parameters of the material: (i) the saturation magnetization (M_s) of the ferrimagnetic component, which reflects a concentration of ferrimagnets, (ii) the saturation remanent magnetization (M_{rs}), *i.e.*, the magnetization remaining in the sample in the absence of the external magnetic field after previous saturation and (iii) the coercive force (H_c), which quantifies a field necessary to induce zero magnetization after the previous saturation (the magnetic hardness). The M_{rs}/M_s ratio is mostly dependent on the particle size being 0.5 for

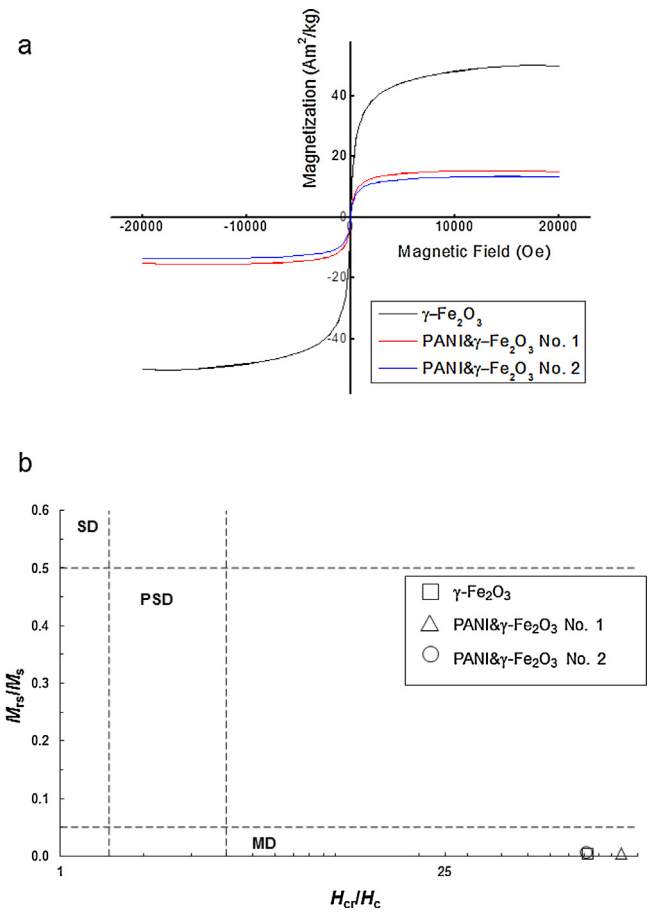

Fig. 3. (a) Hysteresis loops and (b) Day diagram of γ-Fe_2O_3 and γ-Fe_2O_3&PANI nanoparticles. SD, PSD and MD is single, pseudosingle and multidomain, respectively.

randomly oriented single-domain magnetite/maghemite particles <0.5 μm. Additional measurements of the direct-field remagnetization (the remanent magnetization in a direction opposite to the previously acquired saturation remanent magnetization) represent a gradual decay and removal of magnetic remanence. This procedure enables a determination of the coercivity of remanence H_{cr}, *i.e.*, a field necessary to remove the saturation remanence completely. The M_{rs}/M_s and H_{cr}/H_c ratios form the Day diagram [55], which reflects a relative particle size distribution (Fig. 3b). Since in ultrafine superparamagnetic particles $H_c \to 0$ and $M_{rs} \to 0$, points in the Day plot should be at extreme positions. All the γ-Fe_2O_3 and γ-Fe_2O_3&PANI particles Nos. 1 and 2 meet well this assumption (Fig. 3a). The saturation magnetization of uncoated γ-Fe_2O_3 particles, determined from hysteresis loops after subtraction of the linear part, is 49 A m^2/kg suggesting that the concentration of maghemite in the sample is 61.2 wt%, assuming that the saturation magnetization of pure maghemite is 80 Am^2/kg. After the modification with PANI, the magnetization of γ-Fe_2O_3&PANI particles Nos. 1 and 2 decreased to 16.2 A m^2/kg (corresponding to 33.1 wt% γ-Fe_2O_3) and 13.9 A m^2/kg (28.4 wt% γ-Fe_2O_3), respectively (Fig. 3a).

The presence of elements in the γ-Fe_2O_3&PANI nanoparticles was analyzed by EDAX, which provided a direct evidence of PANI on the iron oxide surface (Fig. 4). The γ-Fe_2O_3&PANI particles No. 1 contained 71.1 wt% of carbon (peak at 0.28 keV), 5.9 wt% of nitrogen (0.35 keV), 8.6 wt% oxygen (0.51 keV), 9.6 wt% of chlorine (2.6 and 2.8 keV) and 2.3 wt% of iron at *ca.* 0.65, 6.4 and 7.1 keV. In contrast, the uncoated γ-Fe_2O_3 had 60.7 wt% Fe. It should be noted that chlorine ions in the γ-Fe_2O_3&PANI contribute to conducting properties of the particles.

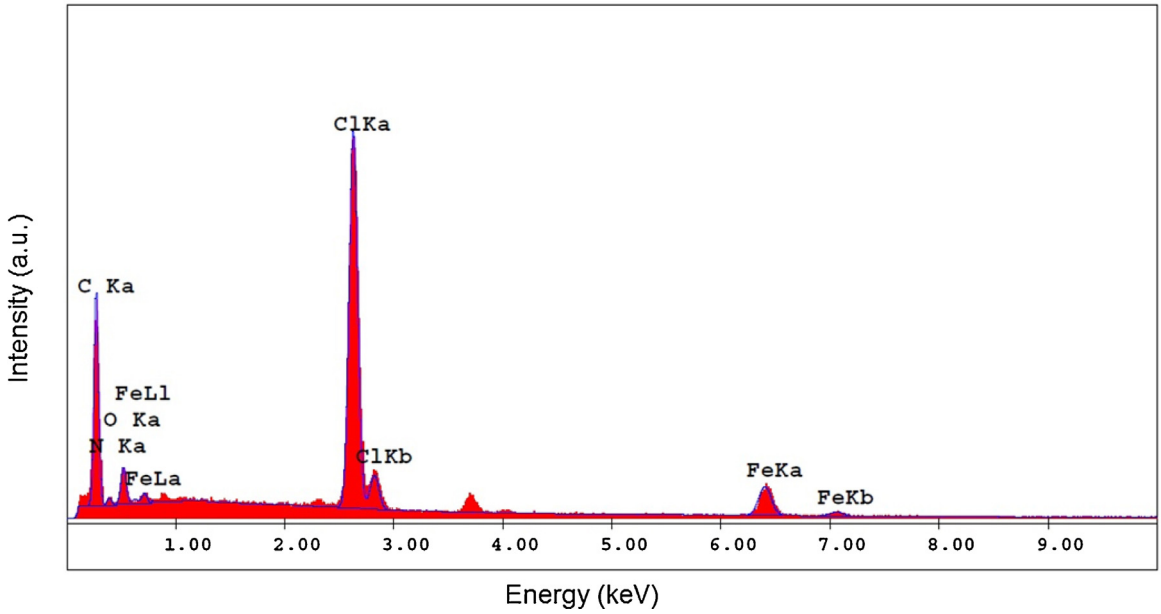

Fig. 4. EDAX analysis of γ-Fe_2O_3&PANI nanoparticles No. 1.

Also the UV–vis spectra of the γ-Fe_2O_3 and γ-Fe_2O_3&PANI particle dispersions clearly demonstrated the formation of the PANI shell (Fig. 5). The spectrum of the γ-Fe_2O_3&PANI dispersion at pH 3 (Fig. 5a) had three absorption maxima typical for a conducting PANI salt: at ~320 nm corresponding to the π–π* transition of the benzenoid rings, and at ~410 and >780 nm associated with the presence of polaron states (charged cation radicals). As the transitions between the PANI salt and non-conducting base takes place at pH 4–6, PANI is in the non-conducting form at pH 7. The absorption maximum of this base at ~ 600 nm corresponds to the *n*–π* quinonoid ring transitions (Fig. 5b). Spectrum of the γ-Fe_2O_3 particle dispersion had maxima at 371 nm (pH 3) and 320 nm (pH 7; Fig. 5). In contrast with PANI, the absorption maxima of γ-Fe_2O_3&PANI salt and base were slightly shifted suggesting interactions between PANI and γ-Fe_2O_3.

3.2. *Evaluation of γ-Fe_2O_3 and γ-Fe_2O_3&PANI particle toxicity*

The potential cytotoxicity of prepared nanoparticles on the SH-SY5Y cells was determined by the xCELLigence system in real-time measurements. The SH-SY5Y cells were used as a biological model of proliferating human neuronal cells. Fig. 6 shows, that five types of the particles were tested on these cells: (A) unmodified γ-Fe_2O_3, (B) γ-Fe_2O_3&PANI No. 1 (pH 3), (C) γ-Fe_2O_3&PANI No. 1 (pH 7), (D) γ-Fe_2O_3&PANI No. 2 (pH 3) and (E) γ-Fe_2O_3&PANI No. 2 (pH 7). The particles were tested at two concentrations (1 and 100 μg/ml), and their effects on the SH-SY5Y cell proliferation were tested for 8 days. The parameter monitoring cell viability and changes in cell morphology — normalized cell index (NCI) — was recorded every 60 min. γ-Fe_2O_3 particles (without shell), similarly to PANI-coated particles Nos. 1 and 2, at concentration 1 and 100 μg/ml did not show detectable cytotoxic effects during the observed time interval (Fig. 6). At the concentration 1 μg/ml, particles with PANI prepared at 0 °C inhibited cell growth to a lower extent than the particles with PANI prepared at 25 °C or neat γ-Fe_2O_3 particles. This can be attributed to the protective effects of the thicker PANI shell on the Fe_2O_3&PANI particles No. 1 compared to the shell on the Fe_2O_3&PANI particles No. 2. The particles at the concentration of 100 μg/ml significantly inhibited cell growth (Fig. 6). The data also show that at the concentration of 1 μg of particles/ml, the γ-Fe_2O_3&PANI particles No. 1 both in protonated (pH 3) and neutral

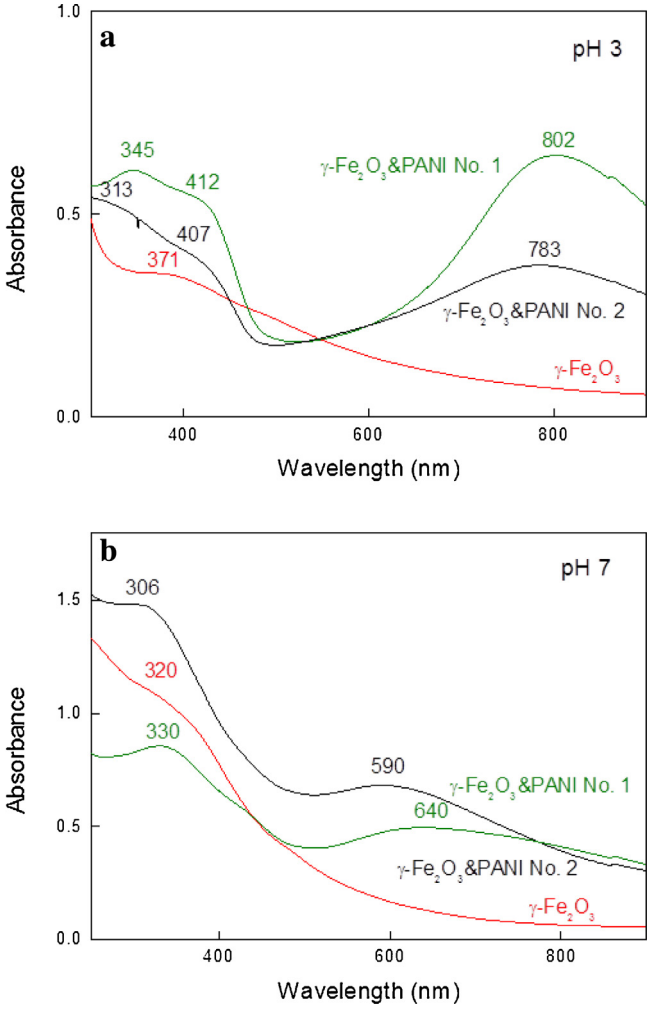

Fig. 5. UV–vis spectra of the γ-Fe_2O_3 and γ-Fe_2O_3&PANI particle dispersions in buffer solutions: (a) pH 3 and (b) pH 7.

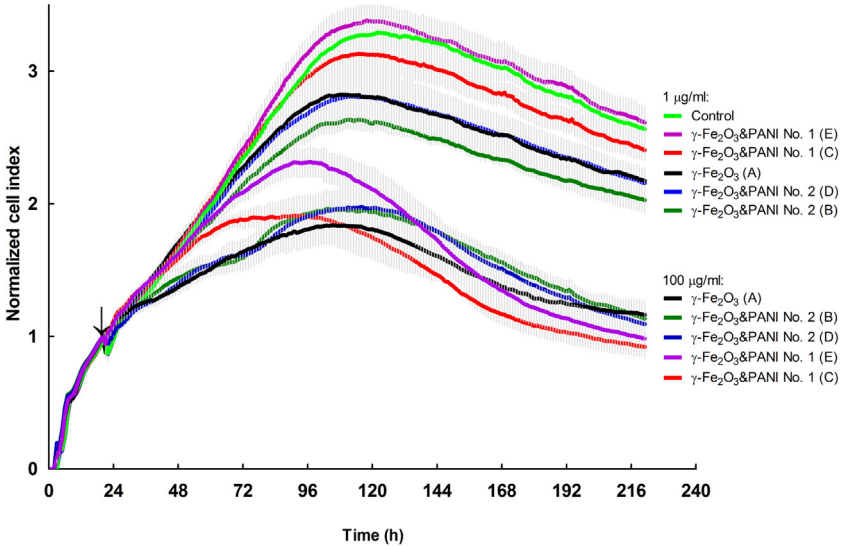

Fig. 6. Impedance-based monitoring of the influence of γ-Fe_2O_3 and γ-Fe_2O_3&PANI nanoparticles on the growth and proliferation of SH-SY5Y human neuronal cells. The particles in two concentrations (1 and 100 μg/ml) were added to cells after 24 h of cell incubation in the E-plate and monitored for next 8 days. PANI prepared on the particles at 0 °C (C, E) caused less inhibition effect on the cell growth in comparison with neat γ-Fe_2O_3 particles (A) or γ-Fe_2O_3&PANI particles with PANI prepared at 25 °C (B, D); pH 3 (B, C) and pH 7 (D, E). The arrow shows time of particle addition. Each curve represents an average of quadruplicate and standard deviation (gray bars).

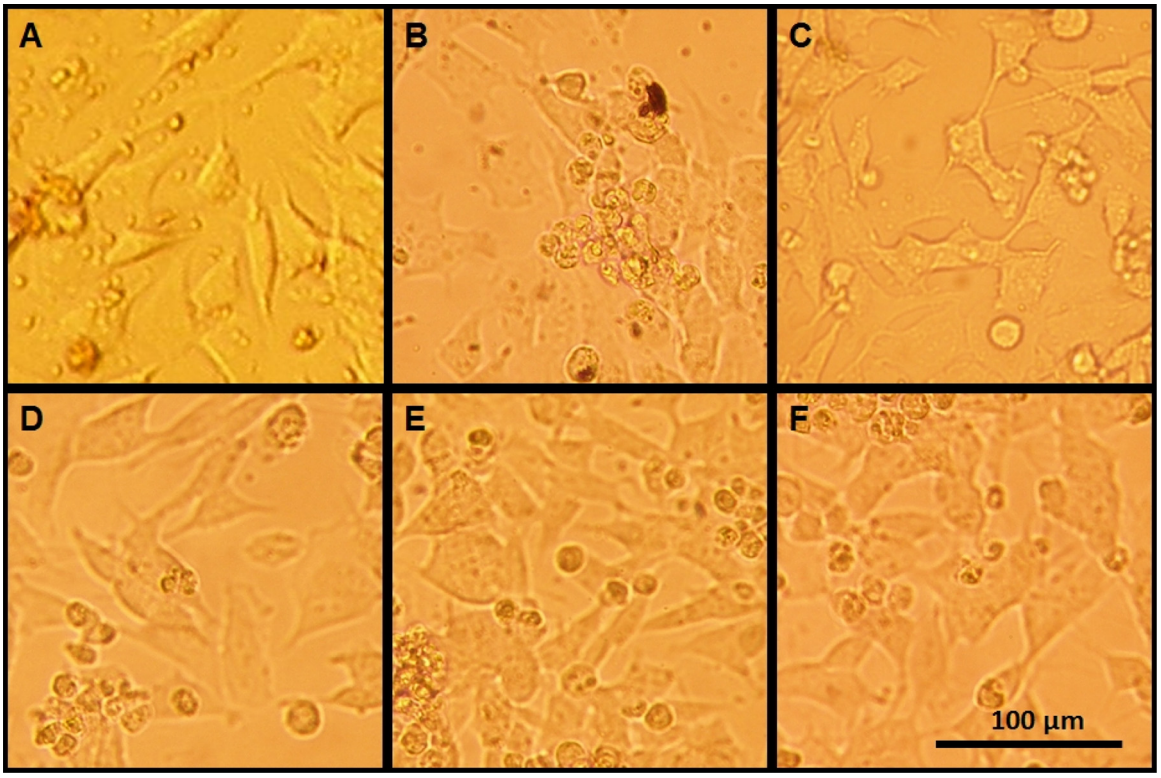

Fig. 7. Micrographs of the SH-SY5Y cells after 72 h incubation with (A) γ-Fe_2O_3, (B) γ-Fe_2O_3&PANI No. 1 (pH 3), (C) γ-Fe_2O_3&PANI No. 2 (pH 3), (D) γ-Fe_2O_3&PANI No. 1 (pH 7) and (E) γ-Fe_2O_3&PANI nanoparticles No. 2 (pH 7; 100 μg/ml); (F) control (cells in the absence of particles). Changes in the cell morphology did not indicate cell death in comparison with control.

forms (pH 7) induced the inhibition of cell growth with a delay in comparison to the γ-Fe_2O_3&PANI particles No. 2. Particles in the protonated form (pH 3) inhibited the cell growth more than the particles in neutral form (pH 7) probably due to a negative effect of acids on cell growth. In spite of the cell growth inhibition by the tested particles at the concentration 100 μg/ml, no changes in the cell morphology, which could be associated with a cell death, were observed after 72 h of the incubation of the SH-SY5Y cells with the particles (Fig. 7). It can be thus concluded that the novel γ-Fe_2O_3&PANI colloid, in particularly that prepared at low temperature, shows an improved biocompatibility *in vitro*.

4. Conclusions

Superparamagnetic γ-Fe_2O_3 nanoparticles were successfully synthesized by a wet chemical method from ferric/ferrous salts and coated with PANI. The coating of the γ-Fe_2O_3 with PANI was confirmed by the EDAX and UV–vis spectroscopy. The col-

loidal character of γ-Fe_2O_3&PANI was confirmed by the DLS analysis. While the dry particles were in tens of nanometers in diameter, the hydrodynamic size, as expected, was substantially larger (~200–250 nm). Measurements of the induced and remanent magnetizations proved the superparamagnetic character of the particles, which makes them sensitive to manipulations in magnetic field and visible in magnetic resonance imaging. Advantage of PANI coating consists in that it provides not only an improved stability of the iron oxide colloid and introduces the conductivity, but it can potentially also electrically stimulate cell growth and/or differentiation. The main benefit of the nanoparticles prepared in this study thus is in the design of hybrid nanoparticles combining together the superparamagnetic and conductivity properties. The magnetic property enables the particle imaging and targeting to specific tissues (such as tumors) in the magnetic field, while does not compromise the particle ability to be dispersed in an aqueous media in the absence of a magnet. The presence of PANI on the particles can then increase the absorption of NIR light boosting thus the hyperthermic effect valuable in the treatment applications, *e.g.*, of cancer. The study highlights that the new, non-toxic maghemite core/polyaniline shell nanoparticles can be a promising candidate for future cancer therapeutics.

The real-time cytotoxicity test determined the influence of particles on the viability of SH-SY5Y cell line. The γ-Fe_2O_3&PANI particles prepared under low temperature (0 °C) showed a lower inhibitory effect on the cell growth than the particles with PANI shell synthetized at 25 °C. The inhibition of cell growth increased at higher particle concentrations, but the morphology of the cells exposed to both uncoated γ-Fe_2O_3 and γ-Fe_2O_3&PANI nanoparticles at the relatively high concentration of 100 μg/ml was unchanged and no cell damage was observed in comparison with control cells. This indicates that the particles have a promising low cytotoxicity for biomedical applications. Ultimately, the magneto-conductive hybrid γ-Fe_2O_3&PANI nanoparticles may represent perspective diagnostic and/or therapeutic agents for treatment of various diseases, as neuroblastoma and lung carcinoma markers, in imaging of biological targets and detection of polysialic acid indicating presence of tumor cells and/or infections.

Author contributions

Zasońska Beata Anna—main contributor, synthesis of samples, writing of the manuscript. Bober Patrycja—polyaniline coatings, UV–vis measurements. Jošt Petr—biological experiments. Eduard Petrovský—magnetic measurements. Boštík Pavel—supervising biological part, english corrections. Horák Daniel—supervising, text corrections.

Acknowledgements

Support of the Ministry of Education, Youth and Sports of the Czech Republic (LH14318 and the National Sustainability Program II BIOCEV-FAR), the Czech Science Foundation (14-05568P) and RECOOP HST Association and Cedars Sinai Medical Center is acknowledged. This publication was also supported by the project, "BIOCEV—Biotechnology and Biomedicine Centre of the Academy of Sciences and Charles University" (CZ.1.05/1.1.00/02.0109) from the European Regional Development Fund and by the Long-term Organization Development Plan 1011 from the Czech Ministry of Defense.

References

[1] A. Chen, H. Wang, B. Zhao, X. Li, Synth. Met. 139 (2003) 411–415.
[2] R. Ladj, A. Bitar, M. Eissa, R. Mugnier, Le Dantec, H. Fessi, A. Elaissari, J. Mater. Chem. B 1 (2013) 1381–1396.
[3] E.A. Ostrakhovitch, J.C. Byers, K.D. O'Neil, O.A. Semenikhin, Arch. Biochem. Biophys. 528 (2012) 21–31.
[4] S. Liu, J.Q. Wang, D. Zhang, P.L. Zhang, J.F. Ou, B. Liu, S.R. Yang, Appl. Surf. Sci. 256 (2010) 3427–3431.
[5] G. Spinks, V. Mottaghitalab, M. Bahrami-Saniani, P. Whitten, G.G. Wallace, Adv. Mater. 18 (2006) 637–640.
[6] A. Chaubey, K. Pande, V. Singh, B. Malhotra, Anal. Chim. Acta 407 (2000) 97–103.
[7] L. Liu, F.H. Tian, M. Zhou, H.P. Guo, X.Y. Wang, Electrochim. Acta 70 (2012) 360–364.
[8] X.Y. Tao, X. Wang, Q. Wei, Q.Y. Wu, J. Macromol. Sci. Part A: Pure Appl. Chem. 44 (2007) 351–354.
[9] T. Lindfors, A. Ivaska, Anal. Chem. 76 (2004) 4387–4394.
[10] T. Lindfors, J. Szücs, F. Sundfors, R. Gyurcsányi, Anal. Chem. 82 (2010) 9425–9432.
[11] J.L. Wang, Z.Z. Zhu, A. Munir, H.S. Zhou, Talanta 84 (2011) 783–788.
[12] C. Oka, K. Ushimaru, N. Horiishi, T. Tsuge, Y. Kitamoto, J. Magn. Magn. Mater. 381 (2015) 278–284.
[13] M.K. Lima-Tenório, E.A. Gómez Pineda, N.M. Ahmad, H. Fessi, A. Elaissari, Int. J. Pharm. 493 (2015) 313–327.
[14] F. Shubitidze, K. Kekalo, R. Stigliano, I. Baker, J. Appl. Phys. 117 (2015) 094302.
[15] S. Sabale, V. Jadhav, V. Khot, X.L. Zhu, M.L. Xin, H.X. Chen, J. Mater. Sci.: Mater. Med. 26 (2015) 127.
[16] S.Y. Zhao, Y.L. Wang, C.S. Gao, J. Zhang, H.D. Bao, Z.Y. Wang, P. Gong, J. Surg. Res. 191 (2014) 290–301.
[17] M.A. Hossain, A.E. Frampton, A. Bagul, Expert Rev. Med. Devices 11 (2015) 9–13.
[18] E. Maltas, S. Malkondu, P. Uyar, M. Ozmen, Mater. Sci. Eng. C 48 (2015) 86–93.
[19] M. Zhang, J. Zhou, J.C. Wang, Q. Zhou, J. Fang, C.Q. Zhou, W.L. Chen, Biotechnol. Lett. 37 (2015) 289–298.
[20] M. Wu, D. Zhang, Y. Zeng, L. Wu, X. Liu, J. Liu, Nanotechnology 26 (2015) 115102.
[21] R. Ladj, A. Bitar, M. Eissa, H. Fessi, Y. Mugnier, R. Le Dantec, A. Elaissari, Int. J. Pharm. 458 (2013) 230–241.
[22] S.F. Medeiros, J.O.C. Filizzola, V.F.M. Fonseca, P.F.M. Oliveira, T.M. Silva, A. Elaissari, A.M. Santos, Mater. Lett. 160 (2015) 522–525.
[23] M. Sababi, J. Pan, P.E. Augustsson, P.E. Sundell, P.M. Claesson, Corros. Sci. 84 (2014) 189–197.
[24] T.K. Mahto, A.R. Chowdhuri, S.K. Sahu, J. Appl. Polym. Sci. 131 (2014) 40840.
[25] R. Devi, C.S. Pundir, Sens. Actuators B 193 (2014) 608–615.
[26] S. Chandra, H. Lang, D. Bahadur, Anal. Chim. Acta 795 (2013) 8–14.
[27] S. Pal, E.C. Alocilja, Biosens. Bioelectron. 24 (2009) 1437–1444.
[28] J.C. Medina-Llamas, A.E. Chávez-Guajardo, C.A. Andrade, K.G. Alves, C.P. de Melo, J. Colloid Interface Sci. 434 (2014) 167–174.
[29] Q. Xiao, X. Tan, L. Ji, J. Xue, Synth. Met. 157 (2007) 784–791.
[30] S. Kant, S. Kalia, A. Kumar, J. Alloys Compd. 578 (2013) 249–256.
[31] J.C. Aphesteguy, S.E. Jacobo, J. Mater. Sci. 42 (2007) 7062–7068.
[32] J. Jiang, L. Li, F. Xu, Mater. Sci. Eng. A 456 (2007) 300–304.
[33] T.H. Hsieh, K.S. Ho, X. Bi, Y.K. Han, Z.L. Chen, C.H. Hsu, Eur. Polym. J. 45 (2009) 613–620.
[34] A.C.V. De Araújo, S. Alves Jr., W.M. Azevedo, Adv. Sci. Technol. 54 (2008) 325–330.
[35] Y. Long, Z. Chen, J.L. Duvail, Z. Zhang, M. Wan, Physica B 370 (2005) 121–130.
[36] L. Kong, X. Lu, W. Zhang, J. Solid State Chem. 181 (2008) 628–636.
[37] T.H. Hsieh, K.S. Ho, C.H. Huang, Y.Z. Wang, Z.L. Chen, Synth. Met. 156 (2006) 1355–1361.
[38] T.H. Hsieh, K.S. Ho, X. Bi, C.H. Huang, Y.Z. Wang, Y.K. Han, Z.L. Chen, C.H. Hsu, P.H. Li, Y.C. Chang, Synth. Met. 160 (2010) 1609–1616.
[39] R. Sharma, S. Lamba, S. Annapoorni, P. Sharma, A. Inoue, J. Appl. Phys. 97 (2005) 1–6.
[40] J. Jiang, L. Li, M. Zhu, React. Funct. Polym. 68 (2008) 57–62.
[41] J. Deng, C.L. He, Y. Peng, J. Wang, X. Long, P. Li, Synth. Met. 139 (2003) 295–301.
[42] Y.J. Zhang, Y.W. Lin, C.C. Chang, T.M. Wu, Synth. Met. 160 (2010) 1086–1091.
[43] I. Haldar, M. Biswas, A. Nayak, Polym. Plast. Technol. 53 (2014) 1317–1326.
[44] A. Khan, A.S. Aldwayyan, M. Alhoshan, M. Alsalhi, Polym. Int. 59 (2010) 1690–1694.
[45] K.R. Reddy, K.P. Lee, A.G. Iyengar, J. Appl. Polym. Sci. 104 (2007) 4127–4134.
[46] S.B. Tiwari, M.M. Amiji, Curr. Drug Deliv. 3 (2006) 219–232.
[47] J. Chen, J. Zhu, H.H. Cho, K. Cui, F. Li, X. Zhou, J.T. Rogers, S.T.C. Wong, X. Huang, Differential cytotoxicity of metal oxide nanoparticles. In 2007 NSTI Nanotechnology Conference and Trade Show—NSTI Nanotech 2007. Technical Proceedings. vol. 2, Santa Clara, 2007, pp. 670–673.
[48] M. Babič, D. Horák, M. Trchová, P. Jendelová, K. Glogarová, P. Lesný, V. Herynek, M. Hájek, E. Syková, Bioconjugate Chem. 19 (2008) 740–750.
[49] D.D. Perrin, B. Dempsey, Buffers for pH and Metal Ion Control, Chapman and Hall, London, 1974.
[50] C.J. Serna, M.P. Morales, Maghemite (γ-Fe_2O_3): a versatile magnetic colloidal material, in: E. Matijevic, M. Borkovec (Eds.), Surface and Colloid Science, 17, Springer, New York, 2004, pp. 27–81.
[51] J. Stejskal, I. Sapurina, Pure Appl. Chem. 77 (2005) 815–826.
[52] J. Stejskal, P. Kratochvíl, A.D. Jenkins, Collect. Czech Chem. Commun. 60 (1995) 1747–1755.
[53] J. Stejskal, I. Sapurina, J. Prokeš, J. Zemek, Synth. Met. 105 (1999) 195–202.
[54] D.E. Koppel, J. Chem. Phys. 57 (1972) 4814–4820.
[55] R. Day, M. Fuller, V.A. Schmidt, Phys. Earth Planet Inter. 13 (1977) 260–267.

Publication No. 5

ACS APPLIED MATERIALS & INTERFACES

Research Article

www.acsami.org

Thionine-Modified Poly(glycidyl methacrylate) Nanospheres as Labels of Antibodies for Biosensing Applications

Beata Zasonská,[†] Michaela Čadková,[‡,§] Aneta Kovářová,[‡] Zuzana Bílková,[‡] Lucie Korecká,[‡] and Daniel Horák*[,†]

[†]Institute of Macromolecular Chemistry AS CR, Heyrovský Sq. 2, 162 06 Prague 6, Czech Republic

[‡]Department of Biological and Biochemical Sciences, Faculty of Chemical Technology, University of Pardubice, Studentská 573, 532 10 Pardubice, Czech Republic

[§]Department of Analytical Chemistry, Faculty of Chemical Technology, University of Pardubice, Studentská 573, 532 10 Pardubice, Czech Republic

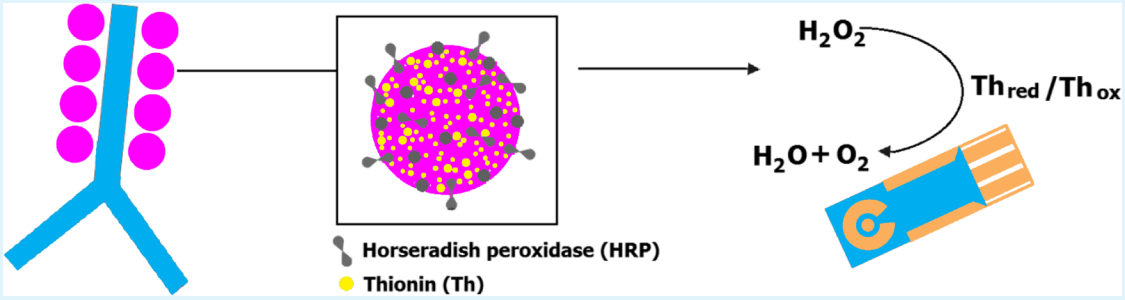

ABSTRACT: Monodisperse poly(glycidyl methacrylate) (PGMA) nanospheres were obtained by emulsifier-free emulsion polymerization and characterized by physicochemical methods. The effects of various reaction parameters on the particle properties were investigated. The particle size was controlled in the range of 350−420 nm. To introduce carboxyl groups, the PGMA nanospheres were hydrolyzed and oxidized with $KMnO_4$. Subsequently, the enzyme horseradish peroxidase (HRP) and the electron mediator thionine were covalently attached to the PGMA nanospheres to obtain an antibody indicator suitable for enzyme-based electrochemical immunosensors. Combined HRP and thionine binding to the nanospheres had beneficial effects for the labeling efficiency and at the same time prevented the formation of soluble electron mediators.

KEYWORDS: *glycidyl methacrylate, nanospheres, thionine, biosensor, electrochemistry, horseradish peroxidase*

INTRODUCTION

Electrochemical sandwich-type immunosensors are becoming increasingly attractive for the detection of proteins and other biomolecules, especially when compared with classical enzyme-linked immunosorbent assays (ELISAs). ELISAs associated with spectrophotometric detection suffer from several disadvantages, including a long analysis time, nonlinearity of the signal, the need for complex equipment, and possible interference of some admixtures. These can be overcome through the use of sensitive, selective, and portable electrochemical immunosensors, which are already associated with a broad spectrum of detection techniques.[1−3] The choice of a suitable enzyme, such as horseradish peroxidase (HRP), alkaline phosphatase, and glucose oxidase, is important when used as a detection label for antibodies because the enzyme influences the sensitivity of the whole system and because the final enzyme activity corresponds to the concentration of the analyzed protein.[3−5] The detection sensitivity is particularly crucial in the analysis of biologically active compounds, e.g., disease biomarkers, at low concentrations in complex biologic media, such as serum, urine, and cerebrospinal fluid. Biosensors enable the use of electron mediators and may be used in combination with various nanomaterials, such as nanoparticles used as carriers for fixation and enhancement of the amounts of biospecific labels. In contrast, neither electron mediators nor nanomaterials may be used in the classical ELISA format.[4,6] Thionine (Th), a thiazine dye, is an example of such mediators used in both electrochemical and photochemical biosensors. Th may be added as a solution directly at the final detection stage, or, alternatively it may be covalently bound together with HRP onto suitable particles and subsequently used for antibody labeling.[1,3,7]

In this report, poly(glycidyl methacrylate) (PGMA) nanospheres were selected as a support because their oxirane groups facilitate modification by a large variety of reagents, including ligands and/or other molecules.[8−10] Although emulsifier-free emulsion polymerization of styrene or methyl methacrylate seems to be well established,[11] the polymerization of GMA had not yet been fully described and was used as the method of choice in this work to obtain particles in the nanometer size range. In the emulsifier-free emulsion polymerization system,

Received: September 9, 2015
Accepted: October 19, 2015
Published: October 19, 2015

DOI: 10.1021/acsami.5b08469
ACS Appl. Mater. Interfaces 2015, 7, 24926−24931

polymer particles are stabilized using either ionizable initiators or ionic comonomers.[12] Several mechanisms have been proposed for particle nucleation and growth during polymerization in the absence of emulsifier;[13] however, it is generally agreed that the actual process depends on the solubility of the monomer in water.[14] For example, it has been proposed that slightly water-soluble monomers, such as styrene, polymerize in the aqueous phase in the presence of the water-soluble initiator potassium persulfate to form oligomeric radicals. The resulting radicals have sulfate end groups that are surface-active and form micelles in an emulsion polymerization.[15,16] However, for more water-soluble monomers such as (meth)acrylates, the particles are formed by the precipitation of growing chains once the chains reach a critical length, which is 60−80 monomer units for methyl methacrylate.[15,17] This phenomenon is termed homogeneous nucleation. In both cases, subsequent polymerization occurs in monomer-swollen particles.

The PGMA nanospheres were subsequently hydrolyzed and oxidized to poly(carboxymethyl methacrylate) (PCMMA) and modified by the covalent attachment of a Th electron mediator and a HRP enzyme. The resulting particles have the potential to be universal antibody labels with enhanced sensitivity in sandwich-type electrochemical immunosensors (Figure 1).

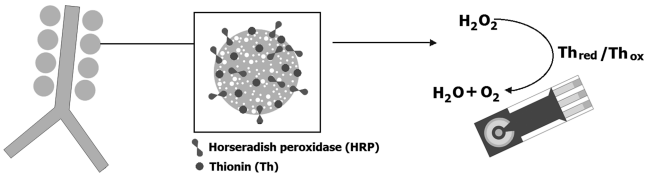

Figure 1. Schematic illustration of the use of PCMMA−Th−HRP nanospheres for electrochemical detection.

EXPERIMENTAL SECTION

Materials. Glycidyl methacrylate (GMA), *N*-[3-(dimethylamino)-propyl]-*N*′-ethylcarbodiimide hydrochloride (EDC), 3-morpholino-2-hydroxypropanesulfonic acid (MOPSO), phosphate-buffered saline (PBS; pH 7.4), potassium persulfate, sodium salt of *N*-hydroxysulfosuccinimide (sulfo-NHS), thionine (Th) acetate, 30% hydrogen peroxide, horseradish peroxidase (HRP; P8415-5KU), 2-morpholinoethane-1-sulfonic acid, and *o*-phenylenediamine (OPD) were purchased from Sigma-Aldrich (St. Louis, MO). Hydrochloric acid, potassium permanganate, sodium hydroxide, and sulfuric acid were obtained from Lach-Ner (Neratovice, Czech Republic). Ultrapure Q-water from a Milli-Q Gradient A10 system (Millipore, Molsheim, France) was used for the preparation of solutions.

Emulsifier-Free Emulsion Polymerization of GMA. Monodisperse poly(glycidyl methacrylate) (PGMA) nanospheres were synthesized by surfactant-free emulsion polymerization. The reaction was carried out in a 100-mL glass reaction vessel equipped with an anchor-type stirrer. In a typical experiment, the $K_2S_2O_8$ initiator (0.075 g) was dissolved in Q-water (75 g) at 80 °C, the monomer GMA (5.25 g) was added after 5 min, and the mixture was stirred (500 rpm) at this temperature for 18 h. The resulting PGMA nanospheres were left to sediment before being washed five times with Q-water. Polymer yields reached >97 wt %.

Hydrolysis and Oxidation of PGMA Nanospheres. In the next step, oxirane groups of PGMA nanospheres (1 g) were hydrolyzed in 2 M sulfuric acid (20 mL) at room temperature for 2 h using the modified procedure described previously.[18] The hydrolyzed nanospheres were then oxidized by a 2 wt % aqueous solution of $KMnO_4$ at room temperature for 3 h. The obtained poly(carboxymethyl methacrylate) (PCMMA) nanospheres were washed with 10 wt % oxalic acid (20 mL) and Q-water to neutralize the reaction mixture. The particles were then stirred in 1 M hydrochloric acid (15 mL) at room temperature for 7 h and finally washed five times with Q-water.

Attachment of Thionine Acetate on the Nanospheres. The PCMMA nanospheres (1 g) were dispersed in MOPSO buffer (50 mL) containing EDC (1.2 mg) and sulfo-NHS (0.725 mg) at 0 °C for 30 min. Thionene acetate (1.81 mg) was then added to the mixture and the reaction allowed to proceed at room temperature for 48 h at pH 9. The reaction was stopped by increasing the pH to 11 using 0.5 M NaOH. The resulting PCMMA−Th nanospheres were washed once with 0.01 M HCl (100 mL) and three times with PBS buffer (50 mL; pH 7.4).

Immobilization of HRP on the PCMMA and PCMMA−Th Nanospheres and Determination of the Enzyme Activity. HRP was immobilized on the surface of PCMMA or PCMMA−Th nanospheres using the conventional, single-step carbodiimide/sulfo-NHS method.[19] Briefly, the nanoparticles (1 mg) were washed eight times with 0.1 M phosphate buffer (PB; 1 mL; pH 7.3) and separated by centrifugation (5000 rpm for 5 min). EDC (7.5 mg) and sulfo-NHS (1.25 mg), each in 250 μL of PB (pH 7.3), and HRP in PB (0.5 mL) were added, and the mixture was incubated at 4 °C for 16 h under slow rotation. After immobilization, the resulting PCMMA−HRP or PCMMA−Th−HRP nanospheres were washed three times with 0.1 M PB (1 mL each; pH 7.3), three times with 0.1 M PB containing 1 M NaCl (1 mL each; pH 7.3) to remove unbound HRP, and finally five times with 0.1 M PB (1 mL each; pH 7.3).

The activity of the immobilized HRP was determined spectrophotometrically according to the literature,[20] where a suspension of either the PCMMA−Th−HRP or PCMMA−HRP nanospheres (100 μg) in 0.1 M PB (50 μL; pH 6.2) was mixed with 100 μL of a substrate solution (5 mg OPD with 5 μL of 30% H_2O_2 in 10 mL of 0.1 M PB; pH 6.2) and incubated at 37 °C for 10 min in the dark under slow rotation conditions. The reaction was stopped by the addition of 1 M H_2SO_4 (50 μL), the particles were separated by centrifugation at 5000 rpm, the supernatant (200 μL) was transferred to a microwell plate, and the absorbance was measured at 492 nm on a Multiskan GO spectrophotometer (Thermo Fisher Scientific; Waltham, MA). The conjugation efficiency was determined by SDS-PAGE electrophoresis with densitometric evaluation of polyacrylamide gels using Chemi-Doc XRS and *Image Lab* software (Biorad, USA). The densities of the bands correlating with the amount of the protein were compared in the fractions before and after the immobilization.

Electrochemical Measurement. A decrease in the current resulting from HRP-mediated H_2O_2 oxidation was electrochemically measured by linear sweep voltammetry (LSV) at 0.35 V. PCMMA−HRP and PCMMA−Th−HRP nanospheres (100 μg each) were washed four times with 0.1 M PB (pH 7.3) and separated by centrifugation (5000 rpm, 5 min). The nanosphere suspension (40 μL) was then incubated with H_2O_2 (1 mg/L; 800 μL) in 0.1 M PB (pH 7.3) with 0.15 M NaCl. For the LSV measurement, 40 μL of the reaction mixture was added to a BST-120 screen-printed three-electrode sensor with platinum working and auxiliary electrodes and an Ag/AgCl pseudoreference electrode (Pt−Pt−Ag/AgCl; Bio Sensor Technology, Berlin, Germany) connected with a PalmSens compact electrochemical sensor interface (Utrecht, The Netherlands). The current response was recorded at the wave maximum at 5 min intervals for a total time of 15 min. The detection conditions were as follows: potential range 0−0.8 V, potential step 0.005 V, scan rate 50 mV/s, and equilibration time 2 s.

Particle Characterization. Scanning electron microscopy (SEM) micrographs were performed on a Quanta 200F microscope (Brno, Czech Republic) equipped with an energy-dispersive spectrometer (Mahwah, NJ). The number-average diameter (D_n), weight-average diameter (D_w), and dispersity index (DI = D_w/D_n) characterizing the particle-size distributions were calculated using Atlas software (Tescan Digital Microscopy Imaging, Brno, Czech Republic) by counting at least 400 individual microspheres. D_n and D_w were expressed as $D_n = \sum n_i D_i / \sum n_i$ and $D_w = \sum n_i D_i^4 / \sum n_i D_i^3$, where n_i and D_i are the number and diameter of the ith microsphere, respectively. The particle hydrodynamic diameter D_h in water was determined using a ZEN3600 Zetasizer Nano-ZS instrument (Malvern Instruments, Malvern, U.K.).

DOI: 10.1021/acsami.5b08469
ACS Appl. Mater. Interfaces 2015, 7, 24926−24931

IR spectra were measured using a PerkinElmer PARAGON 1000 PC Fourier transform infrared (FT-IR) spectrometer (Norwalk, CT).

RESULTS AND DISCUSSION

PGMA Nanospheres. Potassium persulfate initiated emulsifier-free emulsion polymerization of GMA was selected as the method of choice for the preparation of polymer nanospheres. The advantage of this method is the absence of emulsifier in the polymerization system because the presence of an emulsifier might hamper the coating and adhesive applications. Emulsifier-free emulsion polymerization produces highly charged, clean, and monodisperse particles that are stabilized by the sulfate cations originating from the initiator. In this report, the effects of two reaction parameters on the properties of the particles were investigated. While the polymerization temperature was held constant at 80 °C, the concentrations of GMA monomer and $K_2S_2O_8$ initiator in water were varied from 6 to 8 wt % and from 0.1 to 0.3 wt %, respectively.

Effect of the GMA Concentration. In this set of experiments, the PGMA nanospheres were prepared at the same concentration of the initiator (0.2 wt % $K_2S_2O_8$ in water) and at five different concentrations of GMA in water: 6, 6.5, 7, 7.5, and 8 wt % (Figure 2). The low concentration of the monomer

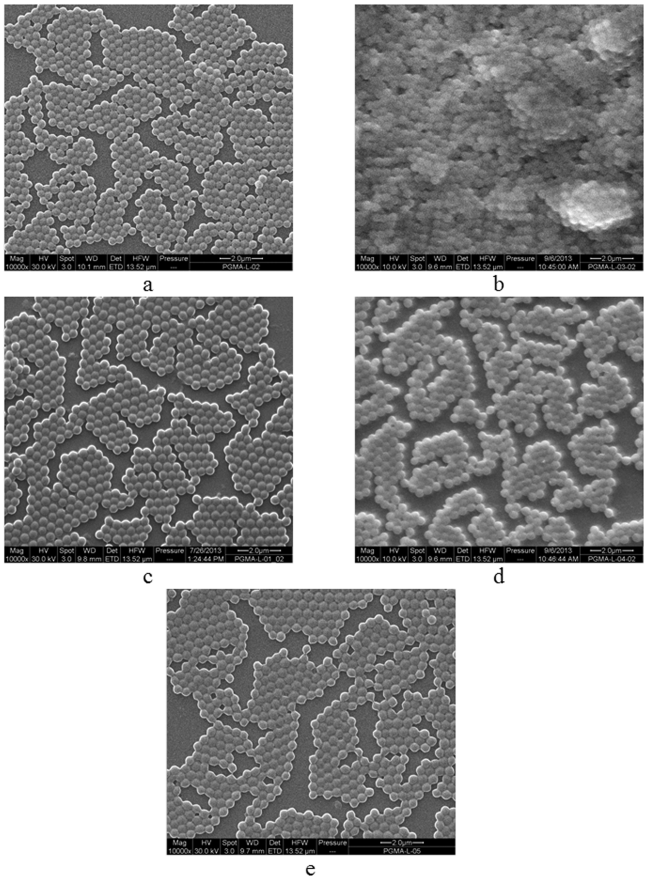

Figure 2. SEM micrographs of PGMA nanospheres prepared at (a) 6, (b) 6.5, (c) 7, (d) 7.5, and (e) 8 wt % GMA and 0.2 wt % $K_2S_2O_8$ in water.

was necessary to obtain stable and monodisperse PGMA lattices. The particles had a spherical shape with number-average diameters D_n (SEM) ranging from ~350 to 400 nm depending on the concentration of GMA in water (Table 1). The PGMA nanosphere diameters slightly increased with

Table 1. Dependence of the Number-Average Diameter D_n and Dispersity Index DI of PGMA Nanospheres on the Concentrations of GMA (c_{GMA}) and $K_2S_2O_8$ Initiator in Water ($c_{K_2S_2O_8}$)

c_{GMA} (wt %)	$c_{K_2S_2O_8}$ (wt %)	D_n (nm)	DI	$c_{K_2S_2O_8}$ (wt %)	c_{GMA} (wt %)	D_n (nm)	DI
6	0.2	348	1.023	0.1	7	357	1.024
6.5	0.2	387	1.022	0.15	7	382	1.028
7	0.2	387	1.02	0.2	7	387	1.02
7.5	0.2	387	1.024	0.25	7	400	1.026
8	0.2	396	1.023	0.3	7	415	1.026

increasing monomer concentration in good agreement with previous reports.[21,22] This can be ascribed to the fact that the monomer is a good solvent for the polymer, thus increasing the oligomer critical chain length before precipitation. It should also be noted that a homogeneous nucleation mechanism is generally recognized as superior for the polymerization of slightly water-soluble monomers such as GMA.[23] The delayed precipitation of polymeric oligomers reduces the numbers and increases the size of the resulting nanospheres. This relatively large particle size obtained at a high monomer concentration may also be explained by rapid particle growth during the polymerization. The resulting particles had DI values <1.025, which confirmed a very narrow distribution of sizes (Table 1). According to the literature,[24] the size of the nanospheres is considered as monodisperse if DI < 1.05. For the sake of comparison, D_h of the PGMA nanospheres prepared at 7 wt % GMA was also measured by dynamic light scattering (DLS). As expected, D_h of the particles in water was substantially larger (508 nm) than D_n of the dry particles determined from SEM (387 nm). This can be ascribed to swelling of the particles in water and the considerably different nature of both characterization methods. It is worth noting that the larger particles induce a much higher intensity of scattered light in DLS than the smaller ones do. In contrast, determination of the particle size from the SEM micrographs is not influenced by the presence of large particles.

Effect of the Initiator Concentration. In the next series ofexperiments, the PGMA nanospheres were prepared at 7 wt % GMA in water with five different $K_2S_2O_8$ concentrations: 0.1, 0.15, 0.2, 0.25, and 0.3 wt % (Figure 3). Similar to the previous experiments, spherical particles were obtained with sizes ranging from ~360 to 420 nm. The dependence of the PGMA nanoparticle diameters on the concentration of the initiator in water showed that the particle size increased with increasing initiator concentration (Table 1). This was likely due to an increase of the radical-to-monomer molar ratio. It should be noted that increases in the $K_2S_2O_8$ concentrations also increased the ionic strength of the aqueous phase; as a result, larger particles were formed. The increase in the particle size with increasing initiator concentration is also attributed to a larger number of growing chains participating in the aggregation step to form one particle (i.e., stronger aggregation).[25] Low DIs (1.02−1.03) confirm the very narrow particle-size distributions (Table 1).

PGMA particles of 392 nm diameter (DI = 1.015) prepared under moderate reaction conditions (7 wt % GMA and 0.2 wt % $K_2S_2O_8$ in water) were selected for the experiments examining hydrolysis, oxidation, and attachment of Th.

Introduction of Carboxyl Groups and Attachment of Th. To introduce reactive carboxyl groups necessary for Th

DOI: 10.1021/acsami.5b08469
ACS Appl. Mater. Interfaces 2015, 7, 24926−24931

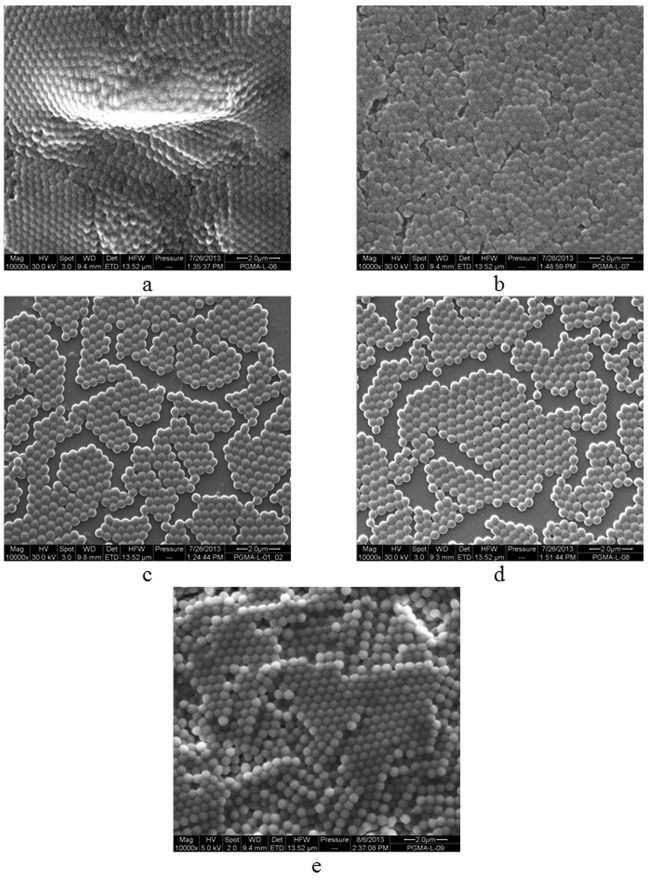

Figure 3. SEM micrographs of PGMA nanospheres prepared at (a) 0.1, (b) 0.15, (c) 0.2, (d) 0.25, and (e) 0.3 wt % $K_2S_2O_8$ (in water). The monomer concentration was 7 wt % in water.

binding, the oxirane groups of the PGMA nanospheres were hydrolyzed with sulfuric acid and the resulting diol groups were subsequently oxidized by $KMnO_4$ to yield PCMMA nanospheres (Figure 4). In analogy with earlier prepared particles,[26]

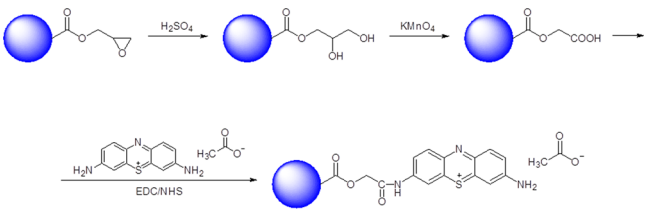

Figure 4. Schematic illustration of the preparation of PCMMA−ThAc nanospheres by hydrolysis of PGMA, oxidation, and reaction with thionine.

where COOH groups were determined by titration with 0.1 M NaOH, the content of the carboxyl groups in the PCMA nanospheres was estimated to be ca. 6.8 μmol of COOH/g. Reaction of the PCMMA nanospheres with Th was achieved using EDC/sulfo-NHS chemistry (Figure 4). A low COOH/Th acetate ratio is recommended to enable removal of unreacted compounds from the reaction mixture during washing. SEM micrograph images of the PCMMA−Th nanospheres confirmed that neither the size nor the dispersity was substantially affected by the reaction (Figure 5). Similarly, like with the PGMA nanospheres, D_h of water-solvated PCMMA−Th particles was larger (775 nm) compared with D_n (~390 nm).

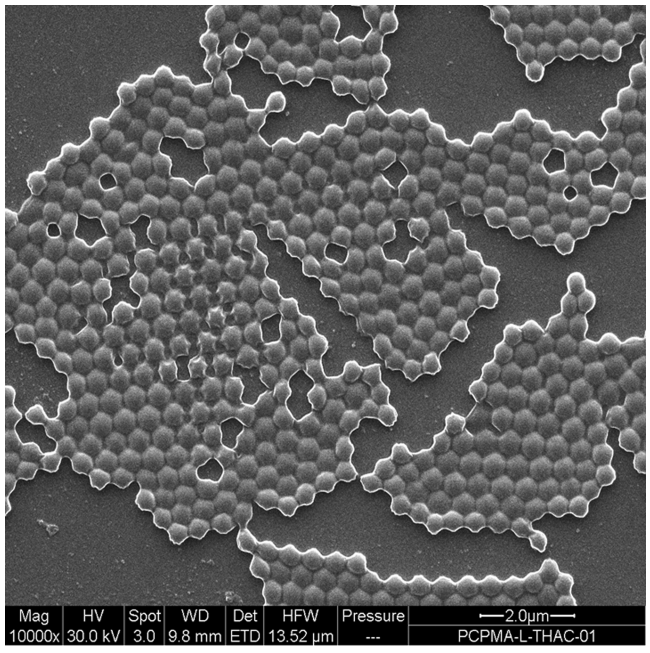

Figure 5. SEM micrograph of PCMMA−Th nanospheres prepared at 7 wt % GMA and 0.2 wt % $K_2S_2O_8$ in water.

FT-IR spectra of PCMMA and PCMMA−Th nanospheres are shown in Figure 6. In the spectrum of the PCMMA−Th

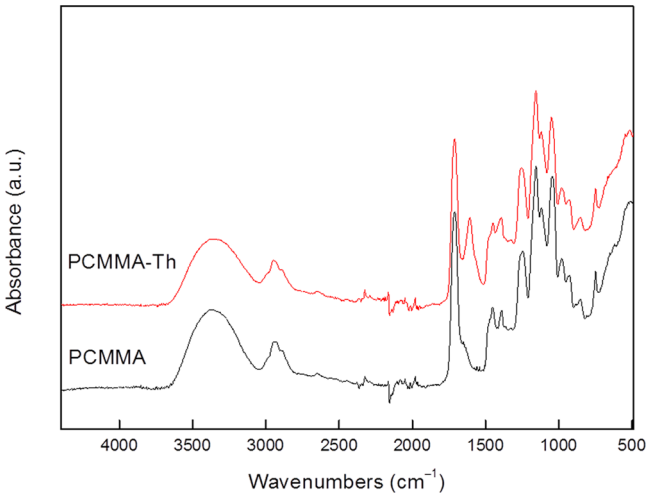

Figure 6. FT-IR spectroscopies of PCMMA (black) and PCMMA−Th nanospheres (red).

particles, a peak characteristic of the $-CO-NH_2$ bond was observed at 1614 cm^{-1} and confirmed the formation of chemical bonds between the amino groups of Th and the carboxyl groups of the particles. Absorption bands at 1600 and 1500 cm^{-1} were assigned to vibration of the Th phenyl rings.[27] Peaks at 1716 and 1410 cm^{-1} in both spectra were ascribed to COOH dimers. On the basis of the amount of Th added in the reaction, the PCMMA−Th nanospheres were assumed to contain ca. 2.8 μmol of Th/g. To further verify the presence of Th on the particles, the PCMMA−Th nanospheres were analyzed by energy-dispersive spectroscopy (EDX), and 6.1 wt % nitrogen was found (Figure 7). It should be also pointed out that the white color of PCMMA changed to blue PCMMA−Th nanospheres, indicating Th attachment.

DOI: 10.1021/acsami.5b08469
ACS Appl. Mater. Interfaces 2015, 7, 24926−24931

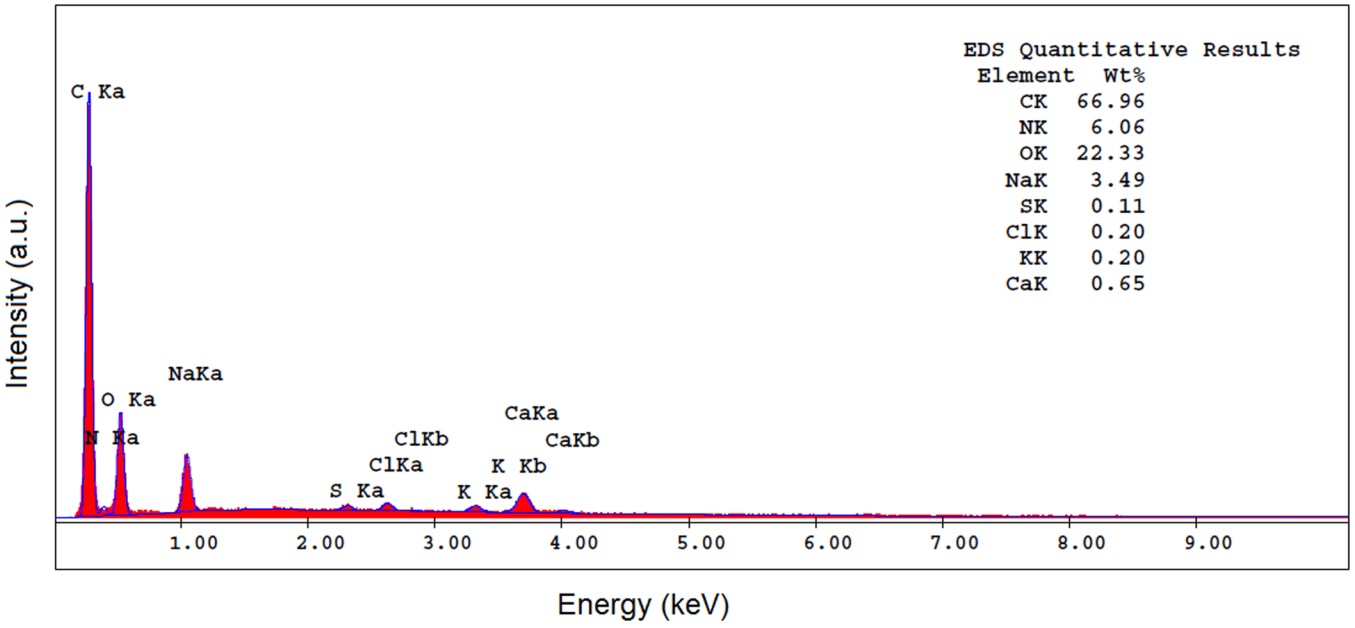

Figure 7. EDX analysis of PCMMA−Th nanospheres.

Immobilization of HRP on the Nanospheres and Electrochemical Measurements. The functionality of the nanospheres to be used as antiobody labels in enzyme-based immunosensors was verified electrochemically. HRP was immobilized on both PCMMA and PCMMA−Th nanospheres via conventional EDC/sulfo-NHS chemistry. Four amounts of HRP were tested: 50, 100, 200, and 500 μg/mg of nanospheres. The immobilization efficiency was determined spectrophotometrically by measuring the HRP activity using a chromogenic substrate solution and by densitometric evaluation of SDS-PAGE gels. On the basis of the results, the use of 200 μg of HRP/mg of nanospheres was found to be optimal, and 1025 ng of HRP was immobilized per 1 mg of the particles. The use of higher amounts of HRP (500 μg) in PB led to almost 4 times lower immobilization efficiency, reaching 258 ng of HRP/mg.

Low concentrations of samples and consumption of reagents are desirable, especially in biosensing applications. Therefore, miniaturized screen-printed three-electrode sensors enabling analysis of droplets with a volume of 40 μL were used for the electrochemical measurements. Because electrochemical signals induced by H_2O_2 consumption by HRP were targeted for detection, sensors with platinum working electrodes (Pt−Pt−Ag/AgCl) were chosen. Decreases in the current versus time responses of both PCMMA−HRP and PCMMA−Th−HRP nanospheres were monitored by LSV, and the current values were recorded at 0.35 V.

As expected, the covalently bound Th electron mediator of the PCMMA−Th−HRP nanospheres had a positive effect on the resulting electrochemical signal. In contrast, a similar effect was not confirmed with PCMMA−HRP (Figure 8). Both the PCMMA−HRP and PCMMA−Th−HRP nanospheres were found to have similar electrochemical stability after almost 1 month of storage. The direct attachment of Th on the nanosphere surface proved superior because it eliminates the disadvantages of Th leaching in the analyzed solutions when Th solutions are added directly to the analyzed samples. Solutions of Th at high concentrations have limited solubility[7] and result in high background signals that may negatively influence electron transfer on the working electrode.

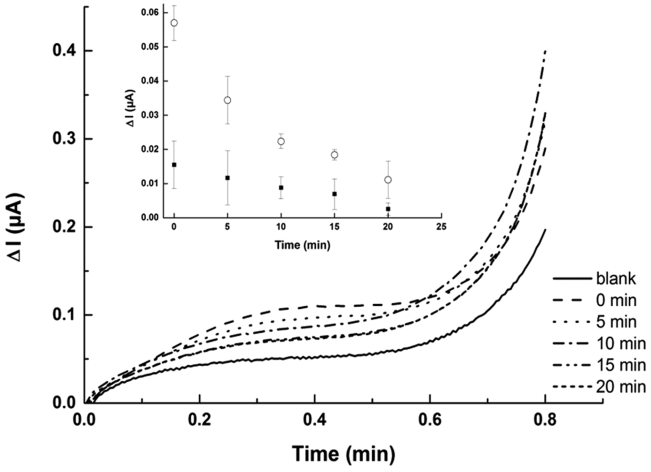

Figure 8. Linear sweep voltammogram of H_2O_2 consumption by the PCMMA−Th−HRP nanospheres. Inset: time dependence of the current response at 0.35 V induced by conversion of H_2O_2 by PCMMA−HRP (■) and PCMMA−Th−HRP nanospheres (○). Conditions: thick film sensor Pt/Pt/Ag/AgCl, 1 mg/L H_2O_2 in 0.1 M PB (pH 7.3) with 0.15 M NaCl, measurements at 5 min intervals for 20 min.

CONCLUSIONS

Uniformly sized PCMMA−Th nanospheres were prepared by emulsifier-free emulsion polymerization with low amounts of GMA. Hydrolysis and oxidation of the PGMA particles were then used to prepare the support, enabling the attachment of Th on the surface. The ability of emulsifier-free emulsion polymerization to produce small monodisperse particles was previously described for the synthesis of poly(methyl methacrylate)[28] or polystyrene particles.[29] Upon investigation of the effects of the concentrations of both the GMA monomer and the $K_2S_2O_8$ initiator, the PGMA particle size was found to increase with increasing values of both parameters. The particle size was controlled within the 350−420 nm range. For subsequent experiments, 390 nm size particles were used for electrochemical experiments. Covalent attachments of both Th and HRP on the PCMMA nanospheres were performed using

DOI: 10.1021/acsami.5b08469
ACS Appl. Mater. Interfaces 2015, 7, 24926−24931

carbodiimide chemistry. The immobilized enzyme was found to retain its activity for a long period of time. Both the PCMMA−HRP and PCMMA−Th−HRP nanospheres were compared in terms of the electrochemical detection of H_2O_2 to examine the effect of Th as an electron mediator for increasing the electrochemical signal. The PCMMA−Th−HRP nanospheres increased the electrochemical response in comparison to PCMMA−HRP. As LSV confirmed, the PCMMA−Th−HRP nanospheres amplified the electrochemical signal and improved the sensitivity and other analytical parameters of biosensors. The reported PCMMA−Th nanospheres represent a highly sensitive, universal potential tool for labeling of antibodies in enzyme-based sandwich-type immunosensors.

AUTHOR INFORMATION

Corresponding Author

*E-mail: horak@imc.cas.cz.

Notes

The authors declare no competing financial interest.

ACKNOWLEDGMENTS

Support of Biotechnology and Biomedicine Centre of Academy of Sciences and Charles University from the European Regional Development Fund (CZ.1.05/1.1.00/02.0109), the Czech Science Foundation (Grant 15-16549S), and the University of Pardubice (SGFCHT 07/2015) is acknowledged.

REFERENCES

(1) Fang, Y.-S.; Huang, X.-J.; Wang, L.-S.; Wang, J.-F. An Enhanced Sensitive Electrochemical Immunosensor Based on Efficient Encapsulation of Enzyme in Silica Matrix for the Detection of Human Immunodeficiency Virus P24. *Biosens. Bioelectron.* **2015**, *64*, 324−332.

(2) Wang, R.; Chen, X.; Ma, J.; Ma, Z. Ultrasensitive Detection of Carcinoembryonic Antigen by a Simple Label-Free Immunosensor. *Sens. Actuators, B* **2013**, *176*, 1044−1050.

(3) Li, X.-M.; Yang, X.-Y.; Zhang, S.-S. Electrochemical Enzyme Immunoassay Using Model Labels. *TrAC, Trends Anal. Chem.* **2008**, *27*, 543−553.

(4) Yang, M.; Li, H.; Javadi, A.; Gong, S. Multifunctional Mesoporous Silica Nanoparticles as Labels for the Preparation of Ultrasensitive Electrochemical Immunosensors. *Biomaterials* **2010**, *31*, 3281−3286.

(5) Abuknesha, R. A.; Luk, C. Y.; Griffith, H. H. M.; Maragkou, A.; Iakovaki, D. Efficient Labelling of Antibodies with Horseradish Peroxidase Using Cyanuric Chloride. *J. Immunol. Methods* **2005**, *306*, 211−217.

(6) Rusling, J. F.; Sotzing, G.; Papadimitrakopoulosa, F. Designing Nanomaterial-Enhanced Electrochemical Immunosensors for Bancer Biomarker Proteins. *Bioelectrochemistry* **2009**, *76*, 189−194.

(7) Čadková, M.; Metelka, R.; Holubová, L.; Horák, D.; Dvořáková, V.; Bílková, Z.; Korecká, L. Magnetic Beads-Based Electrochemical Immunosensor for Monitoring Allergenic Food Proteins. *Anal. Biochem.* **2015**, *484*, 4−8.

(8) *Epoxy Resins: Chemistry and Technology*; May, C. A., Tanaka, Y., Eds.; Decker: New York, 1973.

(9) Horák, D.; Pelzbauer, Z.; Bleha, M.; Ilavský, M.; Švec, F.; Kálal, J. Reactive Polymers XXXII. Effect of Composition of Polymerization Feed on Morphology and Some Physical Properties of Macroporous Suspension Copolymers Glycidyl Methacrylate-Ethylene Dimethacrylate. *J. Appl. Polym. Sci.* **1981**, *26*, 411−421.

(10) Zhao, R.; Lu, J.; Tan, T. Preparation of Polyglycidylmethacrylate Macropore Beads and Application in *Candida Species 99−125* Lipase Immobilization. *Chem. Eng. Technol.* **2011**, *34*, 93−99.

(11) Shouldice, G. T. D.; Vandezande, G. A.; Rudin, A. Practical Aspects of the Emulsifier-Free Emulsion Polymerization of Styrene. *Eur. Polym. J.* **1994**, *30*, 179−183.

(12) Ottewill, R. H.; Shaw, J. N. Studies on Preparation and Characterization of Monodisperse Polystyrene Latices. I. Preparation. *Colloid Polym. Sci.* **1967**, *215*, 161−166.

(13) Sharifi-Sanjani, N.; Soltan-Dehghan, M.; Naderi, N.; Ranji, A. Emulsifier-Free Emulsion Polymerization of Styrene. *J. Appl. Polym. Sci.* **2004**, *94*, 1898−1904.

(14) Munro, D.; Goodall, A. R.; Wilkinson, M. C.; Randle, K.; Hearn, J. Study of Particle Nucleation, Flocculation, and Growth in the Emulsifier-Free Polymerization of Styrene in Water by Total Intensity Light-Scattering and Photon Correlation Spectroscopy. *J. Colloid Interface Sci.* **1979**, *68*, 1−13.

(15) Song, Z.; Poehlein, G. W. Particle Nucleation in Emulsifier-Free Aqueous-Phase Polymerization: Stage 1. *J. Colloid Interface Sci.* **1989**, *128*, 486−500.

(16) Goodall, A. R.; Wilkinson, M. C.; Hearn, J. Mechanism of Emulsion Polymerization of Styrene in Soap-Free Systems. *J. Polym. Sci., Polym. Chem. Ed.* **1977**, *15*, 2193−2218.

(17) Watson, R.; Fitch, R. M.; Bakker, D. Kinetics of Particle Nucleation and Initial Growth in Latex Polymerization: Light Scattering and Laser Interferometric Observations. *Abstr. Pap. Jt. Conf. - Chem. Inst. Can. Am. Chem. Soc.* **1975**, *16*, 109−113.

(18) Horák, D.; Rittich, B.; Španová, A. Carboxyl-Functionalized Magnetic Microparticle Carrier for Isolation and Identification of DNA in Dairy Products. *J. Magn. Magn. Mater.* **2007**, *311*, 249−254.

(19) Hermanson, G. T.; Mallia, A. K.; Smith, P. K. *Immobilized Affinity Ligand Techniques*; Academic Press: San Diego, 1992.

(20) Bovaird, J. H.; Ngo, T. T.; Lenhoff, H. M. Optimizing the *o*-Phenylendiamine Assay for Horseradish Peroxidase: Effect of Phosphate and pH, Substrate and Enzyme Concentrations, and Stopping Reagents. *Clin. Chem.* **1982**, *28*, 2423−2426.

(21) Tanrisever, T.; Okay, O.; Sonmezoglu, I. C. Kinetics of Emulsifier-Free Emulsion Polymerization of Methyl Methacrylate. *J. Appl. Polym. Sci.* **1996**, *61*, 485−493.

(22) Chen, M.-Q.; Serizawa, T.; Akashi, M. Graft Copolymers Having Hydrophobic Backbone and Hydrophilic Branches. XVI. Polystyrene Microspheres with Poly(*N*-isopropylacrylamide) Branches on Their Surfaces: Size Control Factors and Thermosensitive Behavior. *Polym. Adv. Technol.* **1999**, *10*, 120−126.

(23) Horák, D.; Semenyuk, N.; Lednický, F. Effect of the Reaction Parameters on the Particle Size in the Dispersion Polymerization of 2-Hydroxyethyl and Glycidyl Methacrylate in the Presence of a Ferrofluid. *J. Polym. Sci., Part A: Polym. Chem.* **2003**, *41*, 1848−1863.

(24) Chen, M.-Q.; Serizawa, T.; Kishida, A.; Akashi, M. Graft Copolymers Having Hydrophobic Backbone and Hydrophilic Branches. XXIII. Particle Size Control of Poly(ethylene glycol)-Coated Polystyrene Nanoparticles Prepared by Macromonomer Method. *J. Polym. Sci., Part A: Polym. Chem.* **1999**, *37*, 2155−2166.

(25) Horák, D.; Shapoval, P. Reactive Poly(glycidyl Methacrylate) Microspheres Prepared by Dispersion Polymerization. *J. Polym. Sci., Part A: Polym. Chem.* **2000**, *38*, 3855−3863.

(26) Horák, D.; Kučerová, J.; Korecká, L.; Jankovičová, B.; Palarčík, J.; Mikulášek, P.; Bílková, Z. New Monodisperse Magnetic Polymer Microspheres Biofunctionalized for Enzyme Catalysis and Bioaffinity Separations. *Macromol. Biosci.* **2012**, *12*, 647−655.

(27) Cho, M. S.; Yoon, K. J.; Song, B. K. Dispersion Polymerization of Acrylamide in Aqueous Solution of Ammonium Sulfate: Synthesis and Characterization. *J. Appl. Polym. Sci.* **2002**, *83*, 1397−1405.

(28) Tanrisever, T.; Okay, O.; Sonmezoglu, I. C. Kinetics of Emulsifier-Free Emulsion Polymerizatin of Methyl Methacrylate. *J. Appl. Polym. Sci.* **1996**, *61*, 485−493.

(29) Sharifi-Sanjani, N.; Soltan-Dehghan, M.; Naderi, N.; Ranji, A. Emulsifier-Free Emulsion Polymerization of Styrene. *J. Appl. Polym. Sci.* **2004**, *94*, 1898−1904.

DOI: 10.1021/acsami.5b08469
ACS Appl. Mater. Interfaces 2015, 7, 24926−24931